Identification and Characterization of a Cardiomyopathy Syndrome Resulting from Loss of the Melanocortin 4 Receptor

By

Michael Litt

Dissertation

Submitted to the Faculty of the

Graduate School of Vanderbilt

University In partial fulfillment of the

requirements for the degree of

DOCTOR OF PHILOSOPHY

in

Molecular Biology and Biophysics

August 31, 2017

Nashville, Tennessee

Approved:
David Wasserman Ph.D.
Roger Cone Ph.D.
Owen McGuinness Ph.D.
Danny Winder Ph.D.
David Weaver Ph.D.

To Papa Jay and Papa Duck.

עֹשֶׂה שָׁלוֹם בִּמְרוֹמָיו, הוּא יַעֲשֶׂה שָׁלוֹם עָלֵינוּ וְעַל כָּל
יִשְׂרָאֵל, וְאִמְרוּ: אָמֵן.

ACKNOWLEDGEMENTS

Any perception of my success in graduate school is a direct reflection of the tremendous guidance and support that I have received.

First and foremost, I would like to thank Roger Cone for his tireless mentorship and unwavering support. It takes an extremely special mentor to train a graduate student working on an unfunded side project. His 'sink or swim' style has given me a confidence I will draw on for the rest of my career. For that, I am forever indebted.

I will always be grateful to the guidance of Dr. Javid Moslehi. His ability to provide honest and critical feedback has been sine qua non. His willingness to find the time to help me with my project while simultaneously starting a lab and clinical department are a true testament to his dedication as a mentor.

I would like to extend the deepest of thanks to the members of my thesis committee: Dave Wasserman, Owen McGuinness, Danny Winder and Dave Weaver. Their astute and timely insights into my project have provided a sense of clarity to both my science and professional development.

I would also like to thank Josh, Masoud, Isin, Max, Luis, my fellow cone lab graduate students, Donald and Savannah for all of the spectacular advice, friendship, and technical acumen. I owe a debt of gratitude to Roger Colbran and Richard O'Brien for their wiliness to work with me under these unique circumstances. Furthermore, I want to thank the entirety of MPB for providing a wonderful environment in which to develop as a scientist. Lastly, I would like to thank the entirety of the MSTP leadership

team, including Chris Williams, Terry Dermody, Danny Winder, Larry Swift, Sally York, and Melissa Krassnove for supporting me throughout this time.

To My Parents: Thank you for giving me a loving home and always believing in my dreams. Despite my many flaws, your confidence in my abilities has never wavered – even when I got that D- in spelling class. While it may have seemed like I was not listening, the countless words of wisdom you have given to/yelled at me over the years have shaped me into who I am today.

To Becca: The ups and downs of graduate school have been your daily source of laughter and concern. You may never believe in things that are microscopic, but your belief in me has given me the strength to push through the low points. You are my rock.

To Alex: Your competitive drive and passion are something I strive towards every day. Thank you for being patient with me and always pointing me in the right direction. Maybe one day I will be as cu as you.

To my grandparents: Thank you for the trips to Panera, rounds at Sawgrass, art lessons and unending love. It has been my greatest joy to have you all in my life.

To my uncles, aunts, and cousins: Thank you for visiting me in Nashville, following me down ski runs, and demonstrating interest in what I am up to. I love you all very much.

Lastly I would like to thank all of my friends. You all have helped make Nashville an amazing place to live, work and have fun. Without you guys, I would have lost my mind far before I did.

TABLE OF CONTENTS

LIST OF TABLES

Table Page

LIST OF FIGURES

Figure Page

CHAPTER 1

[1]BACKGROUND AND SIGNIFICANCE

The Central Melanocortin System

The melanocortin receptors were first understood in terms of the biological actions of α-melanocyte stimulating hormone (α-MSH) on pigmentation via the melanocyte stimulating hormone receptor (MSH-R) and adrenocorticotropic hormone (ACTH) on adrenocortical glucocorticoid production via the adrenocorticotropin receptor (ACTH-R). Subsequently, a family of five melanocortin receptors were cloned, with the MSH-R and ACTH-R renamed the MC1-R and MC2-R, and 3 new receptors termed the MC3R, MC4R, and MC5R respectively. The combined detection of POMC and MC4R expression in the brain has since sparked a decades long investigation into the roles of POMC and MC4R in neurobiology. MC4R, its agonist α-MSH – a POMC cleavage product, and its inverse agonist AgRP are now known to regulate a diverse array of physiological processes including food intake, sympathetic tone, adaptive thermogenesis, reproductive biology, and glucose homeostasis. This line of inquiry has resulted in a new understanding of MC4R's role in human health. Heterozygous loss of function of the MC4R is now known to be the most common cause of

[1] Text and figures have been modified from Anderson et al. (2016)

monogenetic obesity, accounting for 2-6% of all pediatric obesity cases. MC4R agonists are also being examined for the treatment for common obesity and have been employed as a hormone replacement therapy for patients with POMC null mutations. However, with the exception of a new α-MSH analogue (Setmelanotide/RM493), use has been severely limited by cardiopressor side effects.

The cloning of MC4R

The cloning of five melanocortin receptors in 1992 significantly advanced our understanding of the physiological regulation of energy balance (Mountjoy, Robbins, Mortrud, & Cone, 1992). The MC1R is expressed in skin and hair follicle melanocytes and regulates skin pigmentation. α-MSH binds to the MC1R and stimulates the synthesis of eumelanin (brown-black pigments). Agouti (agouti signaling protein or ASP) binds to the receptor and stimulates the synthesis of pheomelanin (yellow-red pigments) by competitively inhibiting the binding of α-MSH. This contrasts with MC2R, which can be activated by physiological levels ACTH, but not α-MSH. The MC2R is exclusively expressed in the adrenal cortex where activation of this receptor regulates cell proliferation and production of glucocorticoids (Cone, 2005). In addition to MC1R and MC2R, three orphan melanocortin receptors were identified and cloned. MC3R was cloned in 1993 (Roselli-Rehfuss et al., 1993) and was found to be expressed in the arcuate nucleus (ARC), ventromedial nucleus of the hypothalamus (VMH), ventral tegmental area (VTA), central linear nucleus of raphe, with moderate expression in anteroventral preoptic nucleus, lateral hypothalamic area (LH), posterior hypothalamic

area, medial habenular nucleus and paraventricular nucleus of the hypothalamus (PVH) (Gantz, Konda, et al., 1993; Roselli-Rehfuss et al., 1993). Disruption of this gene in knockout mouse models causes increased adiposity, reduced lean body mass, and increased feed efficiency (Butler et al., 2000; A. S. Chen et al., 2000).

Two independent laboratories then identified MC4R using homology-based cloning (Gantz, Miwa, et al., 1993; Mountjoy, Mortrud, Low, Simerly, & Cone, 1994). The gene, identified on chromosome 18 (q21.3) in humans, consisted of one large exon with an open reading frame of 1 kb encoding a protein of 332 amino acids. Based on sequence alignment analysis, the closest identified receptor was MC3R, with 58% homology (Gantz, Konda, et al., 1993; Magenis et al., 1994). As there was no known physiological function, this gene was then termed MC4R. Later studies also identified the MC5R, which is expressed primarily in exocrine glands and stimulates the synthesis and secretion of a variety of exocrine gland products (W. Chen et al., 1997; Morgan & Cone, 2006). *In situ* hybridization studies of MC4R revealed wide expression throughout the central nervous system (Mountjoy et al., 1994), peripheral nervous system and later within L cells of the colon – a neuroendocrine cell type (B. L. Panaro et al., 2014). In the hypothalamus, MC4R localized to the PVH, LH, and dorsomedial nucleus (DMH) (Figure 1). Outside of the hypothalamus, MC4R was found in numerous brain regions including in the dorsal motor nucleus of the vagus (DMX), the intermediolateral (IML) column of the spinal cord, the amygdala, and bed nucleus of the stria terminalis (BNST). The high expression of MC4R in hypothalamic and brainstem nuclei suggested a role in neuroendocrine and autonomic control (Mountjoy et al., 1994).

The role of MC4R signaling in feeding behavior

The earliest physiological evidence of MC4R's role in feeding behavior is a series of reports that demonstrated how intracerebroventricular injection of ACTH or α-MSH can inhibit the feeding drive induced by intraperitoneal injection of an opiate receptor agonist in rats (Poggioli, Vergoni, & Bertolini, 1986; Vergoni, Poggioli, & Bertolini, 1986). However, the breakthrough in understanding the MC4R physiological function came from discoveries made in MC1R physiology and pharmacology (Lu et al., 1994). In these studies, Agouti, a 132-amino-acid protein that is produced in the hair follicle, was found to be a high affinity antagonist of MC1R where it competitively blocks α-MSH binding and inhibits cAMP production (Lu et al., 1994). This finding correlated with observations *in vivo* that agouti blocked eumelanin production.

During the course of these studies, agouti was also found to be a high affinity competitive antagonist of α-MSH action at MC4R, but not other melanocortin receptors (Lu et al., 1994). Thing finding was coupled with the observation the obese yellow A^y mouse. This mouse was found to have a gene rearrangement in the Agouti locus that produced ectopic expression of agouti in the brain (Yen, Gill, Frigeri, Barsh, & Wolff, 1994). From these studies, it was inferred that the inhibition of melanocortin receptor(s) in the brain underlies the obesity and metabolic syndrome observed in A^y mouse (Lu et al., 1994).

Several additional studies were published providing direct evidence supporting this hypothesis and established a central role of MC4R signaling in regulation of energy homeostasis. Intracerebroventricular injection of MTII, a cyclic analog of α-MSH, was

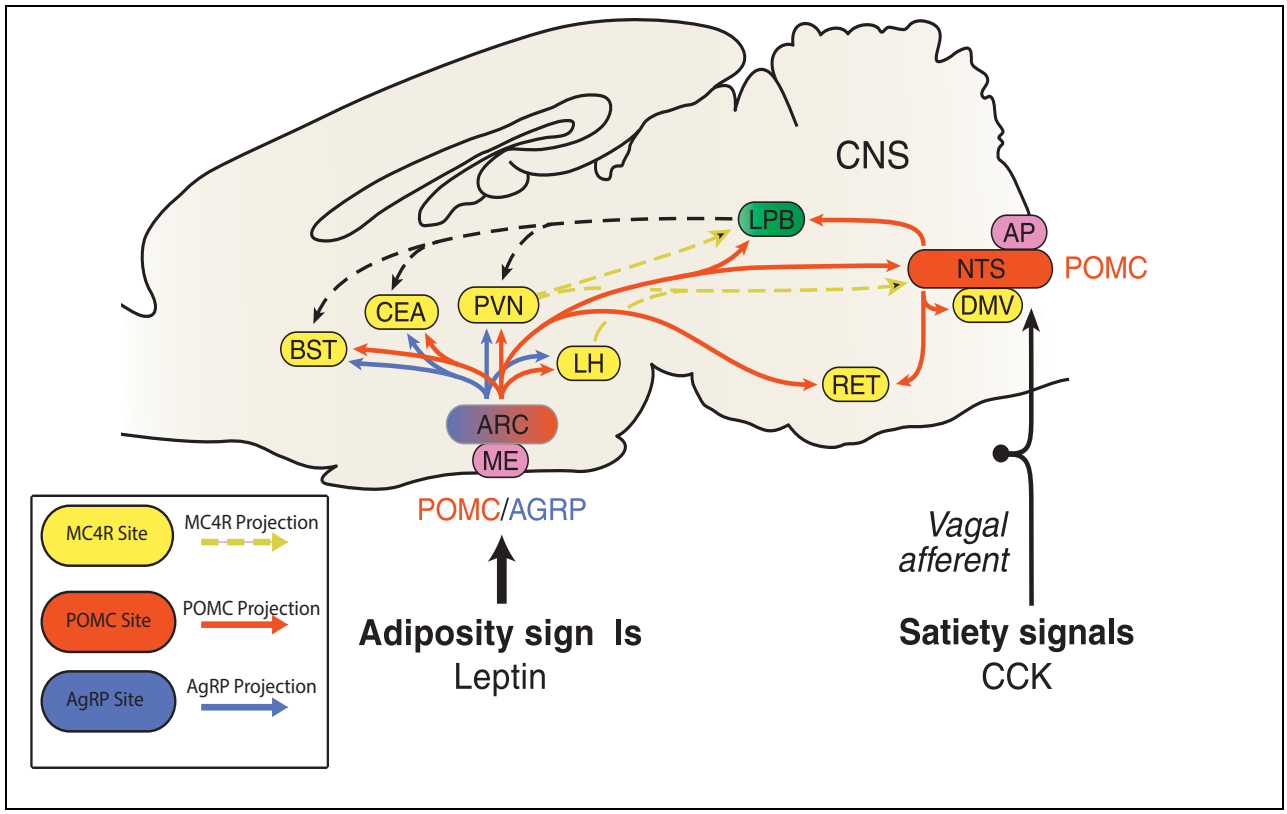

Figure 1 A highly simplified schematic of the central melanocortin system.

Receipt of long-term adipostatic signals and acute satiety signals by neurons in arcuate nucleus and brainstem, respectively. Light blue boxes indicate nuclei containing POMC neurons; yellow boxes indicate nuclei containing MC4R neurons that may serve to integrate adipostatic and satiety signals; and pink boxes show some circumventricular organs involved in energy homeostasis. Red arrows designate projections of POMC neurons; blue arrows show projections of agouti-related protein (AgRP neurons). AP, area postrema; ARC, arcuate nucleus; BST, bed nucleus of the stria terminalis; CCK, cholecystokinin; CEA, central nucleus of the amygdala; DMV, dorsal motor nucleus of the vagus; LH, lateral hypothalamic area; LPB, lateral parabrachial nucleus; ME, median eminence; NTS, nucleus tractus solitarius; PVH, paraventricular nucleus of the hypothalamus; RET, reticular formation. For simplicity, only a fraction of the >100 MC4R target sites are shown, and none of the MC3R target nuclei is indicated. Adapted, with permission, from Fan W, Boston BA, Kesterson RA, Hruby VJ & Cone RD (1997) Role of melanocortin neurons in feeding and the agouti obesity syndrome. *Nature* **385** 165–168.

found to suppress food intake in four different mouse models: fasted C57BL/6J, *ob/ob*, A^y, and mice injected with neuropeptide Y. Co-injection of SHU9119, a cyclic peptide antagonist of MC3R and MC4R, was able to block this effect. Furthermore, intracerebroventricular injection of SHU9119 alone increased food intake in mice (Fan et al., 1997; Hruby et al., 1995) indicating the potential for bi-directional melanocortin signaling and basal receptor activity. Furthermore, chronic blockade of this signaling pathway by the MC1/4R antagonist agouti was deemed responsible for the obesity phenotype observed in the A^y yellow mouse (Fan et al., 1997).Together, these findings supported the hypothesis that hypothalamic POMC expressing neurons release α-MSH tonically and inhibit feeding via activation of MC4R target neurons.

Knockout and transgenic mice have been pivotal to further advancing our understanding of MC4R's role in energy homeostasis. Using a neomycin-targeting cassette, the MC4R was knocked out in embryonic stem cells and these cells were used to create the MC4R knockout mouse. This mouse model was then used to further test the hypothesis that deletion of MC4R would recapitulate the agouti obesity syndrome (Huszar, Lynch, Fairchild-Huntress, et al., 1997). Mice lacking both MC4R alleles displayed early-onset obesity, hyperphagia, increased linear growth, hyperinsulinemia, and hyperglycemia while loss of a single allele resulted in an intermediate phenotype. This indicated the MC4R exhibited a gene dosage effect – an uncommon feature of GPCRs (Huszar, Lynch, Fairchild-Huntress, et al., 1997). Later, a reversible MC4R knockout model was generated through the insertion of a floxed transcriptional blocking cassette in the 5' region of the gene (MC4R-loxTB) (Balthasar et al., 2005). Along with

the $MC4R^{loxP/loxP}$ mouse (Sohn et al., 2013), these tools have enable site-specific re-expression and deletion of MC4R in mice.

AgRP – An endogenous MC4R antagonist

In parallel with the discovery of MC4R as a physiological regulator of energy balance, an analog of Agouti, termed Agouti related peptide (AgRP), was characterized (Fong et al., 1997; Graham, Shutter, Sarmiento, Sarosi, & Stark, 1997; Ollmann et al., 1997) and found to be an endogenous antagonist of the MC4R. AgRP was identified by homology mapping with Agouti and its expression was found in the ARC and adrenal gland, with very low expression in lung, kidney, testis and ovaries (Ollmann et al., 1997; Shutter et al., 1997). Based on its expression profile and homology with Agouti, it was proposed that AgRP was a melanocortin receptor antagonist. Further studies found that AgRP mRNA levels are significantly increased during fasting and in the hyperphagic *ob/ob* mouse. Later studies showed that AgRP binds to MC3R and MC4R with high affinity (Chai et al., 2003) and acts as competitive antagonist of α-MSH at these receptors (Ollmann et al., 1997). Unlike agouti however, AgRP has low affinity for MC1R (Ollmann et al., 1997). AgRP was also found to have a rather unique pharmacological profile. A one time 1-nmol intracerebroventricular injection of AgRP was found to increase food intake for a week. Further more, co-injection of α-MSH was unable to blunt this orexigenic effect (Hagan et al., 2000). Together with AgRP's ability to suppress N-terminal tethered ligand mediated basal MC4R activity, suggested that AgRP functions *in vivo* as an inverse agonist, as well as a competitive antagonist (Chai et al., 2003; Haskell-Luevano, Cone, Monck, & Wan, 2001; Nijenhuis, Oosterom, &

Adan, 2001). This finding further substantiated the now canonical yin/yang view of feeding regulation. In this model, POMC neurons suppress food intake and energy storage through activation of MC4R signaling, while NPY/AgRP neurons stimulate hunger drive in part through AgRP antagonism of MC4R signaling (Figure 2).

In concordance with this model, transgenic mice ubiquitously overexpressing human AgRP were found to exhibit hyperphagic obesity.,Unlike the A^y mouse, however, these mice did not have yellow fur (Graham et al., 1997; Ollmann et al., 1997). This finding led to speculation that AgRP knockout mice might exhibit leanness. Despite such expectation, these mice exhibited normal food intake, body composition, growth rate, and responses to starvation (Qian et al., 2002). Subsequent work demonstrated that homozygous AgRP knockout mice exhibit a very modest reduction in body weight and adiposity at 6-months of age with increased metabolic rate, body temperature, and locomotor activity (Wortley et al., 2005). These mice also were found to exhibit a blunted fast-induced refeeding response, a finding also seen in MC3R knockouts. Further studies revealed that AgRP is part of a larger class of neurotransmitters within the AgRP neuron that stimulate feeding. AgRP neurons also express GABA and NPY, and all three ligands act to inhibit MC4R neurons and promote food intake (Q. Wu & Palmiter, 2011). Despite this redundancy, the kinetics for each neurotransmitter is unique. GABA functions in a fast acting manner, regulating bout to bout food intake, while NPY and AgRP act over longer periods and dictate long term energy homeostasis (Michael J. Krashes, Bhavik P. Shah, Shuichi Koda, & Bradford B. Lowell, 2013). These findings underscore the immense complexity of the AgRP neuronal population and

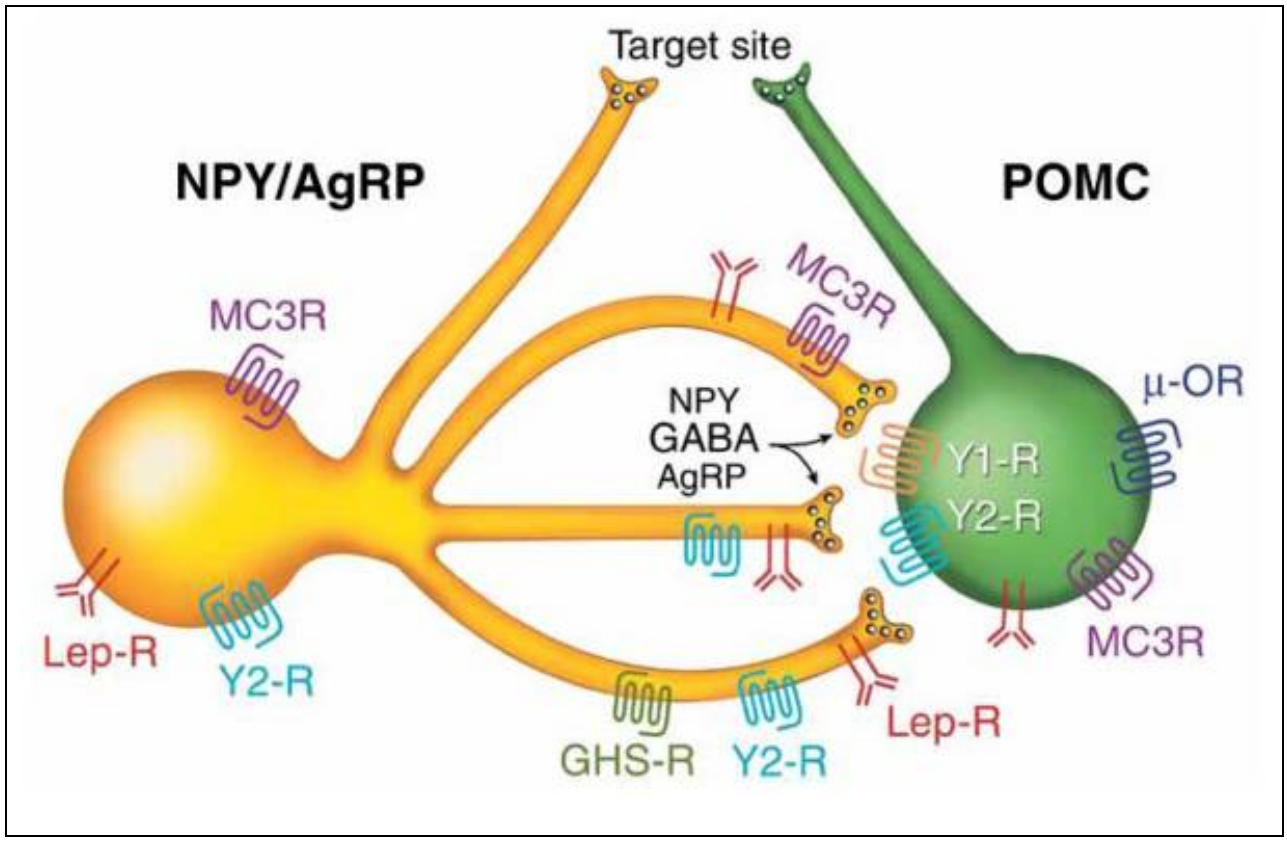

Figure 2 Yin–Yang model of control of feeding behavior and energy homeostasis.

NPY/AgRP and POMC neurons within the arcuate nucleus form a coordinately regulated network due to dense NPY/ AgRP fibers that project to POMC cell bodies. Some of the receptors for a large number of hormones and neuropeptides known to regulate the network are indicated. These fibers project to many of the same nuclei, where dual release of α-MSH and AgRP were proposed to compete for MC4R binding, to coordinately regulate food intake and energy homeostasis. AgRP, agouti-related peptide; GABA, γ-aminobutyric acid; GHS, growth-hormone secretagogue receptor; Lep, leptin; MC3R, melanocortin 3 receptor; NPY, neuropeptide Y; μ-OR, μ-opiate receptor; R, receptor; GLP-1, glucagon-like peptide 1. Modified, with permission, from Cowley MA, Smart JL, Rubinstein M, Cerdan MG, Diano S, Horvath TL, Cone RD & Low MJ (2001) Leptin activates anorexigenic POMC neurons through a neural network in the arcuate nucleus.

ability to modulate MC4R mediated hunger and satiety.

POMC & AGRP neurons

Neurons expressing POMC, and AgRP constitute the primary input components of the central melanocortin system (Figure 1) Within the CNS, AgRP neurons are restricted to the arcuate nucleus of the hypothalamus (ARC^{AgRP}). Most AgRP neurons (~90%) also express the orexigenic peptide hormone, neuropeptide Y (NPY) and the fast neurotransmitter GABA. Unlike AgRP, NPY is widely expressed in the mammalian brain. Likewise, POMC neurons within the ARC (ARC^{POMC}) express another gene coding for an anorectic peptide called cocaine- and amphetamine-regulated transcript (CART). $ARC^{NPY/AgRP}$ and $ARC^{POMC/CART}$ neurons, henceforth referred to as ARC^{AgRP} and ARC^{POMC} neurons, are chemically and anatomically distinct. However, approximately 25% of the ARC^{NPY} neurons are derived from the same lineage as ARC^{POMC} neurons during development (Padilla, Carmody, & Zeltser, 2010). In the rodent, ARC^{AgRP} neurons are present throughout the rostrocaudal axis of the ARC. Conversely, most ARC^{POMC} neurons are located in the anterior and medial portion of the ARC. In the rat, ARC^{POMC} neurons are more laterally distributed compared to the mouse (Cowley et al., 2001). Early studies quantifying ARC^{POMC} neurons, by β-endorphin immunohistochemistry (Huo, Grill, & Bjorbaek, 2006) or using mice expressing GFP under the POMC promoter, (Cowley et al., 2001) have reported around 3000-3500 POMC neurons in rodent ARC. However a recent report quantifying POMC neurons using an antibody specific to the POMC precursor, found closer to 9000 POMC cells (Lemus et al., 2015). The number of ARC^{AgRP} neurons, as analyzed using mice

expressing GFP in an AgRP promoter-dependent manner, has been estimated to be between 8000-10,000 (Betley, Cao, Ritola, & Sternson, 2013; Lemus et al., 2015).

In adult rodents, POMC mRNA was detected by northern blot in hypothalamus, amygdala and the cerebral cortex but was not detectable in midbrain or cerebellar RNA preparations (Civelli, 1982). A 5' truncated version of POMC mRNA lacking the signal sequence was also detected in amygdala, midbrain and cortex as well as in several peripheral tissues. The role of this truncated version is unclear, however, as it does not produce functional POMC peptides (Clark, Lavender, Coates, Johnson, & Rees, 1990). POMC was also detected in the NTS and lateral reticular formation of the rat brainstem initially by immunohistochemistry against ACTH (Joseph, Pilcher, & Bennett-Clarke, 1983; Schwartzberg & Nakane, 1983) and later by *in situ* hybridization (Bronstein, Schafer, Watson, & Akil, 1992). Most neurons identified as POMC positive by labeling strategies involving POMC-Cre mediated recombination do not express POMC in the adult brain. This is due to transient POMC expression that does not persist into adulthood. In this context, mice expressing GFP under the POMC promoter yielded more satisfactory anatomical data (Pinto et al., 2004). More recent and comprehensive studies comparing POMC-Cre, POMC-GFP and sensitive in situ hybridization techniques have concluded that POMC expression in the adult mouse brain is restricted to ARC and NTS (Figure 1)(Padilla, Reef, & Zeltser, 2012).

ARC^{POMC} and ARC^{AgRP} neurons receive inputs from other hypothalamic nuclei including the PVH, DMH, VMH and LH. Extra-hypothalamic nuclei such as the lateral septum and BNST also innervate these neurons (D. Wang et al., 2015). Neurons with

cell bodies in the hippocampus, medial mammillary nucleus and ventral tegmental area (VTA) appear to selectively innervate ARC^{POMC} neurons but not ARC^{AgRP} neurons (D. Wang et al., 2015). NTS^{POMC} neurons receive input primarily from other neurons in the brainstem. However neurons originating from PVH and amygdala (D. Wang et al., 2015) also innervate NTS^{POMC} neurons.

ARC^{AgRP} and ARC^{POMC} neurons project to a large number of intra- and extra-hypothalamic brain regions, and many reciprocal connections have been found. Within the hypothalamus, ARC^{AgRP} and ARC^{POMC} neurons send overlapping projections to hypothalamic nuclei including PVH, LH, VMH, PH, DMH, and mPOA (Bagnol et al., 1999). ARC^{AgRP} neurons innervate extra-hypothalamic sites such as the BNST, and the LPB, central nucleus of the amygdala and periaqueductal gray (PAG) (Betley et al., 2013; D. Wang et al., 2015). ARC^{POMC} neurons innervate many extra-hypothalamic regions including BNST, lateral septum, nucleus accumbens, LPB, the periaqueductal gray, and the DMX. NTS^{POMC} neurons innervate other neurons within the brain stem (D. Wang et al., 2015). The large degree of overlap in the regions innervated by both AgRP and POMC neurons also supports the dual regulation of central melanocortin signaling by α-MSH and AgRP (Figure 2). However, POMC neurons appear to innervate important regions not receiving AgRP innervation, such as the DMX.

Besides neuronal inputs, ARC^{AgRP} and ARC^{POMC} neurons are under direct regulation of hormonal and nutrient-related signals. Both neuron populations express LepRb and the insulin receptor while only ARC^{AgRP} neurons express ghrelin receptors. A recent report suggested that the AgRP neurons that project within the hypothalamus

do not express LepRb, which was not the case for ARC^{POMC} neurons (Betley et al., 2013). Around 30-40% of ARC^{AgRP} neurons respond to leptin with increased STAT3 phosphorylation (van de Wall et al., 2008). Virtually no ARC^{POMC} neurons in the NTS exhibit leptin-induced STAT3 phosphorylation or c-Fos expression induction (Huo et al., 2006). Nonetheless, about 60% of ARC^{POMC} neurons are leptin-responsive. In addition, fasting decreases POMC expression in both ARC and NTS, but only ARC POMC expression can be rescued by leptin (Huo et al., 2006; Perello, Stuart, & Nillni, 2007). Further more, deletion of LepRb from ARC^{POMC} or ARC^{AgRP} neurons results in obesity and hyperleptinemia (Balthasar et al., 2004; van de Wall et al., 2008) in both genders of mice. Deletion LepRb from both neuronal populations is additive (van de Wall et al., 2008). Despite the difficulties inherent to the developmental problems associated with the Cre lines, these studies suggest that POMC and AgRP neurons mediate only part of leptin's effects on energy homeostasis (Padilla et al., 2012).

The first circuit level genetic manipulation of the POMC and AgRP neurons involved the targeted expression of DTR in each neuronal subpopulation, followed by administration of DT to ablate the entire neuronal population (Luquet, Perez, Hnasko, & Palmiter, 2005). These studies demonstrated that AgRP neurons are essential for food intake, and that loss of ARC^{POMC} neurons, but not NTS^{POMC}, results in hyperphagia, decreased energy expenditure, and obesity (Zhan et al., 2013). These findings undoubtedly stimulated interest in application of optogenetic and chemogenetic methods to the study of POMC and AgRP neurons. The development of optogenetics and DREADDs has enabled circuit level manipulation of genetically defined neuronal

populations involved in hunger and satiety. Optogenetics (see: (Deisseroth, 2011)) employs microbial opsins to control neuronal firing properties. The principal opsin used in function studies of feeding circuits is humanized channel rhodopsin (hChR2), a nonspecific cation channel that can depolarize cells when activated by 470nm light (Boyden, Zhang, Bamberg, Nagel, & Deisseroth, 2005). By packaging hCh2R into a Cre-inducible adeno-associated viral vector, this construct can be selectively expressed in target populations via stereotactic injections (Atasoy, Aponte, Su, & Sternson, 2008; Sohal, Zhang, Yizhar, & Deisseroth, 2009; Tsai et al., 2009). The connectivity and behavioral relevance of these neurons can then be investigated with *ex vivo* channel rhodopsin assisted circuit mapping (CRACM) and *in vivo* photostimulation (Adamantidis, Zhang, Aravanis, Deisseroth, & de Lecea, 2007; Aravanis et al., 2007; F. Zhang et al., 2010). Designer receptors exclusively activated by designer drugs (DREADDs) (see: (Sternson & Roth, 2014)) are a related strategy that enables remote control of neuronal activity without the need for specialized hardware (Alexander et al., 2009; Armbruster, Li, Pausch, Herlitze, & Roth, 2007). The first generation DREADDs are molecularly evolved human muscarinic receptors that have minimal endogenous activity and can be activated only by clozapine-n-oxide (CNO), an otherwise inert ligand (Armbruster et al., 2007). Importantly, DREADDs can be used to induce either Gq (hM3Gq) or Gi (hM4Gi) signaling pathways to respectively depolarize or silence neurons (Sternson & Roth, 2014). Together, these tools have been used to further understand how AgRP, POMC and MC4R neurons regulate acute and chronic food intake.

Initial studies with optogenetics found that 1-hour hCh2R stimulation of ARC^{AgRP}

neurons induced 0.85g of food intake in satiated mice (Aponte, Atasoy, & Sternson, 2011; Atasoy, Betley, Su, & Sternson, 2012). The frequency of stimulation was proportional to the magnitude of food ingested indicating that this effect was presumably due to increased action potential frequency (Aponte et al., 2011). Interestingly, the acute phase of ARC^{AgRP} stimulated food intake was maintained on the A^{y} background and therefore independent of MC4R inhibition (Aponte et al., 2011). Similar experiments using DREADDs also found that hM3Gq activation of ARC^{AgRP} neurons resulted in increased food intake and reduced oxygen consumption. hM4Gi mediated inhibition reduced food intake indicating that ARC^{AgRP} regulated feeding is bidirectional (Krashes et al., 2011). Furthermore, chronic hM3Gq activation of ARC^{AgRP} neurons was found to cause an obesity phenotype that could be reversed following cessation of CNO administration (Krashes et al., 2011). By combining ARC^{AgRP} targeted DREADDs with existing knockout mouse models, follow up studies revealed that NPY or GABA was necessary for the acute effects on ARC^{AgRP} neuron activation while AgRP was sufficient for long-term effects (M. J. Krashes, B. P. Shah, S. Koda, & B. B. Lowell, 2013). More recent experiments have used hCh2R and DREADDs to further define how ARC^{AgRP} neurons encode a negative balance signal for energy depletion (Betley et al., 2015) and how they evoke typified energy seeking behaviors even in the absence of food (Dietrich, Zimmer, Bober, & Horvath, 2015). Together, these studies establish a critical role of ARC^{AgRP} neurons in the regulation of feeding behavior and serve as a model by which to study the role of other genetically defined populations.

Optogenetics and DREADDs have also been used to study the role of POMC

neurons in feeding behavior. Chronic but not acute optogenetic stimulation of ARC^{POMC} neurons was found to reduce food intake and cause weight loss, but only after several hours of stimulation (Aponte et al., 2011; Zhan et al., 2013). Importantly, unlike ARC^{AgRP} dependent feeding, the satiating effect of ARC^{POMC} stimulation was lost on the A^{y} background and therefore dependent on MC4R signaling (Aponte et al., 2011). This finding has been repeated with hM3Dq activation of ARC^{POMC} neurons whereby animals displayed a 50% reduction of food intake and a 6% drop in their total body mass (Zhan et al., 2013). Furthermore, chronic but not acute hM4Di mediated inhibition of ARC^{POMC} neurons was found to cause hyperphagia, but only after 24 hours. Although this finding points toward a role for α-MSH signaling in regulating long term energy balance, these studies are at odds with pharmacological data that have shown robust acute anorexic effects of MC4R agonists (Fan et al., 1997). While it is possible that supraphysiological α-MSH dosing paradigms used during pharmacological studies might be responsible for some of this effect, NTS^{POMC} neurons have also been implicated in acute feeding behavior. Indeed, acute hM3Dq stimulation of NTS^{POMC} neurons has been found to cause acute anorexia while chronic activation of this population does not seem to effect food intake (Zhan et al., 2013). The mechanism that underlies the discordance between anatomical subsets of POMC neurons remains unknown, however, it is likely a result of their distinct projection fields (D. Wang et al., 2015). Alternatively, acute stimulation of ARC^{POMC} has been shown to promote endocannabinoid evoked feeding which may be responsible for the delayed response of ARC^{POMC} neurons but not NTS^{POMC} neurons (Koch et al., 2015).

MC4R Neurons

MC4R expressing neurons serve to integrate energy status signals from ARC^{AGRP} and ARC^{POMC} neurons and then relay this status throughout the CNS. The MC4R is broadly distributed. It is expressed in many CNS nuclei with a striking presence in the hypothalamus, NuAcc, and DMX. Mapping via *in situ* hybridization localized MC4R to over 100 distinct nuclei (Mountjoy et al., 1994). Hypothalamic nuclei with the highest MC4R expression include the suprachiasmatic preoptic nucleus, anteroventral periventricular nucleus, supraoptic nucleus, PVH, VMH, DMH, tuberomammillary nucleus, and the lateral hypothalamic area. High MC4R expression is also found in brainstem within the superior colliculus, DMX, substantia nigra, raphe, and reticular formation. Regions of the amygdala and cortex have moderate expression. MC4R is also localized in the cortex where it may play a role in olfactory response (K. R. Tucker, Godbey, Thiebaud, & Fadool, 2012). MC4R has also been identified in CA1 and CA2 regions of the hippocampus, throughout the bed nuclei of the stria terminalis (BNST) and striatum, and with minimal expression in the thalamus (Cone, 2005; Cui et al., 2012; Kishi et al., 2003; Mountjoy, 2015; Mountjoy et al., 1994; Mountjoy et al., 1992; Siljee et al., 2013; Y. X. Tao, 2010). MC4R mRNA expression has also been detected in astrocytes, the IML of the spinal cord, and peripherally in the colon, lung, and testis (Caruso, Lagerstrom, Olszewski, Fredriksson, & Schioth, 2014). Localization and distribution of MC4R has been confirmed by studies using a mouse model expressing GFP under control the MC4R promoter (H. Liu et al., 2003).

Genetic and pharmacologic systems inducing or repressing MC4R gene function

in specific neuronal populations have been used to map neuroanatomical functions of each population. For example, MC4R signaling in the PVH is essential for regulating appetite, while MC4R signaling in cholinergic preganglionic parasympathetic neurons is necessary for brown adipose thermogenesis, insulin release and blood pressure regulation (Balthasar et al., 2005; Rossi et al., 2011) (Sohn et al., 2013). One peripheral MC4R-mediated pathway was described after detection of high levels of MC4R expression in enteroendocrine L cells (B. L. Panaro et al., 2014). Data shows the receptor mediates release of L cell products PYY and GLP-1 in either mouse or human, in response to exogenous administration of α-MSH. The physiological role of MC4R at this site, and the origin of the ligand, likely an α-MSH peptide, remains unknown.

Optogenetics and DREADDs have also been used to characterize the MC4R target sites that are necessary and sufficient and for evoked feeding behaviors. Despite evidence of a functional inhibitory ARC^{AgRP} -> ARC^{POMC} projection, co-activation of these two populations did not blunt light evoked ARC^{AgRP} feeding (Atasoy et al., 2012; Betley et al., 2013). However, site-specific photostimulation of GABAergic ARC^{AgRP} efferents within the PVH was found to be sufficient for acute feeding behavior (Atasoy et al., 2012; Garfield et al., 2015). This effect was replicated with hM4Gi mediated silencing of PVH^{SIM1} neurons indicating that inhibition of this population is sufficient for feeding behavior. Furthermore, co-activation of PVH^{SIM1} cell bodies and ARC^{AgRP} efferents did not cause food intake. Initially, PVH^{OXT} neurons (a subpopulation of PVH^{SIM1} neurons) were thought to be the mediators of ARC^{AgRP} -> PVH induced food intake (Atasoy et al., 2012). However, both *ex vivo* and *in vivo* experiments have challenged this finding

(Garfield et al., 2015; Sutton et al., 2014; Z. Wu et al., 2012). Using CRACM, ARC^{AgRP} fibers were found to evoke time locked IPSCs within 83% of PVH MC4R cells and 0% of PVH^{OXT} expressing cells (Garfield et al., 2015). MC4R neurons were also found to be distinct from OXT neurons as evidenced by immunohistochemistry. Co-stimulation of inhibitory ARC^{AgRP} fibers and PVH^{MC4R} were also found to block evoked feeding behavior while PVH^{OXT} did not. PVH^{MC4R} neurons also displayed projections to and elicited activation of the LPBN, thereby provoking a satiety response (Garfield et al., 2015). In addition to the PVH, ARC^{AgRP} neurons are known to project to numerous other brain regions. Using a similar efferent projection stimulation strategy, ARC^{AgRP} fiber activation in the BNST, LH and PVT was sufficient for evoked feeding behavior (Betley et al., 2013). This contrasts with ARC^{AgRP} fibers that project to ARC^{POMC} neurons, PBN, CEA, and PAG which do not evoke feeding. Interestingly, while the BNST and the LH both express MC4R, inhibition of MC4R neurons within these sites does not appear to be responsible for the increased food intake seen with ARC AgRP afferent stimulation (Garfield et al., 2015).

MC4R Signal Transduction

All Melanocortin receptors (MCR) are members of the rhodopsin-like, Class A branch of the seven transmembrane-spanning domain G protein coupled receptor (GPCR) superfamily. Except for MC2R, all melanocortin receptors bind melanocortin peptides containing the conserved heptapeptide core “MEHFRWG,” found in α-MSH. Binding to the MC2R requires an addition C-terminal peptide motif (Gantz, Konda, et al.,

1993). Due to its role in obesity and cachexia, understanding how MC4R transduces information to post synaptic cells has been of particular interest. α-MSH binding to MC4R leads to dissociation of the coupled heterotrimeric G-protein complex by stabilizing an active form of the receptor (Carpenter, Nehmé, Warne, Leslie, & Tate, 2016; Supriya Srinivasan et al., 2004). This process leads to a conformational change in the complex that facilitates the exchange of GDP for GTP on the Gαs (Kleuss, Raw, Lee, Sprang, & Gilman, 1994). Upon dissociation, Gαs associates with and activates adenylyl cyclase through a direct protein-protein interaction (Rasmussen et al., 2011). This process continues until GTP is converted to GDP by the GTPase activity of Gαs. During the time it is activated by Gαs, adenylyl cyclase catalyzes conversion of ATP to cAMP (R. Ho & E. W. Sutherland, 1975; R. J. Ho & E. W. Sutherland, 1975). cAMP goes on to function as a diffusible second messenger until it is cleaved into AMP by phosphodiesterases (Francis, Turko, & Corbin, 2001). cAMP is able to bind to the PKA regulatory subunits causing a conformational change in the protein structure (C. Kim, Xuong, & Taylor, 2005). This enables the catalytic domain of PKA to phosphorylate target proteins including channels that regulate neuronal excitability (Shen, Fu, Cheng, Fu, & Ip, 2013; Shinyama, Masuzaki, Fang, & Flier, 2003). In addition to PKA, cAMP can activate PKA independent pathways including the EPAC pathways (Glas, Muckter, Gudermann, & Breit, 2016). This pathway appears to be essential for MC4R mediated changes in gene transcription in cell lines, but the hypothesis remains to be tested *in vivo.* There is also evidence that MC4R can increase intracellular calcium levels through recruitment of Gαq and IP3 production in heterologous overexpression systems (C. S.

Kim et al., 2002; Konda et al., 1994; Mountjoy, Kong, Taylor, Willard, & Wilkison, 2001). Furthermore, studies on AgRP signaling have found that AgRP leads to MC4R activation of the pertussis toxin sensitive Gi/o inhibitory protein in the hypothalamic GT1-7 cell line (Buch, Heling, Damm, Gudermann, & Breit, 2009). The ability to signal through Gi/o led to the hypothesis that MC4R could potentially couple to GIRKs; known to be activated by Gβγ binding following release from Gi heterotrimers (Lei et al., 2000). These results highlight the possibility that MC4R can signal through different G-proteins with opposing actions depending on the ligand. However, this finding has not been seen in *ex vivo* brain slices.

Physiologically relevant data on the mechanism of α-MSH and AgRP signaling through MC4R relies heavily on the use of electrophysiological slice preparations from mice in which MC4R neurons have been transgenically labeled with GFP (Ghamari-Langroudi, Srisai, & Cone, 2011; Ghamari-Langroudi et al., 2010; H. Liu et al., 2003). Using this method, PKA has been shown to regulate aspects of MC4R signaling in many nuclei (Sohn et al., 2013). PKA mediated MC4R signaling has been shown to cause neuronal hyperpolarization within the DMX through activation of a K_{ATP} channel. In this study, the adenylyl cyclase activator forskolin as well as the PKA activator 8-Br-cAMP were able to mimic the effect of the MC4R agonist MTII. Inhibition of PKA with H89 or KT-5720 was further shown to abolish the MTII mediated hyperpolarization. Within the IML of the spinal chord, PKA was found to be essential for MC4R mediated depolarization. In this cell population, MC4R-PKA signaling was dependent on the activation of a non-specific cation channel. Within the hippocampus, MC4R induces

synaptic strengthening in a PKA dependent manner (Shen et al., 2013). This results in an increase in synaptic spine number and AMPA surface expression via PKA phosphorylation of GluA1. Furthermore, deletion of the inhibitory domain of PKA (RIIβ) is able to reverse the obesity syndrome in A^y mice (Czyzyk, Sikorski, Yang, & McKnight, 2008). Together these studies demonstrate a critical role of PKA in α-MSH induced activation and inhibition of MC4R within the IML, DMX, and hippocampus – regions that lack AgRP innervation. More recent studies have found a distinct MC4R signaling modality within the PVN – a region with high amounts of AgRP innervation (Broberger, Johansen, Johansson, Schalling, & Hökfelt, 1998).

Using a slice preparation of the PVN, α-MSH was found to depolarize MC4R neurons, while AgRP addition led to hyperpolarization. Unlike previous studies, the α-MSH induced depolarization result remained in the presence of the G-protein inhibitors GDPβS and gallein. α-MSH induced depolarization was also retained in the presence of the cAMP inhibitor Rp-cAMPs and the PKA inhibitor H-89 (Ghamari-Langroudi et al., 2015). Subsequent current-voltage ramps indicated that a potassium inward rectifier channel (Kir) was responsible for this effect. In this experiment α-MSH was shown to reduce the inward rectification current of the cell while AgRP was able to increase it. From there, a specific Kir subunit, Kir7.1, was proposed to be a component of the channel responsible for this result using a panel of specific Kir channel blockers. Studies in HEK293 cells reinforced the finding that α-MSH and AgRP regulate Kir7.1 conductance. Furthermore, other inward rectifiers such as Kir2.3 and Kir4.1 channels did not couple to MC4R in cultured cells. However, the molecular mechanism by which

AgRP mediates this effect currently remains unknown and will require further studies to be definitively clarified. As Kir channels form homo and hetero-tetramers, it remains to be determined whether MC4R modulates homo-tetramers of Kir7.1 or hetero-tetramers with other Kir channel subunits. Ghamari-Langroudi et al. (2015) also reported biased agonism at the MC4R. Taken together, these findings reveal a novel MC4R signaling pathway, and the potential for the creation of biased ligands that favor the ion channel direct interaction/activation paradigm over classical G-protein signaling (Z. Zhang et al., 2014).

The discovery of G protein independent coupling of MC4R to Kir7.1 has also revealed that AgRP is also a biased agonist that can act through MC4R to open Kir7.1 and hyperpolarize neurons. New neuroanatomical data supports both the original yin-yang model of α-MSH and AgRP competing for MC4R binding in areas of volume release from POMC and NPY/AgRP neurons (Figure 2) as well as independent α-MSH and AgRP actions in different brain regions and on different subcellular domains of the target MC4R neurons. Confocal (Bouyer & Simerly, 2013) and electron microscopy (Atasoy et al. 2015) of PVH neurons suggests that while there are areas of likely volume release of both peptide, PVH cell bodies receive mostly AgRP synaptic contacts, while small distal dendrites receive mostly POMC synaptic contacts. Thus, the micro-circuitry is far more complex than originally suggested, in turn having profound impact on models of α-MSH and AgRP action *in vivo*.

MC4R and human disease

Two research groups conducted cohort screenings of the MC4R gene in individuals with obesity. Through these studies, frameshift mutations in the MC4R gene were discovered in children with early onset obesity (Vaisse, Clement, Guy-Grand, & Froguel, 1998; Yeo et al., 1998). The vast majority of MC4R deficient obese individuals have heterozygous mutations of the receptor, which further validates the notion of a MC4R gene dosage effect. Initial studies estimated a mutation prevalence of 6% in cohorts of pediatric obesity (Farooqi et al., 2003). More recent estimates place the incidence at closer to 2% in this population (Zakel et al., 2005). In the general population, the rate of MC4R mutations is 0.05% with a substantial enrichment in the obese population to about 0.5-1%. The clinical spectrum of MC4R associated obesity mirrors the syndrome in the mouse. Patients display severe hyperphagic obesity, increased linear growth, severe hyperinsulinemia, incomplete growth hormone suppression, reduced rates of obesity associated hypertension, reduced urine norepinephrine levels, increased lean mass and increased bone mineral density (Farooqi et al., 2003; I. S. Farooqi et al., 2000; Greenfield et al., 2009). Furthermore, loss of the MC4R enhances a preference for fat over sucrose in both mice (Panaro & Cone, 2013; Srisai et al., 2011) and humans (van der Klaauw et al., 2016).

The discovery of MC4R mutations in human cohorts has also furthered the understanding of MC4R receptor pharmacology. 166 MC4R mutations have been identified throughout the coding sequence of the receptor (Hinney, Volckmar, & Knoll, 2013). These mutations fall within 5 distinct classes of mutations (Figure 3). Class I

mutations include nonsense, frameshift, and missense mutations that cause an absence or reduction of protein synthesis, or are hypomorphic alleles. These mutations include the nonsense mutations Y16Stop, Y35Stop, C277Stop and Y287Stop and missense mutations R7C, I69M, M79I, S94N, D146N, & I301T. Class II mutations cause reduced surface expression largely due to defects in receptor folding and/or trafficking. Many of mutations in this class, including S58C, E61K, N62S, I69T, G98R, T162I, R165W, W174C, C271Y, and P272L, P299H, (X. H. Wang, Wang, Zhao, Yu, & Fan, 2014) remained trapped intracellularly, get polyubiquitinated and are degraded by the proteasome (Granell et al., 2012). This process appears reversible with MC4R selective receptor chaperones that act to promote receptor trafficking and indicate a need to use therapies that are mutation specific (Y.-X. Tao & Huang, 2014). Class III mutations exhibit normal expression levels by result in reduced ligand binding and include P48S, V50M, F51L, I102S, D126Y, R165Q, A175T, A219, G238D, L250Q, S295P, and D298A. Class IV mutations have normal receptor expression and ligand binding but have reduced ligand stimulated signaling or reduced basal activity. These include the obesity associated N terminal region mutations R7H, T11S/A, R18C/H/L, S30F, and D37V which have been shown to reduce basal receptor activity without altering ligand mediated signaling (S. Srinivasan et al., 2004) as well as a number of mutations that reduce E_{max}. Class V mutations are mutations with an obesity association without differences in protein expression, ligand binding or signaling. In addition to discovering obesity associated MC4R mutations, the V103I mutation (2-9% of the general population) (Heid et al., 2008) and I251L mutation (0.41-1.21% of the general

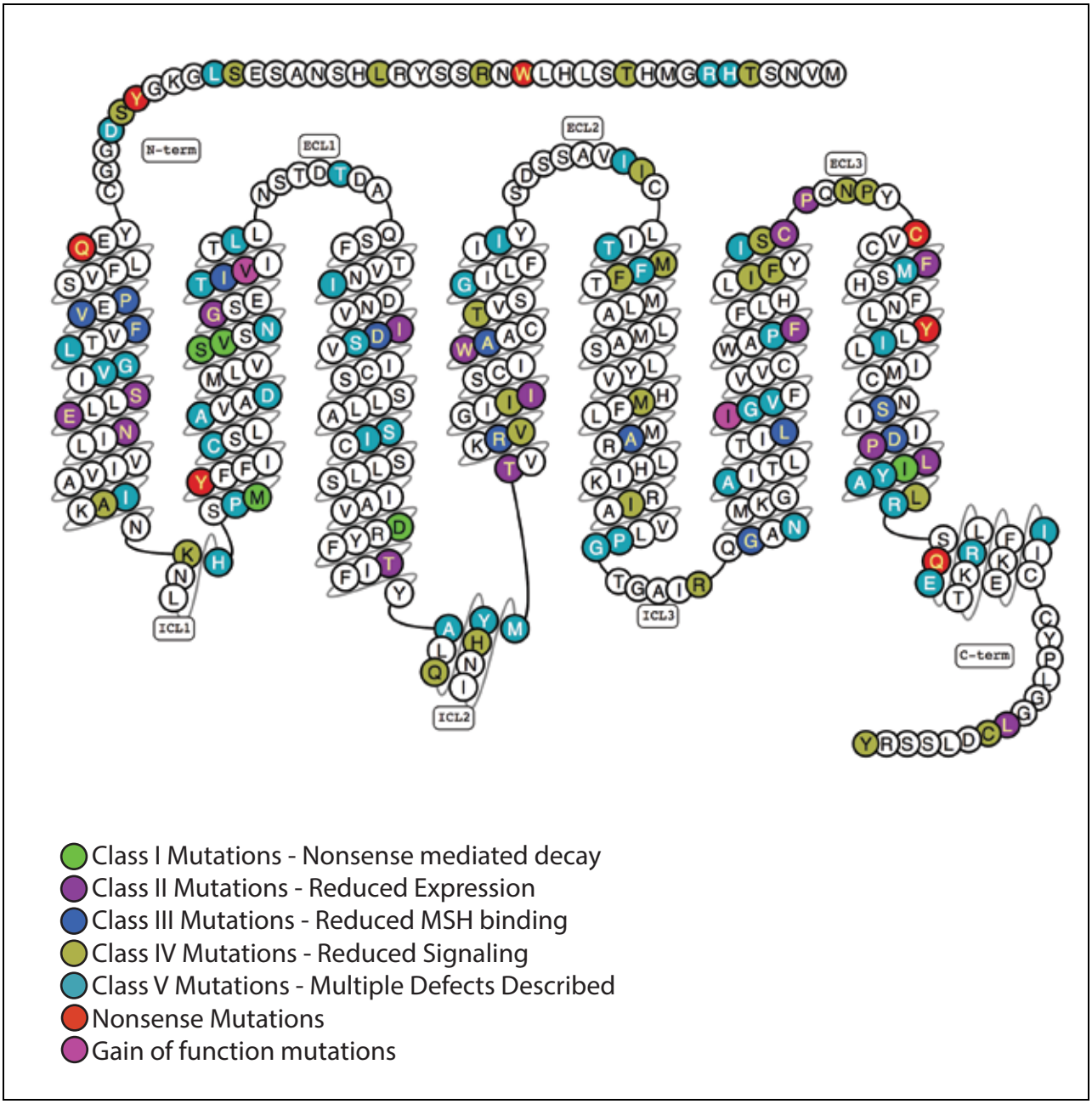

Figure 3 Human mutations of the MC4R

MC4R mutations have been found throughout the receptor and cause obesity. This includes mutations that reduce protein levels, lead to hypomorphic proteins, and reduce basal activity. Certain mutations can also increase receptor activity and are associated with a lean phenotype. Modified from (Cite reference)….

population) (Xiang, Proneth, Dirain, Litherland, & Haskell-Luevano, 2010) have increased ligand mediated receptor activity and basal receptor activity, respectively. Not surprisingly, these receptors are associated with both leanness and reduced serum triglyceride levels (D. Wang et al., 2010).

MC4R and energy expenditure

In addition to its role in regulating food intake, MC4R has been implicated in the regulation of energy expenditure. This hypothesis has been examined across multiple modalities including basal energy expenditure, adaptive thermogenesis, and sympathetic tone. An initial study using indirect calorimetry found a reduction of body weight normalized VO_2 in 8-9 week old male *Mc4r-/-* mice (Ste Marie, Miura, Marsh, Yagaloff, & Palmiter, 2000). However, this time point is after a detectable increase in adiposity (Huszar, Lynch, Fairchild-Huntress, et al., 1997). This fact is critical for the proper interpretation of the experiment as the authors correct VO_2 by dividing by the larger MC4R body weight. Furthermore, this correction assumes a linear relationship between body weight and energy expenditure that does not intersect at Y=0 implying that an organism with a mass of 0g could somehow expend energy. The authors do find that pair feeding was unable to normalize body weight in *Mc4r-/-* females. However, this was not present in males suggesting a sexual dimorphic component to MC4R regulated energy expenditure. Butler et al. (2001) reported no difference in basal VO_2 when dividing by body weight raised to the 0.75 power to correct for allometric scaling (Kleiber, 1932). Rather than dividing by body weight, the body weight-VO_2 interaction should be compared by ANCOVA as is now standard in the field (Kaiyala & Schwartz,

2011). A more recent study compared the basal VO_2 and energy expenditure in *Mc4r-/-* rats using the ANCOVA methodology found no difference in co-variation between body weight and energy expenditure (Almundarij et al., 2016). Despite no difference in basal VO_2, most studies on *Mc4r-/-* mice have found a significant increase in the respiratory exchange ratio suggesting increased glucose utilization in these animals (Almundarij et al., 2016; Butler et al., 2001).

Pharmacological studies have also been used to examine the role of MC4R tone in basal whole animal energy expenditure. Studies have found that administration of an MC4R agonists leads to an increase in basal energy expenditure in mice (Lute et al., 2014), rats (Joyce J. Hwa, Lorraine Ghibaudi, Jun Gao, & Eric M. Parker, 2001; Jonsson et al., 2001) and humans (Kong Y. Chen et al., 2015). In mice, IP administration of MTII causes a biphasic modification of energy expenditure (Lute et al., 2014). Within ten minutes of compound administration, total animal energy expenditure is suppressed while RER is increased for approximately one hour. This effect appears to be non-specific as it occurs in MC4R knockout animals. Following the initial suppression, there is then a dose dependent two-hour increase in energy expenditure and decrease in RER. This effect is mirrored by an increase in body temperature and that is due to brown fat thermogenesis. In rats, MTII administration displayed a dose dependent increase in 3 hour VO_2 in both lean and diet induced obese and lean Zucker rats (J. J. Hwa, L. Ghibaudi, J. Gao, & E. M. Parker, 2001). Furthermore, the respiratory quotient is reduced in animals injected with α-MSH indicating an increase in fat utilization. In humans, subcutaneous administration of RM-493 – an MC4R agonist that

lacks a pressor effect in primates (Kievit et al., 2013) – was able to raise resting energy expenditure by 6.4% (95%CI: 0.68-13.2) as well as lower the respiratory quotient (from 0.848 ± 0.022 to 0.833 ± 0.021)(K. Y. Chen et al., 2015). MC4R modification of whole organism VO_2 has also been shown to be bi-directional. Both acute (TOSHIOINUI, FUJINO, MEGUID, & KASUGA, 2002) and chronic (C. Small et al., 2003) ICV administration of AgRP leads to a suppression of oxygen consumption in rats (C. J. Small et al., 2003). Whether this effect is due to a reduction in basal MC4R signaling is unclear. In some reports, the neutral antagonist HS014 is unable to suppress VO_2 (Jonsson et al., 2001) while in others, HS014 lead to a reduction in energy expenditure and VO2 (Shukla et al., 2015). Thus, while the loss of MC4R plays an unclear role in basal energy expenditure, a change in MC4R signaling tone is able to modulate energy expenditure.

The underlying mechanism behind how MC4R changes energy expenditure has been examined. The degree of MC4R tone has been shown to correlate with the metabolism of several peripheral organs. Brown adipose tissue (BAT) was the first peripheral organ that MC4R was found to regulate. RFP labeled pseudorabies virus injection into the interscapular brown fat pad of MC4R-GFP mice leads to co-localization in nuclei that regulate sympathetic tone (Voss-Andreae et al., 2007). Furthermore, when *Mc4r-/-* mice were placed on high fat diet, there was no induction of the mitochondrial uncoupling protein - UCP1 – within the BAT. An independent study confirmed this finding pharmacologically and further described how MC4R regulates peripheral lipid metabolism (Nogueiras et al., 2007). ICV injection of SHU9119 led to an increase in lipid

uptake and triglyceride storage in white adipose tissue (WAT). *Mc4r-/-* mice were also found to have increased insulin sensitivity of WAT while pharmacological inhibition of MC4R decreased sympathetic nerve activity and muscle/BAT glucose utilization. While the precise mechanism for this effect remains undetermined, it is presumed to due to MC4R regulation of sympathetic tone.

MC4R and cardiovascular function

In addition to BAT, WAT and skeletal muscle metabolism, MC4R has also been shown to regulate peripheral vascular resistance. ICV, but not intravenous, injection of α-MSH has been found to increase heart rate and blood pressure. This effect is lost in *Mc4r-/-* animals and can be blocked through administration of an MC4R antagonist (Matsumura, Tsuchihashi, Abe, & Iida, 2002; Ni, Butler, Cone, & Humphreys, 2006). However, chronic administration of α-MSH eventually led to a reduction in mean arterial pressure (Hill & Dunbar, 2002) and physical activity. The acute effects of α-MSH injection on the cardiovascular system are nucleus dependent. Injection of a MC4R agonist into the PVN causes a subsequent increase in blood pressure and renal sympathetic nerve activity (Li et al., 1996). Likewise, injection of a MC4R agonist directly into the C1-T3 region of the IML was found to increase heart rate without changing blood pressure (Iwasa, Kawabe, & Sapru, 2013) and overexpression of α-MSH in the NTS also increases heart rate (Eerola et al., 2014). This increase in blood pressure and heart rate can be blunted by the addition of a combined α/β blocker thus demonstrating the role of sympathetic nervous system in this process (Kuo, Silva, & Hall, 2003). This

increase in sympathetic output contrasts with what happens when α-MSH is injected into the DMX (Li et al., 1996; Pavia, Schioth, & Morris, 2003). Injection of MTII into this region results in a rapid reduction of blood pressure and heart rate. This effect is MC4R specific as it can be blocked by SHU9119 or HS014 in a dose dependent manner. Similar to the set of energy expenditure experiments discussed above, the ability of MC4R to regulate blood pressure is bi-direction. Inhibition of the MC4R with SHU9119 or AgRP leads to hypotension and bradycardia (Humphreys, Ni, & Pearce, 2011; Tallam, Kuo, da Silva, & Hall, 2004). This effect is centrally mediated, as IV injection does not replicate this effect. Recent reports indicate that some MC4R compounds lack a cardiopressor activity in humans (K. Y. Chen et al., 2015; Royalty, Konradsen, Eskerod, Wulff, & Hansen, 2014), which opens the door for the use of MC4R agonists in the treatment of common obesity.

In addition to acutely regulating blood pressure, MC4R signaling has been shown to be a critical mediator of obesity-associated hypertension. B5lood pressure recordings of *Mc4r-/-* mice showed that they were normotensive despite being profoundly obese, hyperinsulinemic and hyperleptinemic (Tallam, da Silva, & Hall, 2006). Furthermore, the *Mc4r-/-* mice did not become hypertensive on a high salt diet (Tallam, Stec, Willis, da Silva, & Hall, 2005). This effect can be replicated pharmacologically. MC4R inhibition with SHU9119 to obese Zucker rats resulted in a greater reduction of blood pressure than lean controls (do Carmo, da Silva, Rushing, & Hall, 2012). Since both insulin (Ward, Bardgett, Wolfgang, & Stocker, 2011) and leptin (Shek, Brands, & Hall, 1998) have been shown to cause hypertension through increases in sympathetic tone, this

finding has implicated MC4R as a common mediator of this effect. This finding has since been replicated in humans as patients with heterozygous loss of the MC4R are protected from the hypertensive effects of obesity and have reduced 24 hour urinary catecholamine levels (Greenfield et al., 2009). Selective knockout studies have been informative with respect to the nucleus that regulates obesity associated increases in blood pressure. The prevention of leptin-induced hypertension in $POMC^{LepR}$ knockout mice has implicated the hypothalamus and brainstem in this process (do Carmo et al., 2011). An initial attempt was made to see if this effect was specific to the hypothalamus or autonomic neurons by re-expressing MC4R in the loxTB MC4R mouse with SIM-1-Cre as a paraventricular neuron marker (Balthasar et al., 2005) or ChAT as a general autonomic neuron marker (Rossi et al., 2011). While both SIM1-Cre; MC4R lox-$TB^{+/+}$ and ChAT-Cre; MC4R lox-$TB^{+/+}$ became similarly obese, only the ChAT-Cre; MC4R lox-$TB^{+/+}$ animals became hypertensive in response to obesity (Sohn et al., 2013). Based on these studies, it appears that the hindbrain Leptin-> NTS^{POMC} -> IML^{MC4R} pathway is essential in this process but the role of presynaptic parasympathetic MC4R neurons within DMX remains to be determined.

Cardiomyopathy Pathophysiology

In his 1628 treatise *On the Circulation of the Blood,* the physician and physiologist William Harvey refuted centuries of myths concerning the function of the heart. Rather than a seat of intelligence (Bäck, 2014) or heat source (Peltier, 2003) he declared, "The heart's one role is the transmission of the blood and its propulsion, by means of the arteries, to the extremities everywhere" (Harvey, 2006). Since this

fundamental observation, the study of heart physiology has centered on the physical processes necessary for the heart to pump oxygenated blood cells to all organs of the body.

In concert with understanding its function, the study of heart pathology has been of great interest. Indeed, heart disease is the leading cause of death in the United States (Statistics, 2016). Signs of heart disease are well characterized and understood. The sensation of fluttering — atrial fibrillation— is the consequence of an abnormal electrical conducting system (Sénac, 1777) (Lewis, 1919); the feeling of chest pain— angina — is a sign of inadequate cardiac perfusion (Heberden, 1816). Concordantly, lifesaving biomedical advances have given the clinician powerful tools with which to treat these symptoms: electrical pacemakers (Kahn, Hixson, Puffer, & Bakken, 1973), coronary angioplasty (Hurst, 1986), coronary bypass (Goetz, Rohman, Haller, Dee, & Rosenak, 1961), artificial valves (Hufnagel, Harvey, Rabil, & Mc, 1954), and a vast array of pharmacological tools. Indeed, the use of such treatments has prolonged millions of lives (National Heart, 1998). Despite these advances, much remains to be learned about the molecular underpinning of heart physiology and pathophysiology.

One disease process in particular — cardiomyopathy — remains poorly understood and extremely challenging to treat. Rather than a single disease, cardiomyopathy is a broad classification of heart tissue disease. Cardiomyopathy is classically divided into five main categories: Hypertrophic Cardiomyopathy, Dilated Cardiomyopathy, Restrictive Cardiomyopathy, Arrhythmogenic right ventricular dysplasia and Unclassified (Richardson et al., 1996). In addition to morphology,

cardiomyopathy can be defined as either primary or secondary (Maron et al., 2006). Primary cardiomyopathies can result from genetic mutations, noxious environmental stimuli, or mixed – a combination of the two. Secondary cardiomyopathies result from cardiovascular abnormalities such as hypertension, valve disorders, and ischemia. Since secondary cardiomyopathies are the result of other disease processes, debate exists as to if secondary cardiomyopathies should be classified as such. The following review of cardiomyopathy sub-types will focus on primary cardiomyopathies but will highlight the origins of a few important secondary forms.

Dilated Cardiomyopathy

Bedford and Konstam were among the first to describe dilated cardiomyopathy as a distinct disease entity (BEDFORD & KONSTAM, 1946). This form of cardiomyopathy is diagnosed echocardiographically with reduced ejection fraction of one or both cardiac ventricles and ventricular dilation. Gross post mortem analysis of dilated cardiomyopathy reveals cardiomegaly, chamber dilation, normal valves, flaccid myocardium, patchy fibrosis, endocardial thickening, and normal coronary arteries. Normal muscle fibers, nuclear pyknosis, thickened endocardium, increased smooth muscle deposition, normal small vessels and occasional necrosis or inflammation characterizes the histopathology of dilated cardiomyopathy. Ultra-structural analysis often displays mitochondrial hyperplasia with cristae distortion, loss of myofibers and increased myelin figures.

The measured prevalence of idiopathic dilated cardiomyopathy is 36 in 100,000 persons (Dec & Fuster, 1994) but this figure only includes patients with symptomatic

disease. Thus, the actual prevalence is likely higher. The cause of dilated cardiomyopathy is generally idiopathic (50%) but can also occur due to myocarditis (9%), ischemia (7%), infiltrative disease (5%), peripartum cardiomyopathy (4%), hypertension (4%), HIV (4%), substance abuse (3%), connective tissue disease (3%), or doxorubicin administration (1%) (Felker et al., 2000). Idiopathic cardiomyopathy is thought to be the result of a combination of genetic risk factors and noxious environmental stimuli. More than 25% of all dilated cardiomyopathy cases are due to genetic mutations. 90% of all disease is inherited in an autosomal dominant manner with X-linked, recessive or mitochondrial inheritance patterns being less common. Patients with dilated cardiomyopathy without conduction or skeletal muscle abnormalities are by far the most common form (Mestroni et al., 1999). Mutations in the genes encoding sarcomeric proteins (TTN, MYH7, TNNT2, etc.), cytoskeletal proteins (LDB3, ACTN2, ACTC, act.) as well as non-structural genes (ABCC9, PLN, EYA4, etc.) are implicated (Tayal, Prasad, & Cook, 2017). Patients with conduction system disease have mutations in the nuclear membrane structural protein LMNA or the sodium channel SCN5A while patients with mutations in the dystrophin gene (Xp21) display skeletal muscle manifestations.

Hypertrophic Cardiomyopathy

The first modern description of hypertrophic cardiomyopathy was made by Dr. Donald Teare (1958). He identified asymmetric septal hypertrophy and abnormal myofiber arrangement as a cause of sudden death in young adults. This hypertrophy leads to aortic outflow tract obstruction leading to death (Maron, 2005). He also

described the systolic murmur and electrocardiographic changes (T-wave inversion and pathological Q waves) that are now foundational to the diagnostic criteria. Modern echocardiography is the standard of care in confirming these findings. Echocardiography signs include characteristic septal wall thickening >13mm, systolic anterior motion of the mitral valve and outflow tract obstruction (Gersh et al., 2011). Post-mortem histopathology of HCM reveals disorganized hypertrophied myocytes with interstitial fibrosis (Shirani, Pick, Roberts, & Maron, 2000). There are additional vascular abnormalities such as decreased luminal area and reduced vasodilatory capacity. This promotes characteristic angina, as the myocardium is not adequately perfused, thereby resulting in low grade, reversible ischemia leading to myocyte death and subsequent fibrosis. Electron microscopy of HCM is characterized by loss of normal myocyte and Z-disk alignment.

When compared to DCM, the prevalence of HCM is relatively common. Estimates range from 0.2% to 0.5% of the population (Morita et al., 2006) (Semsarian, Ingles, Maron, & Maron, 2015). Similar to DCM, primary HCM is inherited in a predominantly autosomal dominant manner. Most mutations are missense or frameshift mutations in proteins that control contraction of the cardiac sarcomere. This includes the genes that encode cTnT, cTnI, MYL2, MYL3, MYH6, MYH7, MYBPC3, ACTC1, TPM1 and TTN (Ingles, Burns, Barratt, & Semsarian, 2015). In addition to contractile proteins, non-contractile proteins have been also shown to promote HCM including genes involved in RAS/MAP Kinase signaling, myogenic differentiation, glucose uptake, autophagy, and lysosome metabolism (Guertl, Noehammer, & Hoefler, 2000). While the

above pathways are known to play a role in cardiac hypertrophy, the understanding of the disease is further complicated by the fact that HCM often leads to DCM. Since many cases of HCM go undiagnosed, this further complicates an attempt to segregate each clinical entity (Maron et al., 2000). While primary forms of HCM are due to rare genetic abnormalities, secondary HCM is a common compensatory response to outflow tract obstruction such as aortic stenosis or chronic hypertension. This disease is quite common in the elderly and is characterized by a crescendo-decrescendo murmur in the upper right sternal border.

Restrictive Cardiomyopathy

Compared to HCM and DCM, idiopathic restrictive cardiomyopathy is a far less common form of cardiomyopathy (Marty, 1996). As first described by Dr. JNP Davies (Davies & Ball, 1955), the ventricles are neither dilated nor thickened. Rather, the heart is rigid thereby resulting in profound diastolic dysfunction with sparing of systolic function. The causative mechanism for this abnormality can be either primary or secondary and the histopathology for each case of RCM is dependent on the underlying etiology. Primary forms of RCM include Löffler's endocarditis– eosinophilic infiltration of heart tissue due to an unknown tropical disease – and endocardial fibroelastosis — a pathological thickening of cardiac connective tissue in babies. There are also forms of familial RCM due to mutations in sarcomeric genes. The overlap of RCM causing genes with HCM genes has led to speculation that the familial forms of both diseases lie on a continuum (W. Wu et al., 2015). Secondary forms of RCM are more common than primary forms and constitute distinct sub-classes of RCM. Etiologies include cardiac

amyloidosis, sarcoidosis, hemochromatosis, post radiation fibrosis, and diabetic cardiomyopathy. Given the increasing rates of obesity throughout the world and the correlation of diabetes with obesity, diabetic cardiomyopathy is poised to become an increasingly common disorder.

The term diabetic cardiomyopathy was first described in 1972 when four patients with type 2 diabetes died from heart failure in the absence of a known precipitating factor such as hypertension or ischemia (Rubler et al., 1972). The Framingham Heart Study found that up to 19% of all patients with heart failure displayed type two diabetes and that the risk of heart failure is increased two to eight fold in patients with type two diabetes (Jia, DeMarco, & Sowers, 2016). Patients with diabetic cardiomyopathy have either diastolic or systolic dysfunction combined with increased wall thickness and interstitial fibrosis (Isfort, Stevens, Schaffer, Jong, & Wold, 2014). The disease course begins with subtle diastolic dysfunction followed by diastolic heart failure that progresses to systolic dysfunction and reduced ejection fraction. The pathophysiology of diabetic cardiomyopathy is complex and not fully understood but the principal features of diabetic cardiomyopathy are thought to result from long standing insulin resistance which alters the metabolic network of the cells (Boudina & Abel, 2007). However, this fact is complicated by the observation that heart failure can itself promote cardiac insulin resistance (Fragasso et al., 2008).

Arrhythmogenic right ventricular dysplasia

ARVC is an inherited cardiomyopathy that is characterized by ventricular arrhythmias, dyspnea, and chest pain. Gross pathology findings include fibrous tissue

and fat deposition in the right ventricle and posterior-lateral wall. Histological features during active disease include mononuclear infiltration with myocyte necrosis that is replaced with fibrolipomatous tissue after disease progression. Electron microscopy reveals abnormalities in desmosome structure and size. The prevalence of ARVC is estimated to be 0.1% to be 0.2% of the population and is a cause of sudden death in young athletes (Gemayel, Pelliccia, & Thompson, 2001). More than 30% of all ARVC cases have a genetic basis with desmosomal genes being the primary contributor (ARVC1-9) (Mazurek & Kim, 2017).

Unclassified Cardiomyopathies

This catchall category of cardiomyopathy includes diseases such as left ventricular noncompaction, stress induced cardiomyopathy (Takotsubo), and cirrhotic cardiomyopathy. LVNC is extremely rare and is characterized by a structurally abnormal left ventricle with deep abnormal trabeculae that can cause thromboembolisms, arrhythmias, and pump failure (Elliott et al., 2008). Takotsubo or stress induced cardiomyopathy is an increasingly important clinical entity. This syndrome was first described in Japan (Dote, Sato, Tateishi, Uchida, & Ishihara, 1991) and is present in 2% patients who present with myocardial infarction like symptoms (Hachamovitch et al., 1995) (Prasad et al., 2014). A transient ballooning of the left ventricle apex, which resembles a Takotsubo – Japanese for octopus trap, characterizes the disease. This ballooning must be differentiated from that which occurs in the later stages of hypertrophic cardiomyopathy. The underlying pathogenesis is not well characterized but is thought to result from excessive catecholamines and acute vascular spasm (Wittstein

et al., 2005). Cirrhotic cardiomyopathy is poorly understood but is independent of alcohol exposure and is characterized by electrical-mechanical dyssynchrony and the inability to match cardiac output with demand (chronotropic incompetence).

Treatment of Cardiomyopathy

The treatment for cardiomyopathy is focused on reducing the pathophysiological consequences of pump failure and is dependent on the specific sub-type of cardiomyopathy. The initial treatment decision is dictated by whether or not there is symptomatic decompensation in the form of dyspnea, edema, and fatigue. The goal of therapy during acute decompensation is to retain perfusion while also reducing the cardiac workload. This involves diuresis to reduce preload as well as a vasodilatory ionotrope to reduce afterload and increase ejection fraction (Stampfer, Epstein, Beiser, & Braunwald, 1968). In patients with congestive symptoms, the diuretic of choice is a loop diuretic such as furosemide (Owen, MacAllister, & Sofat, 2015). Furosemide inhibits the luminal $Na^+/K^+/Cl^-$ co-transporter on the thick ascending limb of the loop of Henle thereby reducing water reabsorption and blood volume. This reduces the left ventricular end diastolic pressure (pre-load) on the heart as demonstrated by the Frank Starling curve. The Frank Starling curve also exemplifies the effective therapeutic window for diuretics, as excessive diuresis will lead to reduced stroke volume and lower cardiac output.

The vasodilatory ionotropes dobutamine and milrinone are used during acute decompensation to alter the shape of the Frank Starling relationship towards increased stroke volume for a given pre-load. Dobutamine is formulated as a racemic mixture with

the (+) enantiomer being a strong β_1AR (Gs) agonist, a weak β_2AR (Gs) agonist, and α_1AR (Gq11) antagonist while the (-) enantiomer is a weak α_1AR antagonist. β_1AR agonism increases myocardial cAMP levels. This promotes PKA mediated phosphorylation of L-type Ca^{2+} channels, RyR channels, and cardiac troponin leading to increased Ca^{2+} influx and ionotropy. PKA can also phosphorylate PLN leading to increased SERCA activity and a faster relaxation time (lusitropy). Milrinone, a phosphodiesterase-3 inhibitor, inhibits cAMP breakdown thereby increasing cAMP levels and PKA signaling. Dobutamine mediated β_2AR activation in the vascular smooth muscle promotes vasodilitory action via PKA mediated inhibition of myosin light chain kinase while the balance of α_1AR agonist and antagonist activity prevents Gq mediated vasoconstriction. Despite the potency of these therapies, late stage disease is terminal and necessitates the use of a ventricular assist device with eventual heart transplantation

The goal of therapy in patients with stable reduced systolic function is to maintain cardiac output while simultaneously reducing the workload of the heart to prevent long-term cardiac damage associated with chronic adrenergic stimulation. In addition to furosemide, ACE inhibitors are used to treat chronic heart failure. These drugs work by inhibiting the production of ATII which functions directly on the AT_1 receptor (Gq) to cause Ca^{2+} influx mediated vasoconstriction, thirst and kidney fluid retention. ATII also causes the release of antidiuretic hormone and aldosterone, both of which promote fluid retention. Similar to loop diuretics, ACE inhibitors cause a reduction in left ventricular end diastolic pressure through its inhibition of ATII action, while also reducing left

ventricular end systolic pressure (afterload) through the inhibition of ATII mediated vasoconstriction (Metra & Teerlink, 2017). This combined hemodynamic effect is thought to underlie the survival benefit seen in patients with heart failure (Yusuf, Pitt, Davis, Hood, & Cohn, 1992). Additional medications along the RAAS system, such as AT_1 inhibitors and aldosterone antagonists are also useful but are only used if ACE inhibitors are contraindicated.

The selective β_1AR antagonists metoprolol and bisoprolol and nonselective βAR/ α_1AR antagonist carvedilol are essential medications for the treatment of stable heart failure. Although once contraindicated in heart failure, selective βAR antagonists have beneficial effects on multiple nodes of cardiac function and have been shown to reduce all cause mortality in a dose dependent manner (Metra & Teerlink, 2017). β_1AR antagonists block the sympathetic activation seen during heart failure (Metra & Teerlink, 2017). This prevents receptor desensitization, preserves cardiac reserve, and prevents the negative remodeling associated with chronic ionotropic stimulation. β1AR antagonists also provide heart rate control, which reduces the likelihood of a fatal re-entrant arrhythmia. In addition to having β1AR antagonist activity, Carvedilol also antagonizes the α1AR. This property reduces the increase in peripheral vascular resistance (afterload) that occurs during sympathoexcitation. Since carvedilol also a nonselective βAR antagonist, this reduction in afterload further limits cardiac work and negative remodeling while the β1AR antagonist prevents reflect tachycardia.

The last line treatment of dilated cardiomyopathy is the foxglove plant derivative digitalis (Ziff & Kotecha, 2016). Digitalis inhibits the Na^+/K^+ ATPase pump, which

increases intracellular Na^+ content and intracellular Ca^{2+} content. This enables increased contractile force and improved cardiac function. While digitalis is able to provide symptom relief, there is no evidence that if can improve survival mostly due to its small therapeutic window and propensity to evoke fatal arrhythmias.

The therapeutic strategy for HCM is less well understood and is largely based on anecdotal evidence. βAR blockers are the drugs of choice as they prolong diastole and prevent outflow obstruction. Calcium channel blockers such as verapamil are also used for this purpose but they carry a risk of vasodilation, which can precipitate outflow tract obstruction. Treatment of RCM is largely dependent on treating the underlying pathophysiology. If RCM is idiopathic, treatment with β-blocker can prevent negative remodeling while the use of ACE inhibitors, loop diuretics, calcium channel blockers and digoxin can improve heart failure symptoms.

CHAPTER 2

[2]LOSS OF THE MC4R LEADS TO DILATED CARDIOMYOPATHY

Introduction

During the last 30 years, obesity has become a leading cause of morbidity and mortality (Ogden, Carroll, Kit, & Flegal, 2014 Christakis & Fowler, 2007). Health risks associated with obesity include type 2 diabetes, hypertension, and coronary artery disease. Obesity is also an independent risk factor associated with the development of heart failure (Kenchaiah et al., 2002) (Levitan, Yang, Wolk, & Mittleman, 2009). Early studies on obesity associated cardiomyopathy in mice revealed an age dependent cardiomyopathy syndrome in leptin receptor (LepRb) knockout mice (db/db) (Christoffersen et al., 2003) (Semeniuk, Kryski, & Severson, 2002) and leptin knockout (ob/ob) mice (Mazumder et al., 2004). These cardiac findings were attributed to the negative metabolic changes associated with increased adiposity. However, such conclusions are difficult to generalize because mutations in Leptin or the LepRb are extremely rare in humans (Montague et al., 1997). In order to understand how obesity correlates with the development of heart failure, recent studies have used a more clinically relevant 60% high fat diet-induced obesity (DIO) model. Reports on cardiac dysfunction in this model have been mixed. Some groups report a reduction in systolic

[2]Text and figures have been modified from Litt et al. 2017. *E. Life*

function in wild type animals while others do not (Battiprolu et al., 2012; Brainard et al., 2013; Calligaris et al., 2013; Heydemann, 2016; Raher et al., 2008; Q. Wang et al., 2017). Studies in rats have found that high fat diet does not cause cardiomyopathy (Dhahri, Drolet, Roussel, Couet, & Arsenault, 2014) and have even found that a high fat diet is protective in an ischemia reperfusion model of heart failure (Salie, Huisamen, & Lochner, 2014).

Due the uniformity of the db/db model and the variability of the DIO model with respect to heart failure, it has been hypothesized that Leptin and LepRb signaling play a fundamental role in the regulation of db/db associated heart failure (Hall, Harmancey, & Stec, 2015). Since LepRb is expressed widely throughout the body including the CNS and heart, a heart specific LepRb mouse model was created. Deletion of LepRb in myocytes was not found to alter baseline systolic function, but did cause worsened cardiac function in response to coronary ligation (McGaffin et al., 2011). Since heart specific LepRb mutations did not result in overt heart failure, CNS mediators of leptin signaling may be critical in the pathogenesis this disease. MC4R has been shown to be necessary for Leptin's pharmacological action on the autonomic nervous system (A. A. da Silva, Spradley, Granger, Hall, & do Carmo, 2015). However, the contribution of the central Leptin->POMC->MC4R axis on the development of obesity associated heart failure remains unknown.

Haploinsufficiency of the MC4R is the most common monogenetic obesity syndrome in man (Farooqi et al., 2003) and is responsible for 0.5-2.5% of all early onset morbid obesity (Stutzmann et al., 2008) making it an important consideration in

personalized obesity care. The high prevalence of the MC4R obesity syndrome is a result of its dominant inheritance pattern and the presence of dominant negative mutations (Tarnow et al., 2008)' (Biebermann et al., 2003; Y. X. Tao, 2005).

MC4R is expressed almost exclusively in the central nervous system where it plays a critical role in energy balance (Cone, 2005). MC4R expressing neurons within the hypothalamus receive orexigenic and anorexigenic signals from presynaptic neurons (Balthasar et al., 2004; Balthasar et al., 2005) and act to restore energy homeostasis by modifying both food intake (Fan et al., 1997; Huszar, Lynch, FairchildHuntress, et al., 1997) and energy expenditure (Ste Marie et al., 2000). A reduction of MC4R signaling, through either genetic or pharmacological means, results in hyperphagia, bradycardia (Alexandre A. da Silva et al., 2008), and reduced blood pressure. Clinical studies have found that MC4R mutations confer protection from obesity-associated hypertension through a reduction in sympathetic tone (Sweeney, 2010)' (Greenfield et al., 2009) (Sayk et al., 2010). However, *Mc4r-/-* mice and humans experience hyperinsulinemia that exceeds their degree of adiposity due to the role MC4R in the suppression of insulin release (Fan et al., 2000) (Mansour et al., 2010). Furthermore, MC4R haploinsufficient patients have blunted suppression of growth hormone secretion when compared to weight matched obese controls (Martinelli et al., 2011). Thus, the effects of MC4R on heart health are ambiguous. Deletion is protective with respect to reduced peripheral vascular resistance, but other aspects of the MC4R syndrome, such as hyperinsulinemia, incomplete growth hormone suppression, and altered autonomic tone are potentially cardiotoxic. Therefore, we chose to follow a

cohort of *Mc4r-/-* mice and their *Mc4r+/-* and WT siblings for signs of altered cardiac function.

Results

Cardiac Function in Male Heterozygous, and Homozygous MC4R knockout Mice

In order to characterize the effects of MC4R on heart function, age-matched male *Mc4r-/-* , *Mc4r+/-* and WT mice were serially assessed using echocardiography at 16 weeks, 20 weeks, 26 weeks and 30 weeks of age. An age dependent dilated cardiomyopathy phenotype was observed in male *Mc4r-/-* animals (Figure 4A-B), at the 26 and 30-week time points. A significant reduction in fractional shortening (FS)(Equation 1), a measure of myocardial contractility (Figure 4C) was observed in *Mc4r-/-* mice when compared to WT and *Mc4r+/-* sibling controls, indicating depressed systolic function (Two way ANOVA Sidak's multiple comparisons test, 26 weeks adjusted p=0.018 & 30 weeks adjusted p=0.010, n=5-6). This difference also was present when contractility was estimated using the ejection fraction calculation (Equation 3) (Two way ANOVA Sidak's multiple comparisons test, 26 weeks adjusted p=0.030 & 30 weeks adjusted p=0.014, n=5-6) (Figure 4D). A significant increase in left ventricular diameter (LVIDd) was also present in male MC4R -/- mice at 26 and 30 weeks of age (Two way ANOVA Sidak's multiple comparisons test, 26 weeks adjusted p=0.017 & 30 weeks adjusted p=0.013, n=5-6) (Figure 4E). This change is most likely a compensatory response to reduced contractility. As has been shown previously (Stepp, Osakwe, Belin de Chantemele, & Mintz, 2013), a reduction in heart rate was also

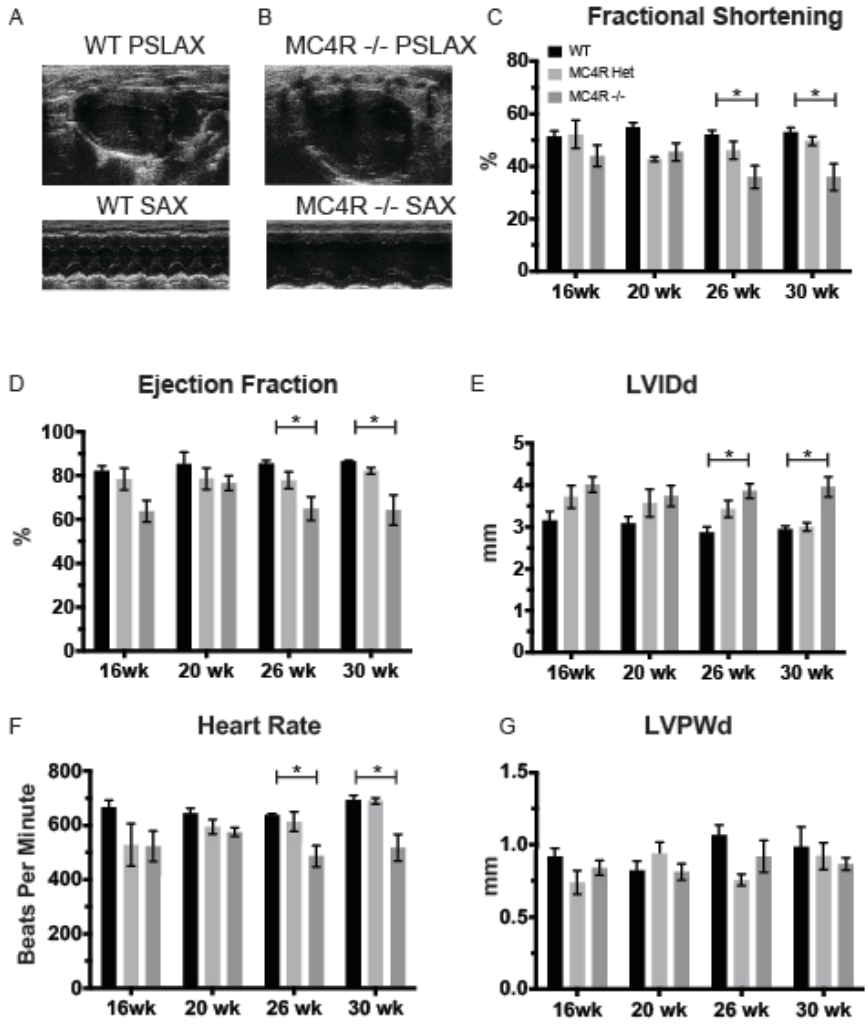

Figure 4 MC4R deletion causes cardiac dilatation and reduced contractility

A) Representative B-mode Parasternal long axis (PSLAX) image at diastole (top) and M-mode short axis (SAX) image of male WT C57B6/J mouse at 26 weeks of age. **B)** Representative B-mode PSLAX image at diastole (top) and M-mode SAX image of male *Mc4r-/-* mouse 26 weeks of age. **C)** Fractional Shortening (FS) of male WT, MC4R-/+, and *Mc4r-/-* mice at 16, 20, 26 and 30 weeks of age. (2-way ANOVA Sidak multiple comparison test, $p<0.05$, n=5-6) **D)** Ejection Fraction (2-way ANOVA Sidak multiple comparison test, $p<0.05$, n=5-6) **E)** Left ventricular internal dimension during diastole (LVIDd) (2-way ANOVA Sidak multiple comparison test, $p<0.05$, n=5-6) **F)** Heart Rate (2-way ANOVA Sidak multiple comparison test, $p<0.05$, n=5-6) **G)** Left ventricle posterior wall thickness during diastole (LVPWd) (2-way ANOVA Sidak multiple comparison test, $p>0.05$, n=5-6)

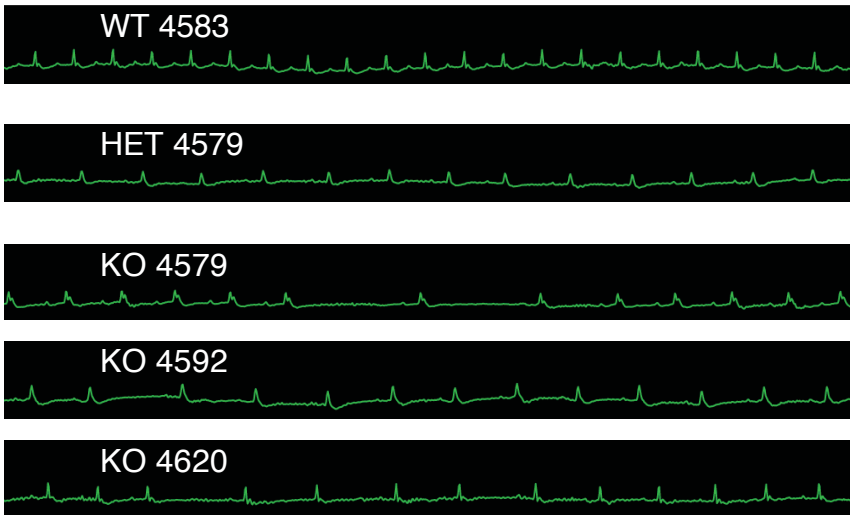

Figure 5 *Mc4r-/-* animals display bradycardic arrhythmias.

Rhythm strips of 30-week-old WT, *Mc4r+/-* and *Mc4r-/-* animals taken during echocardiograms. *Mc4r-/-* mice display sinus bradycardia with abnormal rhythmicity.

observed in the *Mc4r-/-* mice at later time points (Two way ANOVA Sidak's multiple comparisons test, 26 weeks adjusted p=0.018 & 30 weeks adjusted p=0.011, n=5-6) (Figure 4F). Analysis of heart wall thickness (LVPWd) did not reveal any difference by time of genotype indicating the absence of pathological hypertrophy or atrophy (Two way ANOVA, p=0.224, n=5-6) (Figure 4G). This symptomology was further characterized by bradycardic arrhythmias at the 30-week time point (Figure 5).

Cardiovascular Function in female Mc4r+/- mice

Based on these findings in male mice, we next examined female *Mc4r-/-* mice at 26 years of age with echocardiography. *Mc4r-/-* female mice displayed a similar phenotype to their male counterparts at 26 weeks (Figure 6A-B). This included a reduction of FS in *Mc4r-/-* mice when compared to their WT siblings (WT: 53.72±2.24% vs. *Mc4r-/-* : 62.49±7.19%; Unpaired Two-tailed t test; p< 0.0001) (Figure 6C). There was also a reduction in estimated EF (WT: 85.69±1.89% vs. *Mc4r-/-* : 33.74±5.17%; Unpaired Two-tailed t test; p= 0.0001) (Figure 6D). Similar to their male siblings, female *Mc4r-/-* mice have displayed and increase in LVIDd dimension at the 26-week time point (WT: 2.93±0.26mm vs. *Mc4r-/-* : 4.25±0.18mm; Unpaired Two-tailed t test; p< 0.0001) (Figure 6E). Female *Mc4r-/-* mice also displayed a reduction in heart rate (Figure 6F) when compared to WT siblings (WT: 689.±26 bpm vs. *Mc4r-/-* : 474±70 bpm; Unpaired Two-tailed t test; p= 0.0002). However, there was no significant reduction in LVPWd at 26 weeks when comparing between genotypes siblings (WT: 1.027±0.188 bpm vs. *Mc4r-/-* : 0.8124±0.1999 bpm; Unpaired Two-tailed t test; p= 0.1185) (Figure 6G).

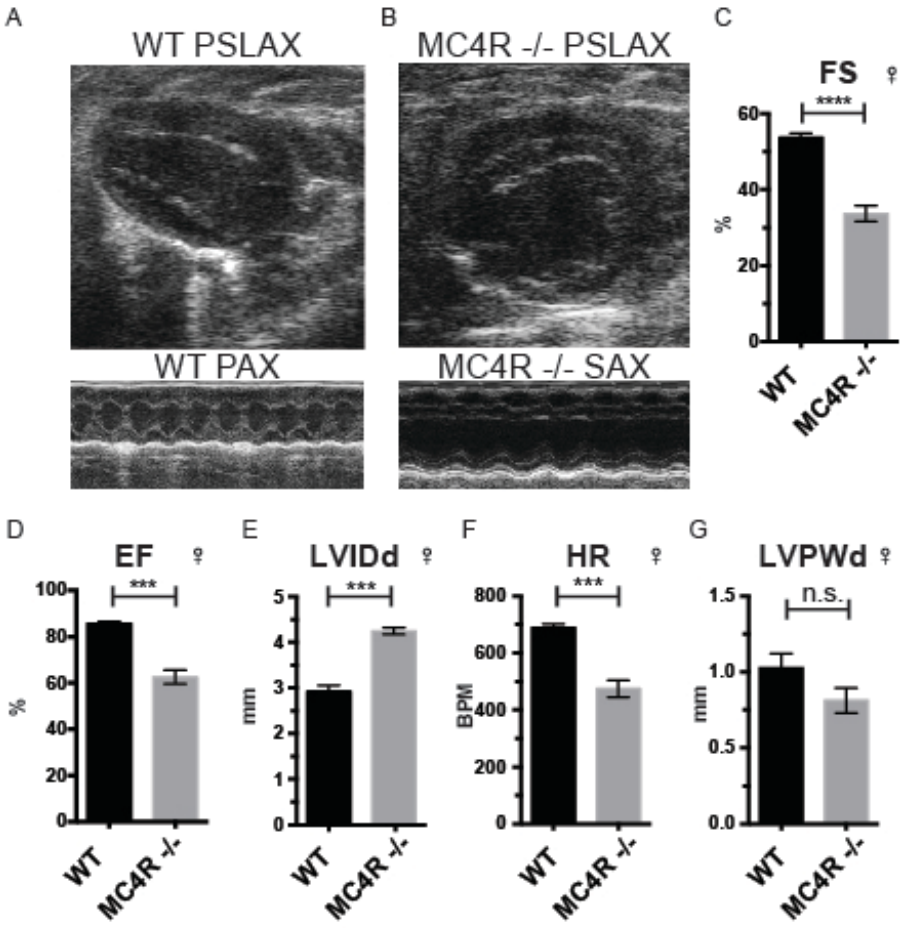

Figure 6 Female MC4R knockout mice display reduced contractility, cardiac dilatation and bradycardia at 26 weeks of age.

A) Representative B-mode PSLAX image at diastole (top) and M-mode SAX image of female WT C57B6/J mouse at 26 weeks of age. **B)** Representative B-mode PSLAX image at diastole (top) and M-mode SAX image of female *Mc4r-/-* C57B6/J mouse 26 weeks of age. **C)** Fractional shortening of female WT and *Mc4r-/-* mice at 26 weeks. (Students t-test $p<0.0001$, n=5) **D)** Ejection fraction of female WT and *Mc4r-/-* mice at 26 weeks. (Students t-test $p<0.001$, n=5) **E)** LVIDd (Students t-test $p<0.0001$, n=5) **F)** HR (Students t-test $p<0.001$, n=5-6) **G)** LVPWd (Students t-test $p=0.1185$, n=5)

Cardiovascular function of MC4R-loxTB$^{+/+}$ mice

Given these observations in male and female mice, we next sought to determine if the cardiac deficits seen in *Mc4r-/-* mice was specific to the loss of MC4R and not due to an anomalous background mutation. In order to accomplish this, the loxTB-MC4R mouse, a distinct MC4R knockout model, was then examined by echocardiography (Balthasar et al., 2005). LoxTB-MC4R knockout animals displayed similar signs of myocardial dysfunction (Figure 7A-B). Findings in the MC4R-loxTB mice included a reduced FS and estimated EF when compared to sibling controls (loxTB-/-: 55.09± 2.78 % vs. loxTB+/+: 38.68± 11.11 %; Unpaired Two-tailed t test; p= 0.0272 & loxTB-/-: 86.11± 2.20 % vs. loxTB+/+: 68.06±13.14 %; Unpaired Two-tailed t test; p= 0.0357) (Figure 7C-D). While *Mc4r-/-* mice had a significant cardiac dilatation at 26 weeks, MC4R-loxTB mice displayed a trend towards increased LVIDd that did not reach statistical significance (loxTB-/-: 3.40± 0.02 mm vs. loxTB+/+: 4.02± 0.66 mm; Unpaired Two-tailed t test; p= 0.1044)(Figure 7E). MC4R-loxTB mice also had a significantly reduced heart rate when compared to controls (loxTB-/-: 629±55 bpm vs. loxTB+/+: 492± 98 bpm; Unpaired Two-tailed t test; p= 0.0455) (Figure 7F) and displayed no signs of heart wall thickness changes (loxTB-/-: 0.94±0.07 mm vs. loxTB+/+: 0.89± 0.27 mm; Unpaired Two-tailed t test; p= 0.664) (Figure 7G). Together with findings from male and female *Mc4r-/-* mice, these results demonstrate that MC4R deletion leads to a progressive cardiomyopathy.

Comparison of Mc4r+/- heart function to weight matched controls

It is plausible that certain effects of the *Mc4r-/-* cardiomyopathy are due to the

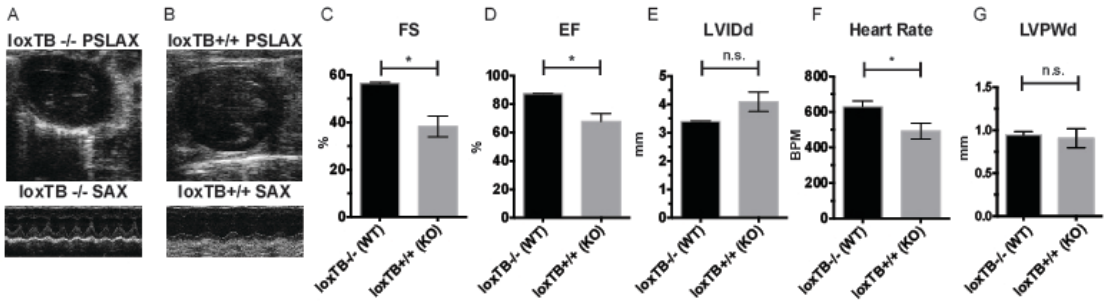

Figure 7 MC4R-loxTB animals phenocopy the reduced cardiac function seen in *Mc4r-/-* mice

A) Representative B-mode PSLAX image at diastole (top) and M-mode SAX image of male MC4R loxTB -/- (WT) mouse at 35 weeks of age. **B)** Representative B-mode PSLAX image at diastole (top) and M-mode SAX image of male MC4R loxTB +/+ (*Mc4r-/-*) mouse 35 weeks of age. **C)** Fractional Shortening (FS) of male MC4R loxTB -/- and MC4R loxTB +/+ mice at 35 weeks. (Student's t-test, $p<0.05$, n=5) **D)** Ejection Fraction (Student's t-test, $p<0.05$, n=5) **E)** Left ventricular internal dimension; diastole (LVIDd) (Student's t-test, $p=0.1044$, n=5) **F)** Heart Rate (Student's t-test, $p<0.05$, n=5) **G)** Left ventricle posterior wall thickness; diastole (Student's t-test, $p>0.05$, n=5)

metabolic consequences of obesity such as insulin resistance, hyperglycemia, and hypertriglyceridemia. Both pre-clinical and epidemiological data support a contributory role of hyperglycemia and insulin resistance in the development heart failure (Bugger & Abel, 2014). However, investigators have observed variable degrees of cardiomyopathy in mouse models of diet-induced obesity by using a high fat diet (DIO)(Battiprolu et al., 2012; Brainard et al., 2013; Calligaris et al., 2013; Heydemann, 2016; Raher et al., 2008; Q. Wang et al., 2017). In order to address the possibility that this phenotype is simply due to adiposity, a cohort of age DIO control mice was generated and evaluated by echocardiography. Male, age matched C57BL/6J wild type mice were placed on a 60% HFD for 35 weeks until they reached the same body weight as the *Mc4r-/-* animals (Figure 8A). Despite their similar body weights, DIO animals and *Mc4r-/-* animals had distinct body compositions, as previously described (Braun et al., 2012). When compared to DIO mice, *Mc4r-/-* mice accumulate more lean mass (Figure 8B-C) while DIO animals preferentially accumulate fat mass (Figure 8D-E). In spite of these differences in body composition, *Mc4r-/-* and DIO animals displayed similar characteristics with respect to glucose tolerance and insulin signaling. When dosed by lean mass, *Mc4r-/-* mice and DIO mice displayed similarly poor glucose tolerance when compared to WT mice as evidenced by an increase in blood glucose at the 60 minute time point (Figure 9A) and in the area under the curve (Figure 9B). Furthermore, *Mc4r-/-* and DIO mice displayed similar increases in heart and liver phospho-AKT T-308 in response to an insulin bolus following a 4 hour fast. Thus, at this age, *Mc4r-/-* mice and DIO mice have distinct body mass, but similar degrees of glucose intolerance and

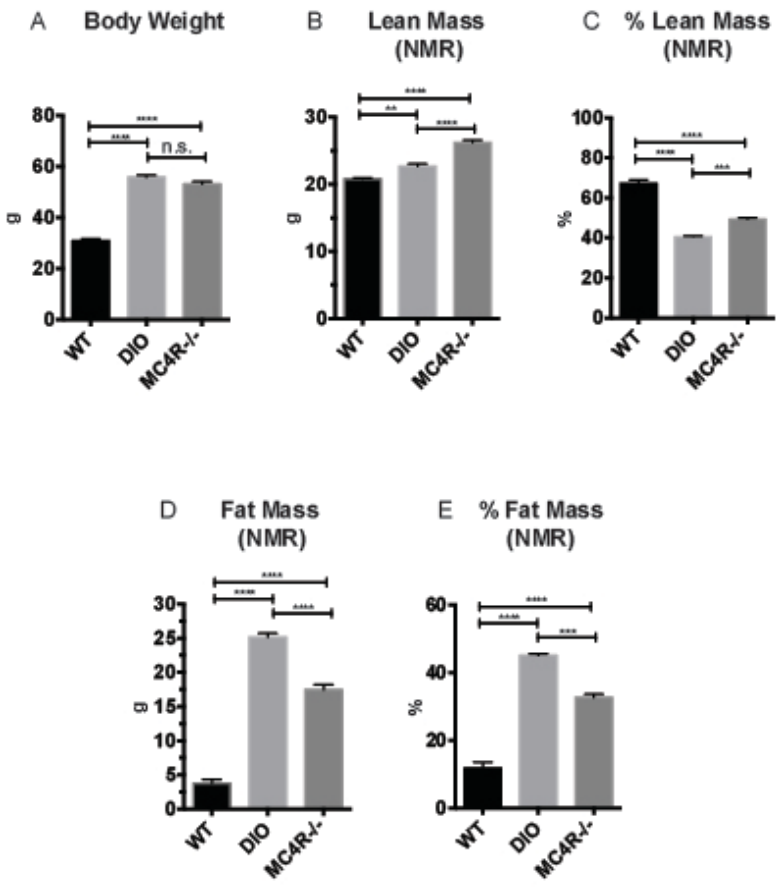

Figure 8 Differences in Body Composition between *Mc4r-/-* obesity and diet induced obesity

A) Body weights of age matched WT, diet induced obese (DIO), and *Mc4r-/-* mice. (1-way ANOVA Sidak multiple comparison test, $p<0.0001$, n=5) **B)** Lean mass of WT, DIO and *Mc4r-/-* mice by NMR (1-way ANOVA Sidak multiple comparison, $p<0.01$, n=5) **C)** Percent Lean Mass comparison of WT, DIO and *Mc4r-/-* mice (1-way ANOVA Sidak multiple comparison, $p<0.001$, n=5) **D)** Fat mass by NMR (1-way ANOVA Sidak multiple comparison, $p<0.0001$, n=5) **E)** Percent Fat Mass (1-way ANOVA Sidak multiple comparison, $p<0.0001$, n=5).

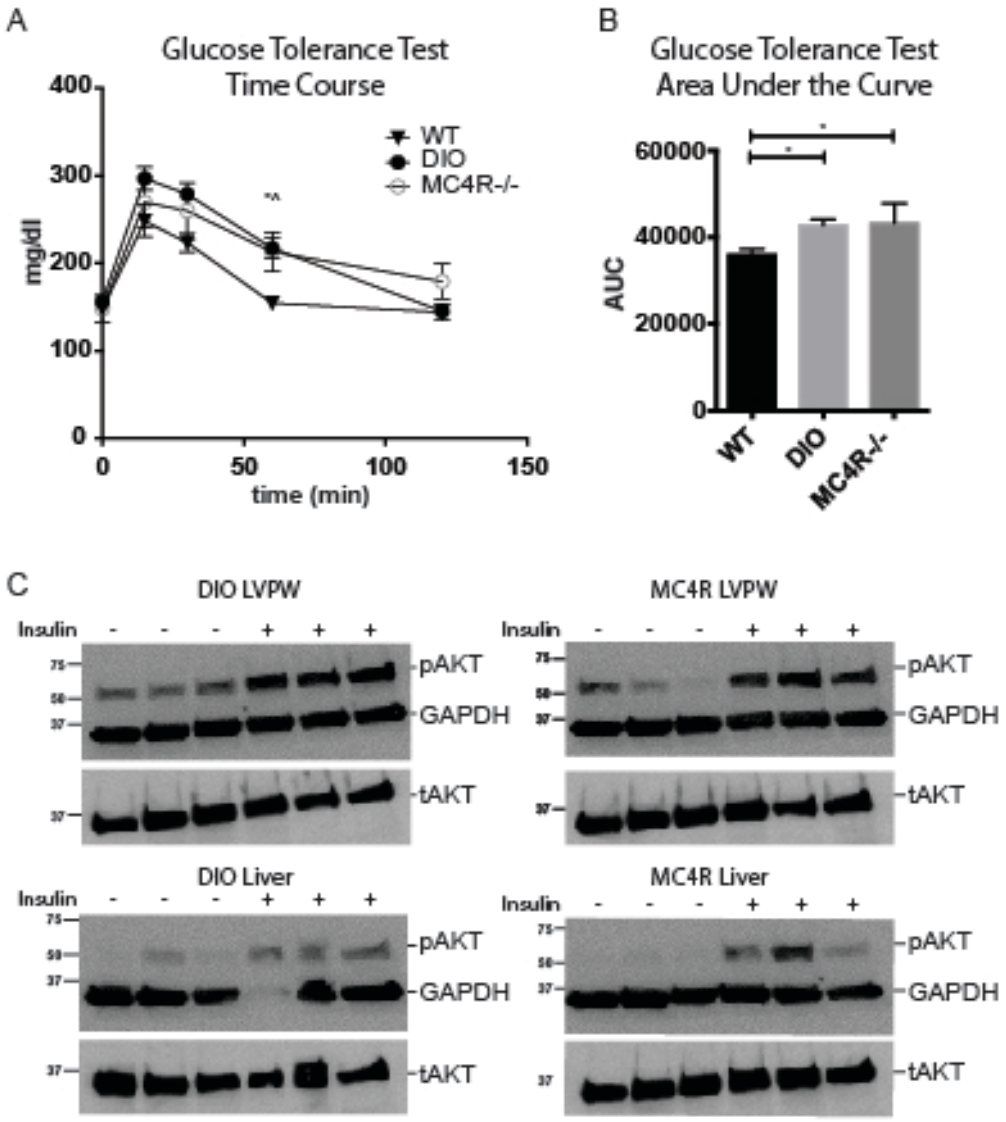

Figure 9 MC4R -/- and DIO mice are indistinguishable with respect to glucose tolerance and insulin sensitivity

A) Glucose tolerance test time course. 2mg glucose per kg lean mass (2-way ANOVA Sidak multiple comparison test, $p<0.05$, n=5) **B)** Area under the curve of glucose tolerance test (Dunn's multiple comparison test, $p<0.05$, n=5) **C)** pAkt T-308 in LVPW and Liver of *Mc4r-/-* and DIO LVPW and Liver tissue samples following the injection of saline or 1U/kg insulin.

insulin sensitivity.

When examined by echocardiography, *Mc4r-/-* animals exhibited reduced cardiac contractility compared to their DIO and WT controls (Figure 10A-B). MC4R knockouts had significantly lower FS (One Way ANOVA Sidak's multiple comparison's test, adjusted p=0.0097, n=5)(Figure 10C) and EF (One Way ANOVA Sidak's multiple comparison's test, adjusted p=0.014, n=5) (Figure 10D) when compared to their DIO and WT controls. Similar the previous results, *Mc4r-/-* mice had a significantly higher LVIDd (One Way ANOVA Sidak's multiple comparison's test, adjusted p=0.0092, n=5) (Figure 10E) when compared to both WT and DIO controls. A trend towards increased LVPWd was observed in DIO animals when compared to lean WT and *Mc4r-/-* mice but this did not reach statistical significance (One Way ANOVA Sidak's multiple comparison's test, adjusted p=0.069, n=5) (Figure 10F). In this cohort, *Mc4r-/-* males also displayed a trend towards a reduction in HR when compared to the DIOs (One Way ANOVA Sidak's multiple comparison's test, adjusted p=0.306 7, n=5) (Figure 10A-B) however this difference did not reach statistical significance. Together, these data demonstrate *Mc4r-/-* cardiomyopathy is independent of body weight.

Expression profile of MC4R

MC4R is primarily expressed in the central and peripheral nervous system and with no MC4R expression reported in mouse myocardium (Gantz, Miwa, et al., 1993). In order to validate this, qRT-PCR was used to characterize the expression pattern of MC4R. Similar to previous studies, a nearly 250-fold enrichment of MC4R mRNA was observed in WT hypothalamus and brain stem as compared to *Mc4r-/-* tissue (Unpaired

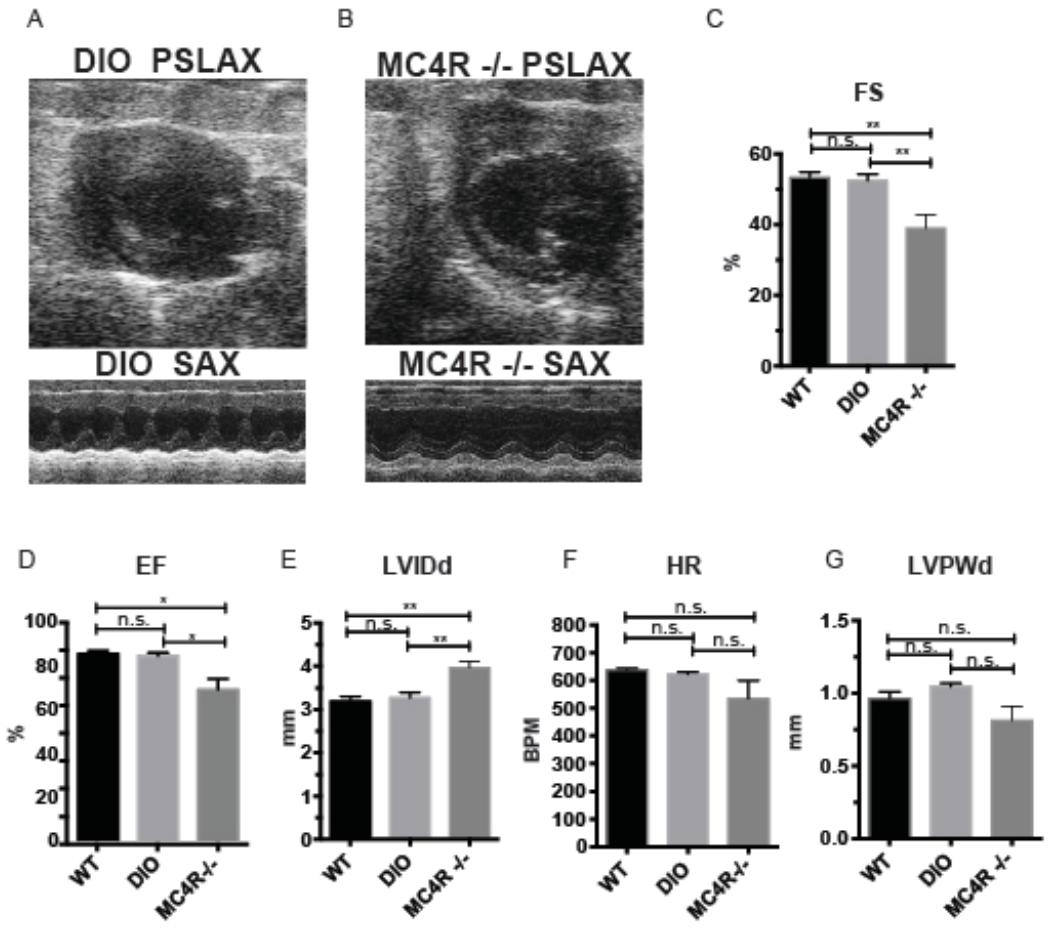

Figure 10 Age and weight matched wild type animals fed a high fat diet do not phenocopy the MC4R-cardiomyopathy.

A) Representative B-mode PSLAX image at diastole (top) and M-mode SAX image of male DIO mice at 30 weeks of age. **B)** Representative B-mode PSLAX image at diastole (top) and M-mode SAX image of male *Mc4r-/-* mouse 30 weeks of age. **C)** Fractional Shortening of WT, DIO and *Mc4r-/-* mice (1-way ANOVA Sidak multiple comparison, $p<0.01$, n=5) **D)** Ejection Fraction of WT, DIO and *Mc4r-/-* mice (1-way ANOVA Sidak multiple comparison, $p<0.05$, n=5) **L)** LVIDd (1-way ANOVA Sidak multiple comparison, $p<0.01$, n=5) **E)** HR (1-way ANOVA Sidak multiple comparison, $p>0.05$, n=5) **F)** LVPWd (1-way ANOVA Sidak multiple comparison, $p>0.05$, n=5).

t test, p=0.0001, n=6) (Figure 11A). However, no fold change in MC4R mRNA in the left ventricle between WT and *Mc4r-/-* (1±0.169, n=6) (Figure 11B) was observed. Furthermore, we did not detect myocardial GFP expression in MC4R-Sapp animals (H. Liu et al., 2003) in either the atrial or ventricular tissue (Figure 11C). Based on these results, loss of MC4R appears to cause cardiomyopathy through an indirect mechanism.

We next examined mice that lack the expression of POMC within the ARC but retained POMC expression in the pituitary and hindbrain. There experiments were conducted as part of a collaboration with Malcolm Low at the University of Michigan. Due to the animal protocol specifications at the University of Michigan Cardiology Core, inhaled isoflurane anesthesia was required during echocardiography. Since isoflurane is a dose dependent cardiac depressant, raw values for this study are lower for contractility and heart rate, but higher for chamber size measurements. Using 52-week-old $ARC^{POMC\text{-}KO}$ mice and their WT siblings, we found them to be significantly more obese as has been previously described ($ARC^{POMC\text{-}WT}$ 30.0±1.5 g vs. $ARC^{POMC\text{-}KO}$: 63.1±7.4 g, Unpaired Two-tailed t test; $p< 0.0001$) (Figure 12A) (Lam et al., 2015). Under these conditions, $ARC^{POMC\text{-}KO}$ and their WT siblings displayed no difference in FS ($ARC^{POMC\text{-}WT}$ 27.37± 3.09 % vs. $ARC^{POMC\text{-}KO}$: 29.9± 4.27 %, Unpaired Two-tailed t test; p=0.2282) (Figure 12B) LVIDd, ($ARC^{POMC\text{-}WT}$ 4.04±0.27 mm vs. $ARC^{POMC\text{-}KO}$: 3.76± 0.53 mm, Unpaired Two-tailed t test; p=0.2535) (Figure 12C) or LVPWd ($ARC^{POMC\text{-}WT}$ 0.80±0.09 mm vs. $ARC^{POMC\text{-}KO}$: 0.90±0.11 mm, Unpaired 2 tailed t test; p=0.0980) (Figure 12D). However, there was a significant increase in the HR of $ARC^{POMC\text{-}KO}$ mice as compared to controls ($ARC^{POMC\text{-}WT}$ 483±48 bpm vs. $ARC^{POMC\text{-}KO}$: 530±37 bpm,

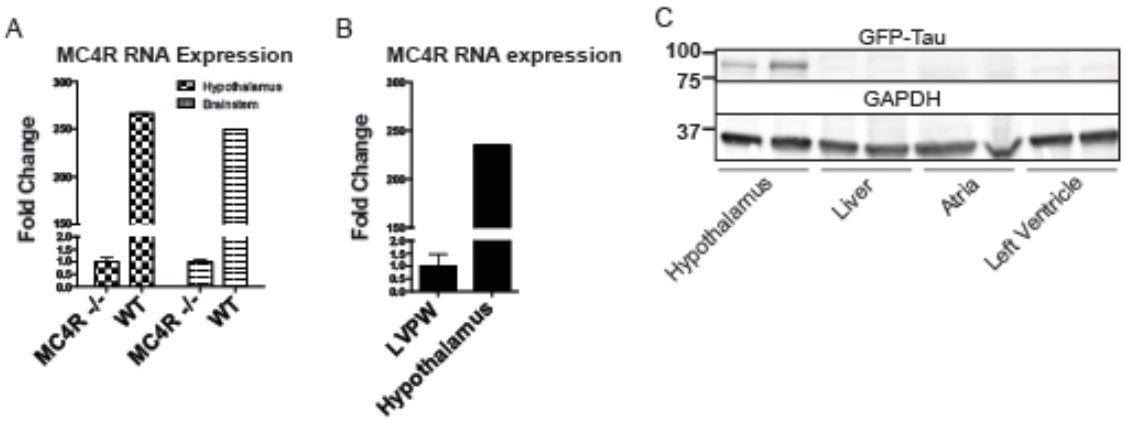

Figure 11 MC4R is not expressed in adult heart tissue.

A) qRT-PCR comparison of MC4R expression in heart and hypothalamus using the ΔΔCT method. (Student's t-test, $p<0.0001$, n=6) **B)** qRT-PCR comparison of MC4R expression in the hypothalamus and brainstem between *Mc4r-/-* and WT tissue demonstrating dynamic range of qRT-PCR primers (Student's t-test, $p<0.0001$, n=6). **C)** Representative western blot of MC4R-Tau-Sapp hypothalamic, hepatic, atrial and ventricular lysates.

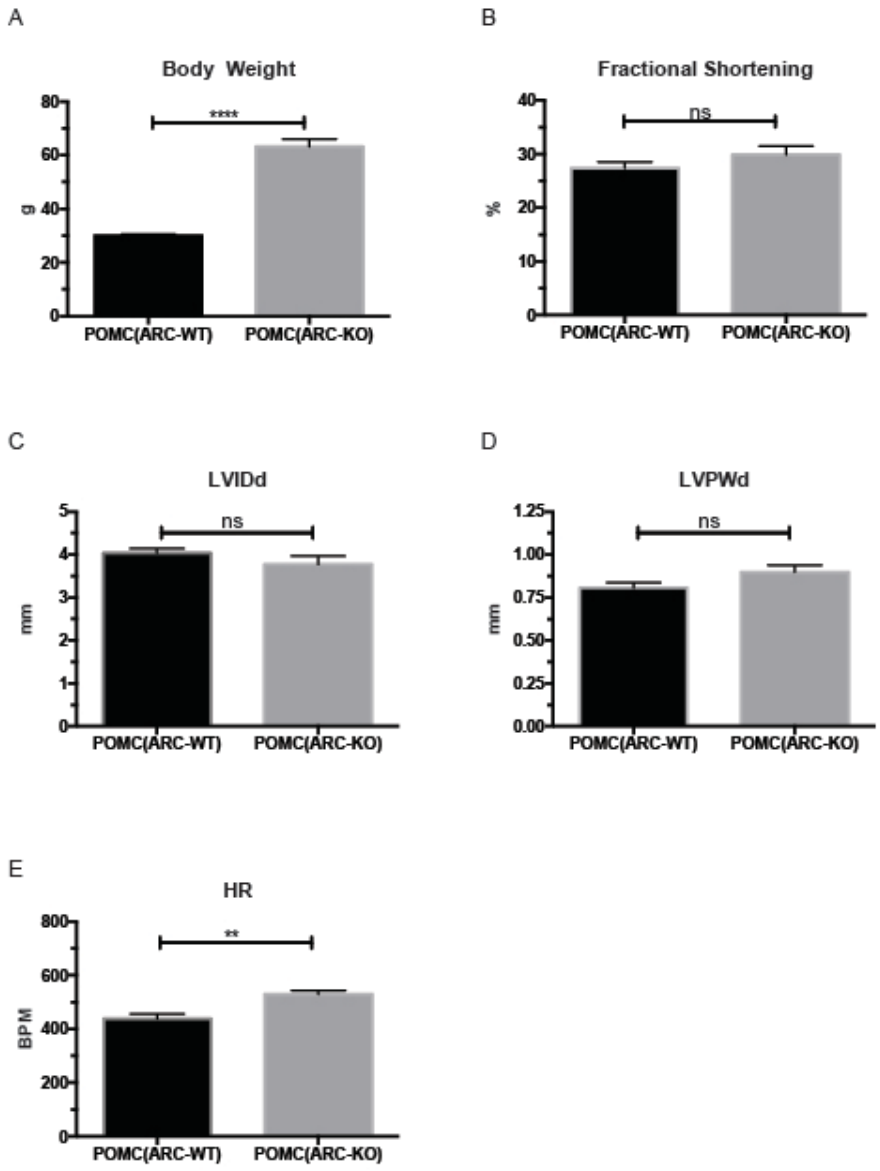

Figure 12 POMC Mice are morbidly obese but appear to have normal cardiac function.

A) Body weights of 52 week old POMC$^{ARC\text{-}KO}$ mice and their WT siblings (unpaired t-test; $p<0.0001$; n=7) **B)** Fractional shortening of POMC$^{ARC\text{-}KO}$ mice and their WT siblings (unpaired t-test; $p>0.05$; n=7) **C)** LVIDd of POMC$^{ARC\text{-}KO}$ mice and their WT siblings (unpaired t-test; $p>0.05$; n=7) **D)** LVPWd of POMC$^{ARC\text{-}KO}$ mice and their WT siblings (unpaired t-test; $p>0.05$; n=7) **E)** Heart rate of POMC$^{ARC\text{-}KO}$ mice and their WT siblings (unpaired t-test; $p<0.01$; n=7)

Unpaired 2 tailed t test; p=0.0019) (Figure 12E). The result to this particular experiment is difficult to interpret. While reduced MC4R signaling within the hypothalamus is correlated with both obesity and reduced heart rate, the observed heart rate data contradicts this fact. Based on this result, it is possible that the $ARC^{POMC\text{-}KO}$ mice were exposed to lower levels of anesthesia (due to a larger biodistribution) and hence were not experiencing the same degree of cardiac depression.

Effect of MC4R Deletion on Myocardial structure

In light of the worse cardiovascular function in MC4R -/- animals, our attention turned towards understanding the cellular basis for the observed pathology. First, *Mc4r-/-* myocardium was examined histologically to determine if the tissue displayed canonical signs of heart failure such as interstitial fibrosis or lipid deposition (Boudina & Abel, 2007). *Mc4r-/-* hearts appeared grossly larger (Figure 13A) and displayed a significantly higher wet weight when compared to WT controls at 30 weeks of age (WT: 142.26±13.56 mg, n=5 vs. MC4R -/-: 184.78±16.08 mg, n=5; Sidak's multiple comparisons test; adjusted p=0.0016) but not at 6 (WT: 105.73±19.44 mg, n=4 vs. MC4R -/-: 110.4±5.13 mg, n=4; Sidak's multiple comparisons test; adjusted p=0.9734) or 12 weeks (WT: 141.14±21.25 mg, n=7 vs. MC4R -/-: 160.57±17.70 mg, n=7; Sidak's multiple comparisons test; adjusted p=0.123) (Figure 13B). This effect is independent of the obesity syndrome as *Mc4r-/-* mice have heavier hearts the DIO mice at 40 weeks of age (DIO: 167.1±9.8 mg, n=5 vs. MC4R -/-: 203.4±18.0 mg, n=5; Unpaired 2 tailed t test; p=0.0007) (Figure 13C). However, there was no difference in the heart weight to lean body weight (HW/LBM) ratio when WT mice are compared to *Mc4r-/-* (WT:

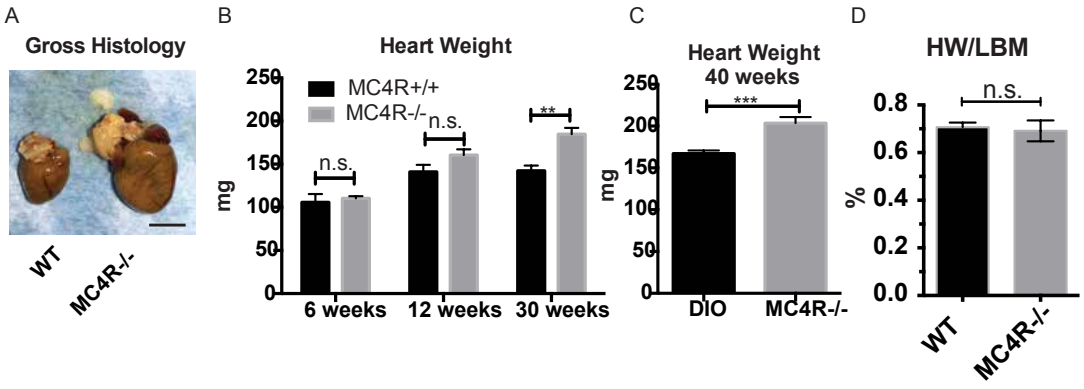

Figure 13 Gross Pathology of *Mc4r-/-* hearts

A) Representative gross pathology of WT and *Mc4r-/-* hearts **B)** Heart wet weight of 6 week old, 12 week old and 30 week old WT and *Mc4r-/-* animals (Two Way ANOVA $p<0.05$, n=4-7). **C)** Heart wet weight of 40-week-old *Mc4r-/-* and DIO animals. (Unpaired 2 tailed t test; $p<0.001$, n=7-8). **D)** Heart weight to lean mass in lean WT mice as compared to *Mc4r-/-* mice (Unpaired 2 tailed t test; $p>0.05$, n=5).

0.00706±0.00044 %, n=5 vs. *Mc4r-/-* : 0.00691±0.000985 %, n=5; Unpaired 2 tailed t test; p=0.7614). (Figure 13D) due to the generalized increase in lean mass seen in *Mc4r-/-* mice. Histological analysis with H&E of *Mc4r-/-* tissue was unremarkable and did not reveal signs of an overt pathological insult such as anoxia, inflammatory infiltration or fibrosis (Figure 14A). Similarly, lipid deposition was not observed by Oil Red O staining (Figure 14B). Furthermore, myocyte size was not altered in *Mc4r-/-* mice (WT: 280.1±88.24 μm^2 vs. *Mc4r-/-* : 274.6±87.77 μm^2, unpaired t-test, p=0.94, n=3 mice x 3 sections x 14 cells/section)(Figure 14C). However, transmission electron microscopy (TEM) showed ultrastructural signs of heart failure. TEM imaging of myocardium in MC4R -/- mice revealed mitochondrial pleomorphy and cardiomyocyte dropout (Figure 15A-B) both of which are cardinal signs of heart failure (Mudhar, Wagner, & Suvarna, 2001).

Summary and Conclusions

In this chapter, an age dependent cardiomyopathy is described in mice that have homozygous loss of function of the MC4R. In this mouse model of obesity, we observed a progressive decline in contractility as well as an increase in cardiac chamber size starting at 26 weeks of age (Figure 4). This age dependent decline in systolic function is paralleled by an increase in total heart weight (Figure 13). This reduction in cardiac function is phenotype is present regardless of animal sex or knockout strategy as we observed a reduction of systolic function in *Mc4r-/-* females (Figure 6) and male MC4R-loxTB mice (Figure 7). The reduction in systolic function was absent in body weight matched, DIO mice as compared to *Mc4r-/-* mice at 35 weeks of age (Figure 10).

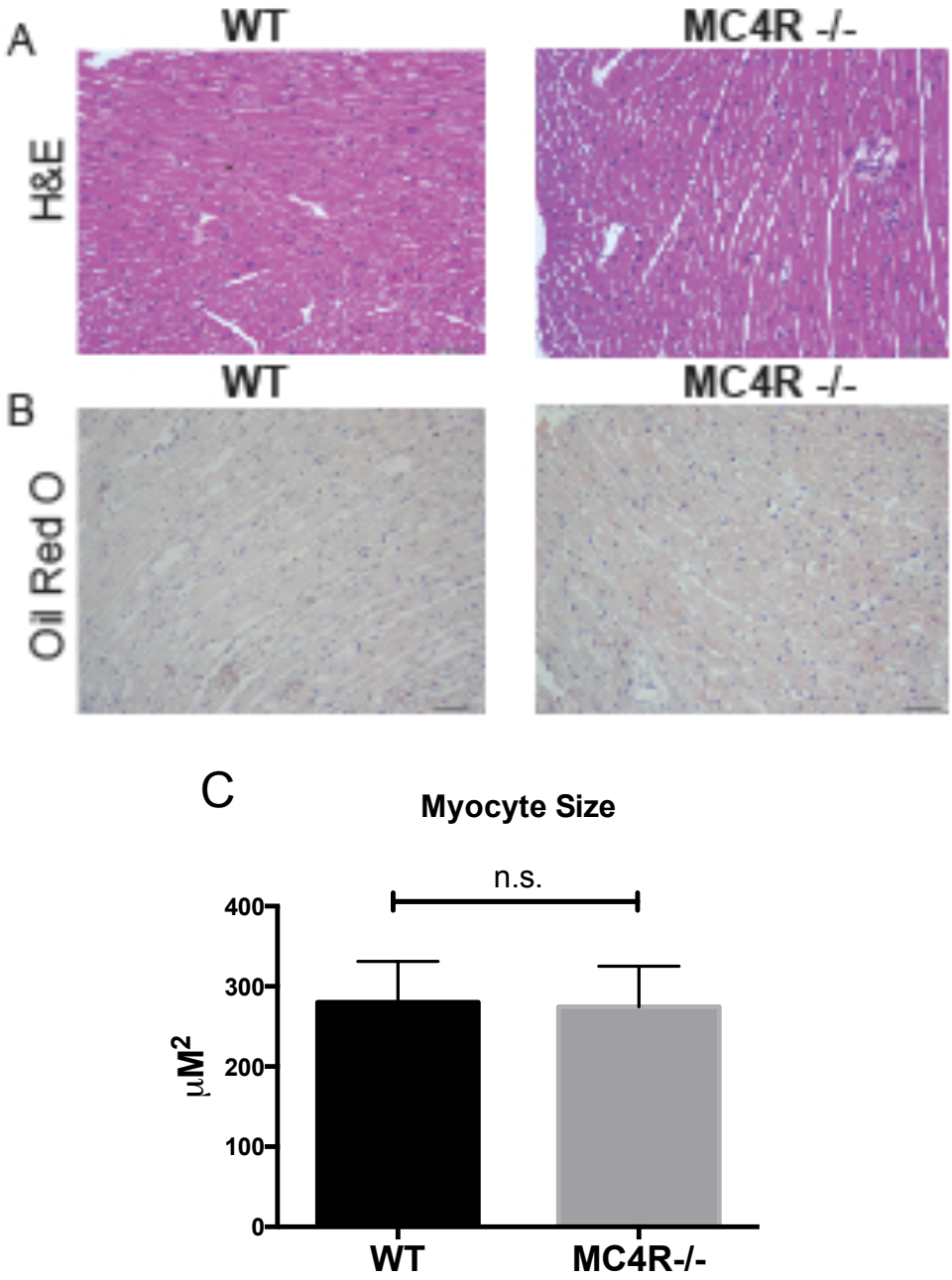

Figure 14 Light Microscopy of *Mc4r-/-* hearts

A) Representative H&E images of WT and *Mc4r-/-* myocardium; scale bar = 500µm **B)** Representative Oil Red O images of WT and *Mc4r-/-* myocardium; scale bar = 500µm **C)** Cross sectional myocyte area. n=3 mice x 3 sections (unpaired t-test, p>0.05).

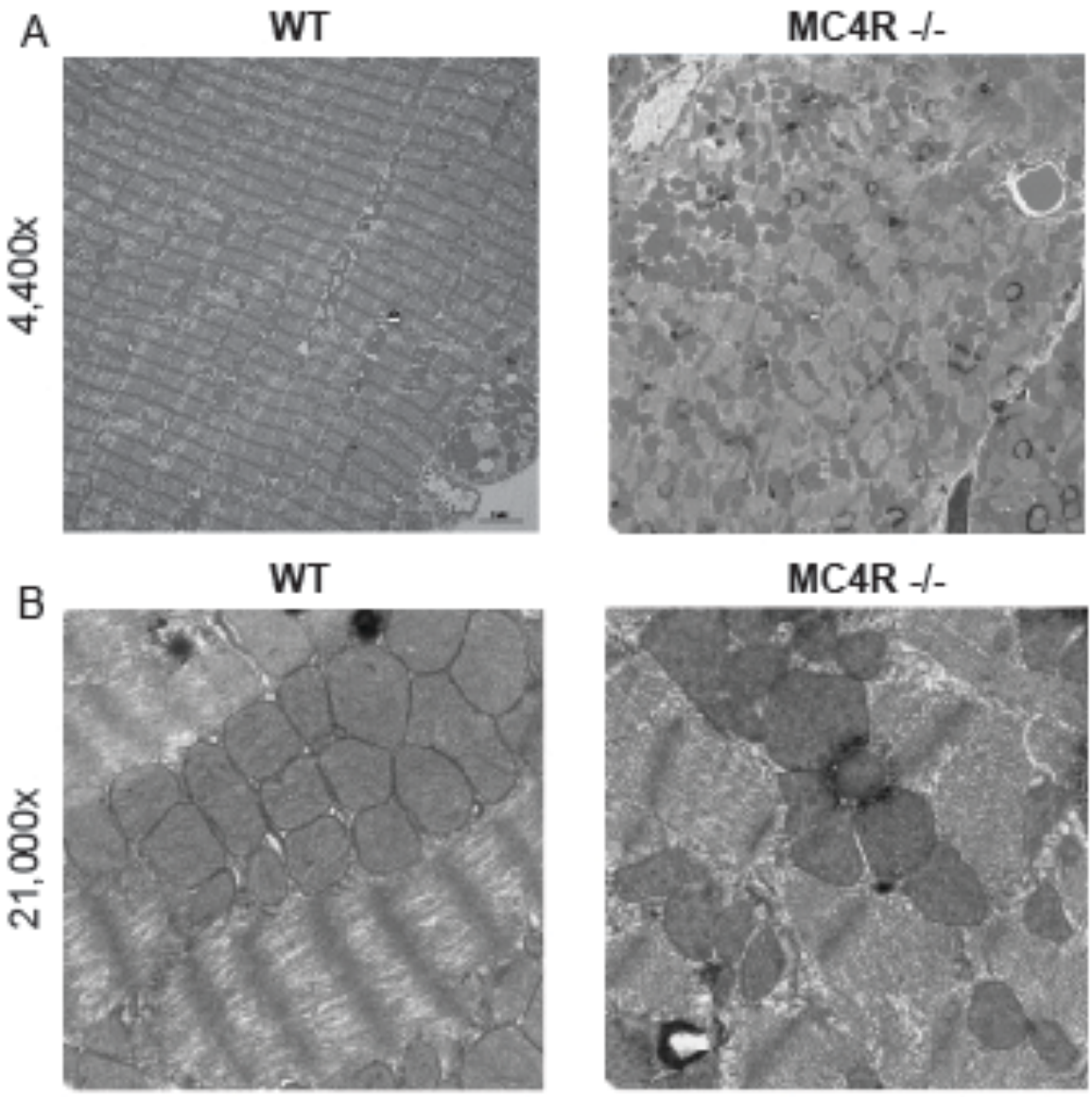

Figure 15 Transmission Electron Microscopy of *Mc4r-/-* hearts

A) Representative TEM images WT and *Mc4r-/-* myocardium at 4400x scale bar= 2µm
B) Representative TEM images WT and *Mc4r-/-* myocardium at 21,000x scale bar=500nm.

Furthermore, *Mc4r-/-* mice had increased heart weight when compared to DIO mice at 40 weeks of age (Figure 13). These underlying changes appear to mirror a global increase in lean mass that is present in *Mc4r-/-* mice as compared to WT and DIO animals (Figure 8) and appear to be independent of glucose homeostasis and insulin signaling (Figure 9). This effect also appears to be indirect, as were unable to detect MC4R in the adult heart by a variety of methods (Figure 11).

Based on this finding, an attempt was made to see if this effect is due to reduced MC4R signaling within the hypothalamus. However, our $ARC^{POMC\text{-}KO}$ mice were difficult to interpret as the mice were echoed under isoflurane anesthesia and the heart rate of $ARC^{POMC\text{-}KO}$ mice was elevated suggesting a difference in anesthesia depth between genotypes. Histologically, *Mc4r-/-* hearts appeared to be normal with no signs of pyknosis, inflammation, hypoxia or fibrosis by H&E staining (Figure 14). Furthermore, there appeared to be no change in lipid deposition by Oil Red O. However, transmission electron micrographs revealed grossly disorganized myofibers and pleomorphic mitochondria in *Mc4r-/-* myocardium (Figure 15).

CHAPTER 3

CHARACTERIZATION OF MITOCHONDRIAL FUNCTION IN *Mc4r-/-* HEARTS

Introduction

Based on the mitochondrial ultrastructure pathology found by TEM, our attention turned towards characterizing the myocardial mitochondrial function of *Mc4r-/-* mice. Proper mitochondrial function is critical for heart function. The ATP turnover in the heart is estimated be 30kg in a day – 100x its own weight (Ashrafian & Frenneaux, 2007). This translates to 300mg of ATP per beat and nearly 10^6 kg of ATP in a lifetime (Ferrari, Censi, Mastrorilli, & Boraso, 2003). The healthy heart is able to oxidize multiple fuel substrates to maintain the mitochondrial proton motive force (Δp) – the driver of ATP synthase (Z. V. Wang, Li, & Hill, 2014). The fuel that the heart burns is dependent on the availability of the substrate and hormonal cues. In the fasted state, fatty acids are responsible for up to 70% of all ATP generated in the heart (van der Vusse, Glatz, Stam, & Reneman, 1992). Following a meal, the heart's substrate preference shifts towards glucose utilization as a result of insulin induced GLUT4 translocation (Stanley, Recchia, & Lopaschuk, 2005). This ability to change fuel substrate preference is termed metabolic flexibility and enables the heart to respond to a changing substrate milieu during periods of fasting, feeding, stress and exercise.

Mitochondrial dysfunction and defects in metabolic flexibility has been observed

in the failing heart. Early in the disease process, the heart relies heavily on fatty acids (Vincenzo Lionetti, Stanley, & Recchia, 2011) and displays insulin resistance. Furthermore, insulin resistance has been shown to alter myocardial metabolism and promote negative cardiac remodeling (L. Zhang, Keung, Samokhvalov, Wang, & Lopaschuk, 2010). This stage is also associated with an increase in serum fatty acid content and a reduction in the cardiac respiratory quotient (Paolisso et al., 1994). In late stages of the disease, total respiration declines. However, the substrate preference of the heart shifts towards glucose utilization. This is due to a decline in total mitochondrial content, which limits the β-oxidation capacity of the myocyte. This change appears compensatory as drugs that limit fatty acid oxidation and promote glucose utilization, such as glucose-insulin-potassium infusion (Kalay et al., 2008) PPAR agonists (Labinskyy et al., 2007), GLP-1 agonists (Margulies et al., 2014) and CPT-1 inhibitors (V. Lionetti et al., 2005) are cardioprotective during heart failure.

While no group has looked at myocardial mitochondrial function in the *Mc4r-/-* heart, studies on other organs in *Mc4r-/-* mice have revealed alterations in both substrate supply and mitochondrial function in other parts of the body. When compared to diet induced obese controls, *Mc4r-/-* mice have elevated serum free fatty acid levels (Itoh et al., 2013). Furthermore, *Mc4r-/-* mice have an early onset hyperinsulinemia phenotype (Fan et al., 2000; Martinelli et al., 2011). Loss of *Mc4r* results in deleterious effects on mitochondrial function within the BAT and kidney. Within the BAT, *Mc4r-/-* mice have reduced cold stimulated UCP1 induction due to reduced norepinephrine stimulated β_3AR signaling (Voss-Andreae et al., 2007). This causes reduced BAT

lipolysis and ineffective adaptive thermogenesis. Within the kidney, no alteration in respiratory rate in isolated mitochondria has been observed. However, *Mc4r-/-* kidneys were found to have increased complex IV function and reactive oxygen species generation when compared to ob/ob or WT mice (Munusamy, do Carmo, Hosler, & Hall, 2015). Furthermore, *Mc4r-/-* mice were found to have reduced kidney ATP content indicating an inability to properly couple respiration with ATP production. Based on these findings and the abnormal mitochondrial structure in our electron microscopy studies, we chose to examine cardiac muscle mitochondrial function of *Mc4r-/-* mice.

Results

Cardiac mitochondria DNA and protein content of Mc4r-/- mice

In order to determine the effect MC4R deletion has on myocardial energetics, mitochondrial content was examined using qPCR. This assay takes advantage of the fact that mitochondria have their own genome, the content of which is proportional to the total number of mitochondria. Using this assay, there was no difference in mitochondrial DNA content relative to genomic DNA content in male *Mc4r-/-* myocardium when compared to WT and *Mc4r+/-* myocardium (WT: 1±0.32, Mc4r+/- : 1.087±0.33, Mc4r-/-: 1.11±0.31, One Way ANOVA, p=0.850) (Figure 16A). Next, mitochondrial protein content was analyzed by western blot. Similar to the qPCR results, there was no difference in the abundance of electron transport chain (ETC) complex I-IV proteins or ATP synthase (Two Way ANOVA, p=0.184, n=5x3)(Figure 16B-C). Due to these negative results and the abnormal mitochondrial morphology on TEM, *Mc4r-/-*

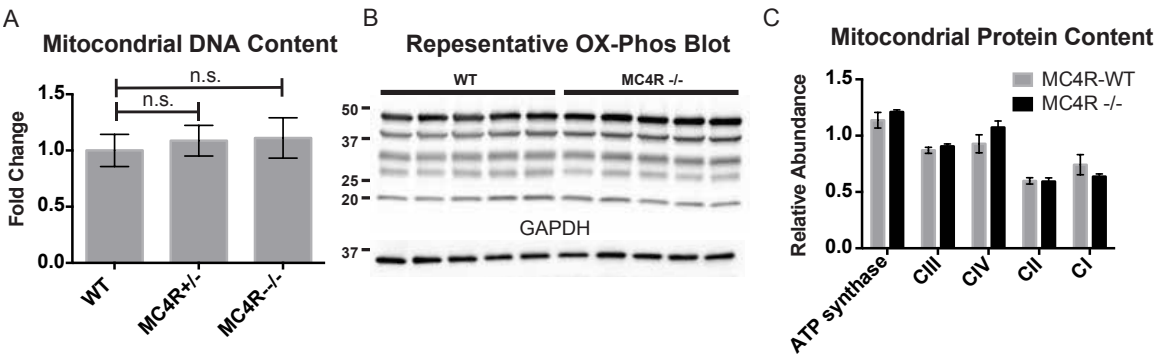

Figure 16 *Mc4r-/-* myocardium displays normal mitochondrial DNA content and OX-Phos protein content

A) qPCR ratio change of mH19 (gDNA) and cytB (mDNA) of *Mc4r-/-* , *Mc4r+/-* and WT myocardium (1-way ANOVA Sidak multiple comparison test, $p>0.05$, n=6). **B)** Representative western blot of WT and *Mc4r-/-* oxidative phosphorylation components. CI subunit NDUFB8 (est. 22kDa) (ab110242), CII (est. 28kDa) (ab14714), CIII-Core protein 2 (est. 49.5kDa) (ab14745) CIV subunit I (est. 37kDa) (ab14705) and CV alpha subunit (est. 53kDa) (ab14748). **C)** Relative quantification of ETC blot normalized to GAPDH content (2 way ANOVA Sidak multiple comparison test, $p>0.05$, n=3 blots x 5 samples per genotype)

myocardial mitochondrial function was examined ex vivo using high-resolution respirometry.

High resolution respirometry of diseased Mc4r-/- myocardium

In order to avoid selecting for healthy mitochondria, mitochondrial function was examined using saponin-permeabilized myocardial fibers. When 30-week-old *Mc4r-/-* myocardium was examined, there was no difference in the O_2 consumption between genotypes when complex I substrates (glutamate and malate) were added to reaction (Holm-Sidak's multiple comparisons test, Adjusted p=0.818, n=5) (Figure 17A). Since this respiration occurs in the absence of ADP (complex I substrates, state IV respiration) this rate is a reflection of the basal leak kinetics of the mitochondria. This is because O_2 is being consumed as an electron acceptor to maintain Δp and Δp is dissipated by ATP synthase only when ADP is present. Therefore, the only respiration that is occurring is the consequence of H^+ ions flowing down their electrochemical gradient through an ATP synthase independent means (i.e. UCPs). Addition of palmitoylcarnitine – a long chain acyl-carnitine that is readily imported in the mitochondria by CAT – in the absence of ADP also did not result in any differential O_2 consumption (Fatty Acid Substrate, state IV respiration) (Holm-Sidak's multiple comparisons test, Adjusted p=0.726, n=5). However, when ADP was added to this reaction (Complex I substrates, state III respiration) *Mc4r-/-* myocardium began to consume more O_2 than control tissue (Holm-Sidak's multiple comparisons test, Adjusted p=0.326, n=5). In this step, ATP synthase mediated translocation of H+ ions greatly increased respiration in both samples as a compensatory response to maintain Δp. While this differential increase did not reach

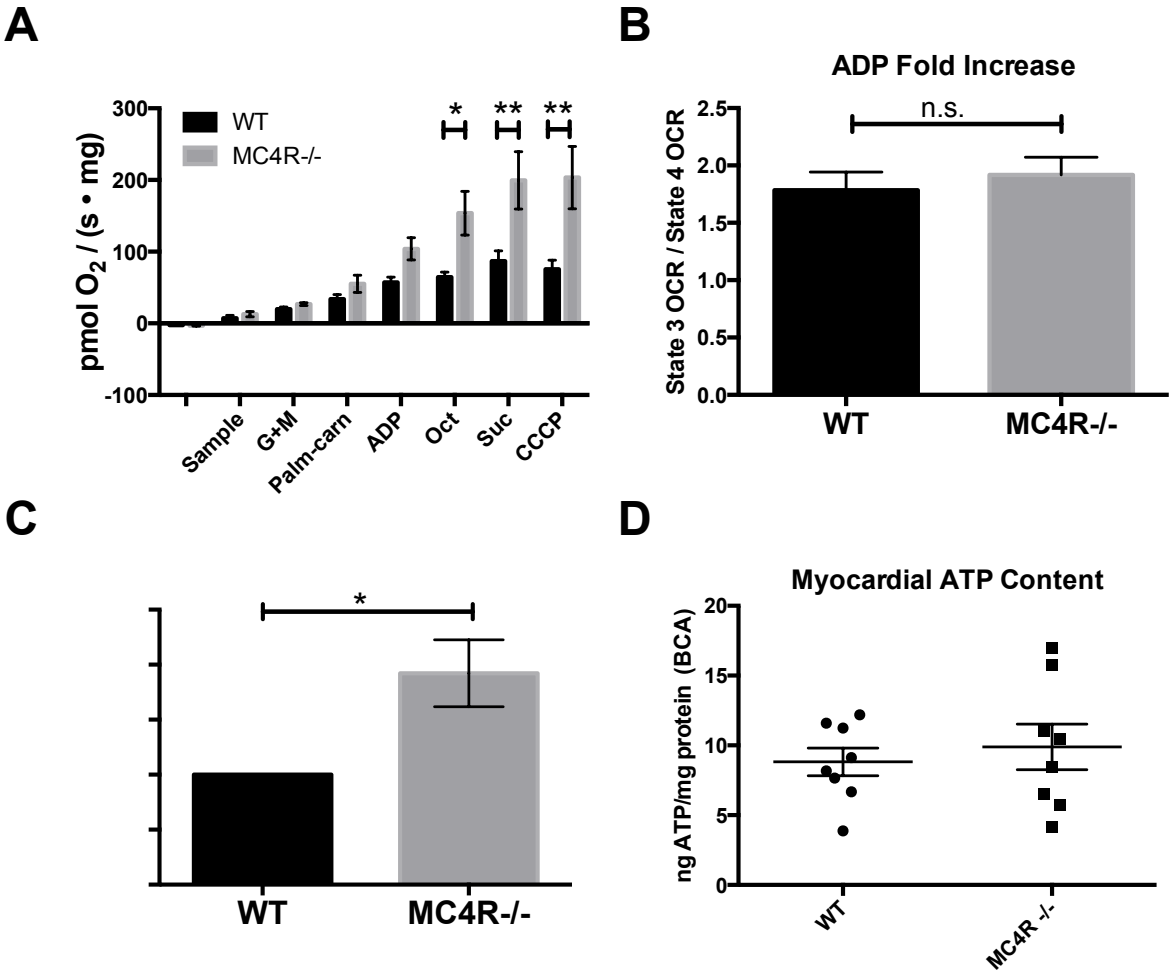

(Figure 17 High-resolution respirometry analysis of permeabilized tissue preparations from cardiomyopathic *Mc4r-/-* myocardium reveal increased oxidative capacity.

A) O_2 consumption rate comparison between permeabilized WT and *Mc4r-/-* myocardial tissue from 30-33 week old mice. (2 way ANOVA, Sidak post test, $p<0.05$, n=5) **B)** ADP dependent O_2 consumption ratio (paired t-test, $p>0.05$, n=5) **C)** Ratio O_2 consumption of *Mc4r-/-* tissue compared to WT (ratio paired t-test, $p<0.05$, n=5) **D)** ATP content of *Mc4r-/-* and WT LVPW (unpaired t-test, $p>0.05$, n=8).

statistical significance, the increase in state III respiration became more pronounced in the presence of a medium chain fatty acid substrate (L-Octanoylcarnitine) and reached statistical significance (Holm-Sidak's multiple comparisons test, Adjusted p=0.0174, n=5). This increase in *Mc4r-/-* myocardial respiration was retained following the addition of succinate (complex II substrate, state III mediated respiration) (Holm-Sidak's multiple comparisons test, Adjusted p=0.0022, n=5). The observed increases in ETC capacity also persisted when the ionophore CCCP was titrated into the reaction indicating that the increase *Mc4r-/-* respiratory capacity was dependent on the electron transport chain and not due to an increase in ATP synthase activity (Holm-Sidak's multiple comparisons test, Adjusted p=0.0005, n=5). When the fold increase following ADP exposure was examined, there was no difference between groups (paired t-test, p=0.270, n=5) (Figure 17B). This ratio is an estimation of the respiratory control ratio used to determine the quality of the mitochondrial within the tissue preparation between experiments (Nicholls, Ferguson, & Ferguson, 2002). When the *Mc4r-/-* maximal oxygen consumption rate was compared as a ratio to that of the control sample's rate, a 2-fold increase in total respiratory capacity in 30-week-old *Mc4r-/-* myocardium was apparent (MC4R/WT: 1.922±0.68, ratio paired t-test, p= 0.031, n=5) (Figure 17C). This increase in respiratory capacity did not translate to increased ATP content by a fluorometric assay (WT: 8.82±2.82 vs. *Mc4r-/-* : 9.89±4.62, unpaired t-test, p=0.583, n=8) (Figure 17D). These results were subsequently validated qualitatively in 2 MC4R-loxTB+/+ animals (Figure 18A-C). Therefore, despite this almost 100% increase in O2 consumption capacity, *Mc4r-/-* heart tissue did not display an increase in the intracellular ATP pool. These

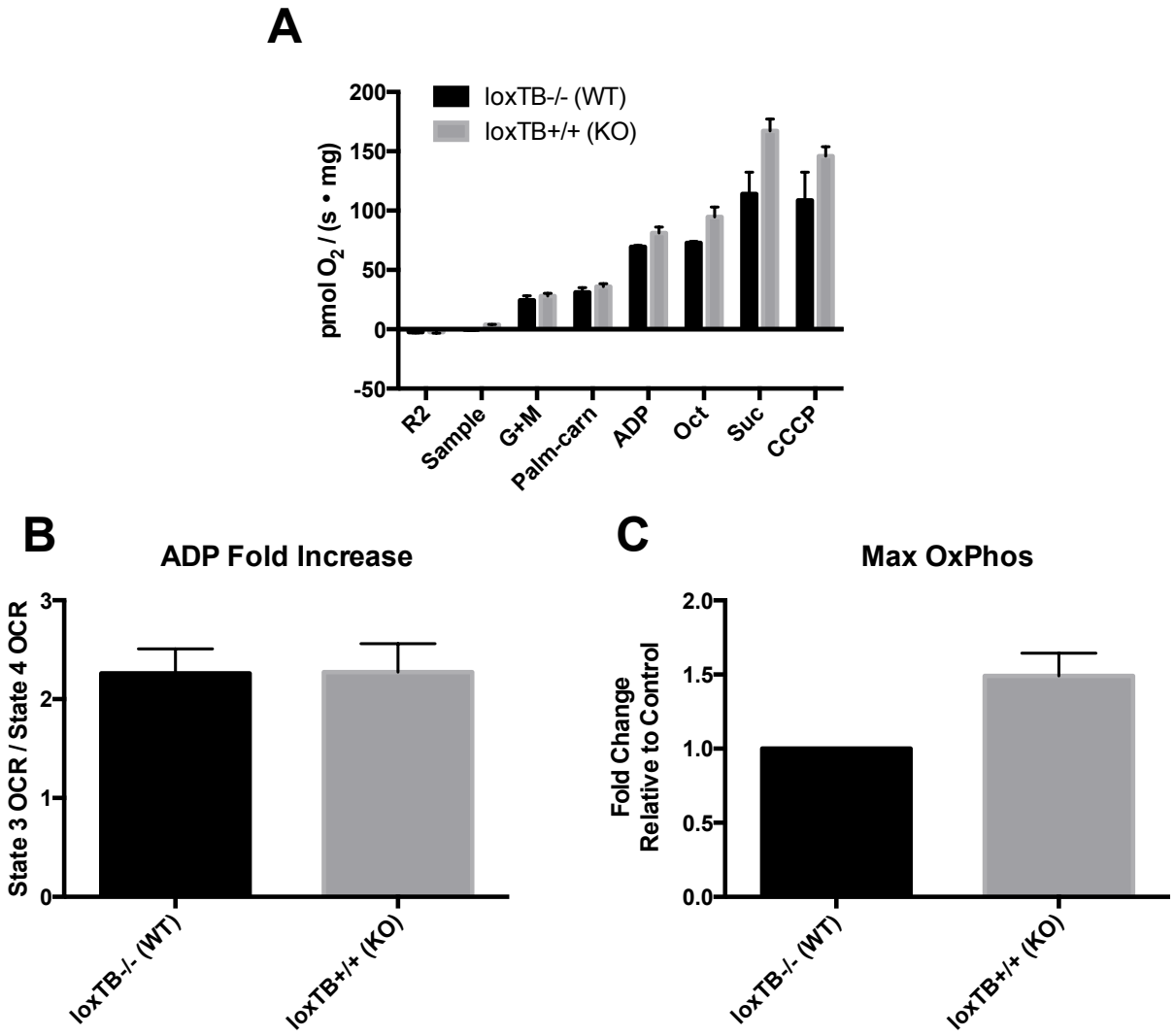

Figure 18 High-resolution respirometry analysis of permeabilized tissue preparations from MC4R-loxTB+/+ myocardium confirm an MC4R specific increase in oxidative capacity.

A) O_2 consumption rate comparison between permeabilized WT and *Mc4r-/-* myocardial tissue from 30-33 week old MC4R-loxTB+/+ mice. (n=2) **B)** ADP dependent O_2 consumption ratio (n=2) **C)** Ratio O_2 consumption of *Mc4r-/-* tissue compared to WT (n=2)

findings are in contrast to what is generally seen in dilated cardiomyopathy and right heart failure (Talati et al., 2016) and more closely mimics what has been observed in hypertrophic cardiomyopathy (Rosca, Tandler, & Hoppel, 2013).

Pre-diseased Mc4r-/- myocardial respirometry

In order to see if the observed mitochondrial phenotype precedes heart failure, the O_2 consuming capacity of 6-12 week old *Mc4r-/-* myocardium was also analyzed using high-resolution respirometry. Similar to the older cohort, young *Mc4r-/-* myocardium display no increase in State IV respiration in the presence of both glutamate/malate and palmitoylcarnitine when compared to controls (Holm-Sidak's multiple comparisons test, Adjusted p=0.962, n=7) (Figure 19A). Likewise, ADP dependent respiration was significantly increased in *Mc4r-/-* myocardium when compared to controls (Holm-Sidak's multiple comparisons test, Adjusted p=0.046 n=7). This relative increase in *Mc4r-/-* myocardial respiration became further exaggerated by the addition of Octanoylcarnitine and succinate (Holm-Sidak's multiple comparisons test, Adjusted p=0.0146 & 0.0001, n=7). Furthermore, maximal ETS capacity as determined by CCCP addition was increased (Holm-Sidak's multiple comparisons test, Adjusted p=0.0001, n=7). These differences were obtained without any difference in ADP fold change between *Mc4r-/-* and WT (WT: 2.07±0.149 vs. *Mc4r-/-* : 2.04±0.192, paired t-test, p=0.128, n=7)(Figure 19B). The ratio between WT and *Mc4r-/-* maximal oxygen consumption further revealed that 12 week old *Mc4r-/-* myocardial tissue displayed a 1.5 increase in O2 consuming capacity compared to WT controls (Mc4r/WT: 1.52±0.412, ratio paired t-test, p=0.0066, n=7) (Figure 19C) indicating a potential derangement of

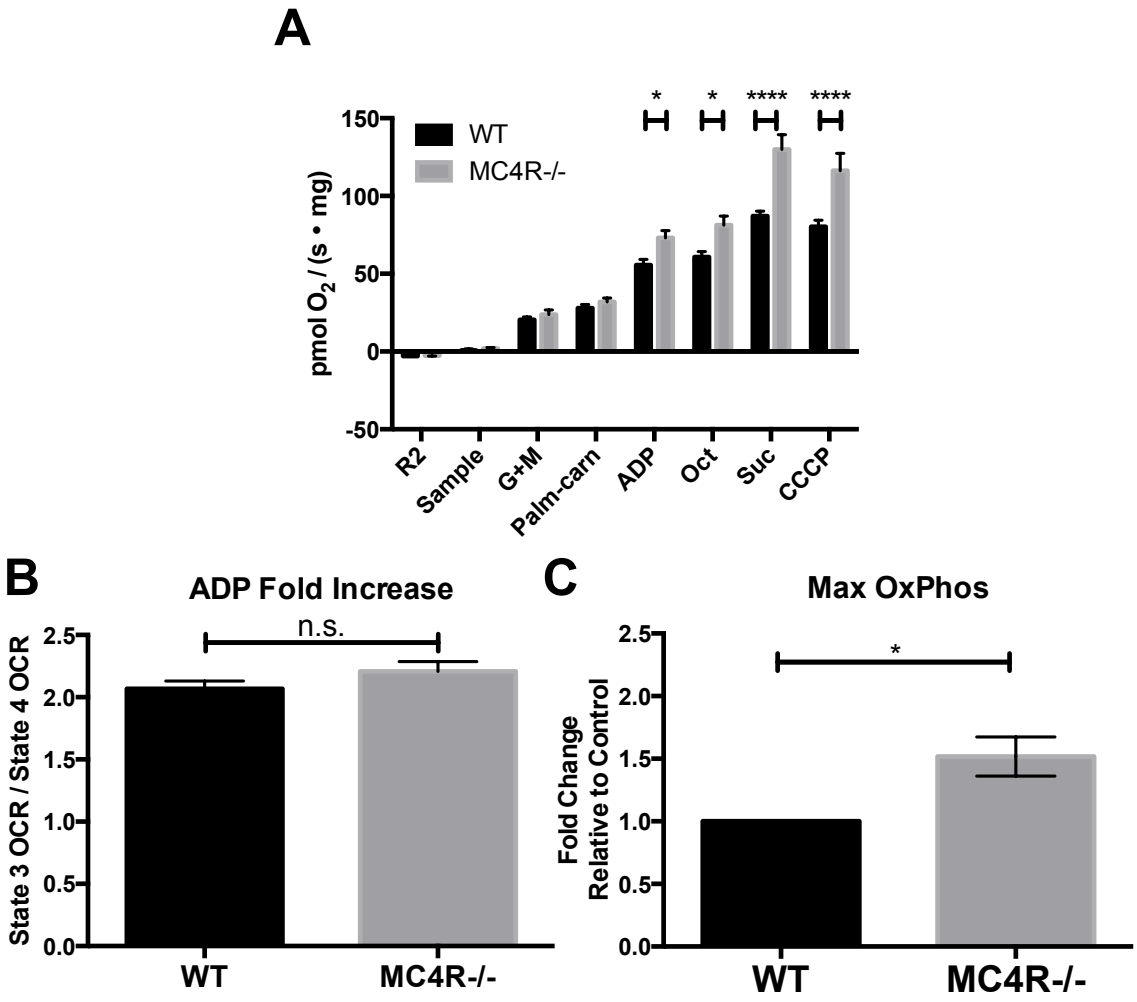

Figure 19 High-resolution respirometry analysis of permeabilized tissue preparations from young, pre-diseased *Mc4r-/-* myocardium also reveals increased oxidative capacity.

A) O_2 consumption rate comparison between WT and *Mc4r-/-* myocardial tissue from 6-12 week old mice. (2 way ANOVA Sidak post test, $p<0.05$, $n=7$) at 6-12 weeks of age **B)** ADP dependent O_2 consumption ratio (paired t-test, $p>0.05$, $n=7$) **C)** Ratio O_2 consumption of *Mc4r-/-* tissue compared to WT (ratio paired t-test, $p<0.05$, $n=7$)

oxygen consumption prior to the onset of heart failure.

Characterization of Mc4r-/- red gastrocnemius fibers

In order to determine if this increase in State III respiration is specific to heart tissue or present throughout the body, permeabilized red gastrocnemius muscle fibers were then examined with high-resolution respirometry. Just like the myocardial tissue experiments, *Mc4r-/-* mouse skeletal muscle had similar O_2 consumption capacity when compared to WT in the presence of glutamate/malate and palmitoylcarnitine but absence of ADP (Holm-Sidak's multiple comparisons test, Adjusted p=0.962, n=6) (Figure 20A). In contrast to *Mc4r-/-* cardiac tissue, *Mc4r-/-* skeletal muscle did not display increased oxygen consumption when ADP was added to the reaction (Holm-Sidak's multiple comparisons test, Adjusted p=0.962, n=6). This finding also persisted following the addition of L-Octanoylcarnitine and succinate indicating no difference in coupled mitochondrial respiration between genotypes (Holm-Sidak's multiple comparisons test, Adjusted p=0.962 & 0.121, n=6). Furthermore, addition of CCCP also failed to reveal any alteration in *Mc4r-/-* red gastrocnemius mitochondrial function (Holm-Sidak's multiple comparisons test, Adjusted p=0.34, n=6). Likewise, there was no alteration in the ADP fold difference (WT: 4.31±0.79 *Mc4r-/-* : 3.69±1.1,paired t-test, p=0.238, n=6) (Figure 20B) and maximal oxygen consumption ratio (MC4R/WT: 1.16±0.0.223, ratio paired t-test, p=0.126, n=6) (Figure 20C) was observed in this muscle type. Based on these results, mitochondrial protein content was examined to ensure that the lack of change was not due to a reduction in mitochondrial protein content. Similar to the heart, there was no difference in the abundance of electron

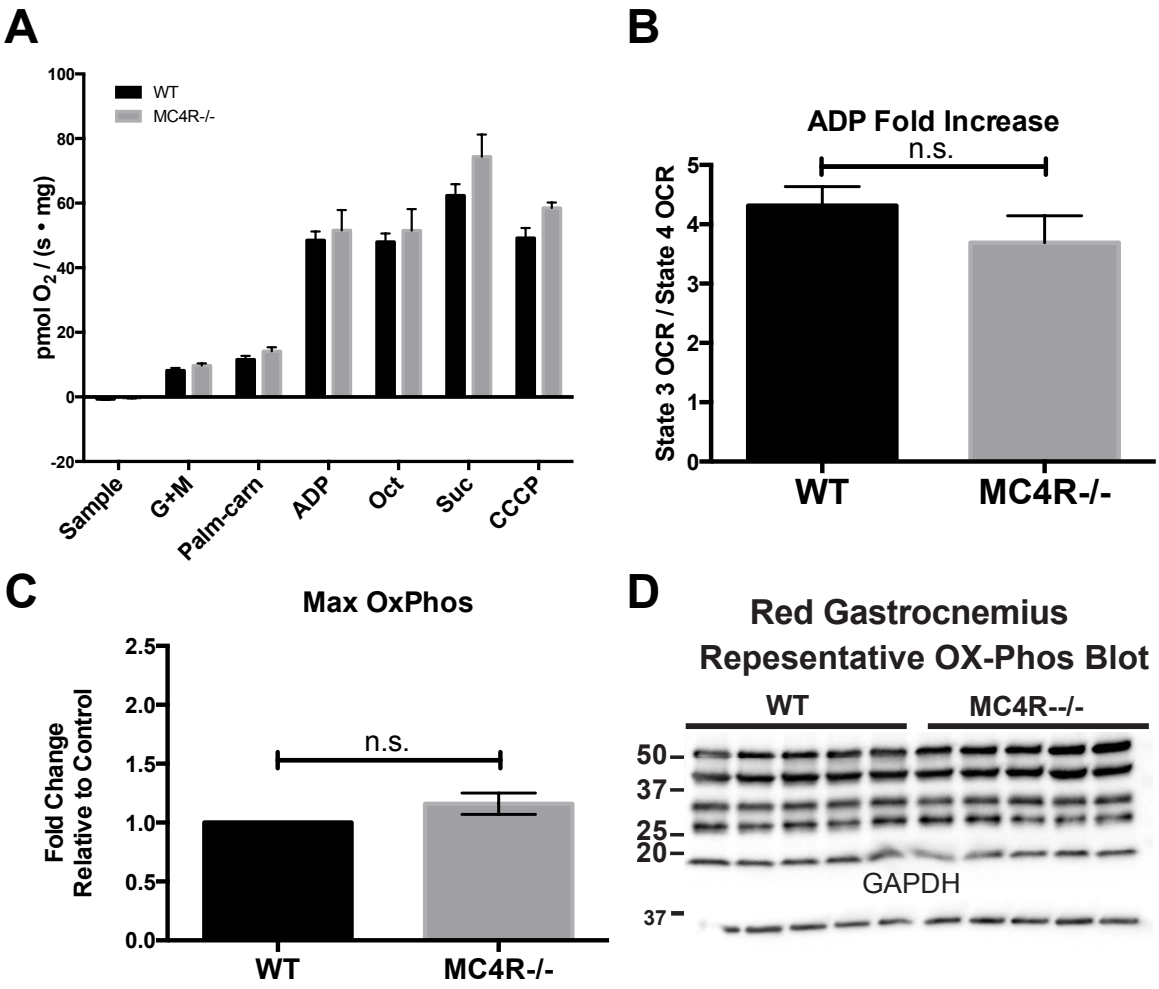

Figure 20 High-resolution respirometry analysis of permeabilized tissue preparations from young *Mc4r-/-* red gastrocnemius tissue fails to show increased oxidative capacity.

A) O_2 consumption rate comparison between WT and *Mc4r-/-* red gastrocnemius tissue from 6-12 week old mice. (2 way ANOVA Sidak post test, p>0.05, n=6) at 12 weeks of age **B)** ADP dependent O_2 consumption ratio of red gastrocnemius tissue from 6-12 week old mice (paired t-test, p>0.05, n=6) **C)** Ratio O_2 consumption of *Mc4r-/-* red gastrocnemius tissue compared to WT red gastrocnemius tissue (ratio paired t-test, p>0.05, n=6) **D)** Representative OxPhos blot from *Mc4r-/-* and WT red gastrocnemius.

transport chain (ETC) complex I-IV proteins or ATP synthase by western blot in muscle fibers (Figure 20D). Based on these results, the observed increase in myocardial oxygen consumption in *Mc4r-/-* mice is specific to the myocardium, independent of obesity, and precedes the development of heart failure.

Respirometry of ARC$^{POMC\text{-}KO}$ myocardium

After demonstrating that the loss of Mc4r causes an increase in myocardial oxygen consumption capacity, ARC$^{POMC\text{-}KO}$ mice were examined to see if the modulation of myocardial oxygen consumption was due to a lack of hypothalamic MC4R signaling. Unlike old *Mc4r-/-* , old MC4R-loxTB+/+ or young *Mc4r-/-* myocardium, old ARC$^{POMC\text{-}KO}$ myocardium did not show any difference in oxygen consumption when compared to controls. This includes no difference in state IV respiration (both following glutamate/malate and palmitoylcarnitine), state III respiration, uncoupled respiration, ADP ratio, and the maximal oxygen consumption ratio Figure 21A-C). Thus, despite being morbidly obese, ARC$^{POMC\text{-}KO}$ mice appear to have normal myocardial oxygen consumption.

Potential role for ROS in Mc4r-/- cardiomyocyte dysfunction

Reactive oxygen species (ROS) are formed as a byproduct of normal aerobic metabolism and play both physiological and pathophysiological roles in the heart (Brown et al., 2017). Excessive mitochondrial ROS production is known to contribute to heart failure through irreversible modifications of cellular lipids, proteins and DNA (Brown et al., 2017). In order to study ROS levels in *Mc4r-/-* myocardium, tissue lysates were examined using the reduced form of 2', 7' –dichlorofluorescein (DCFH-DioxyQ

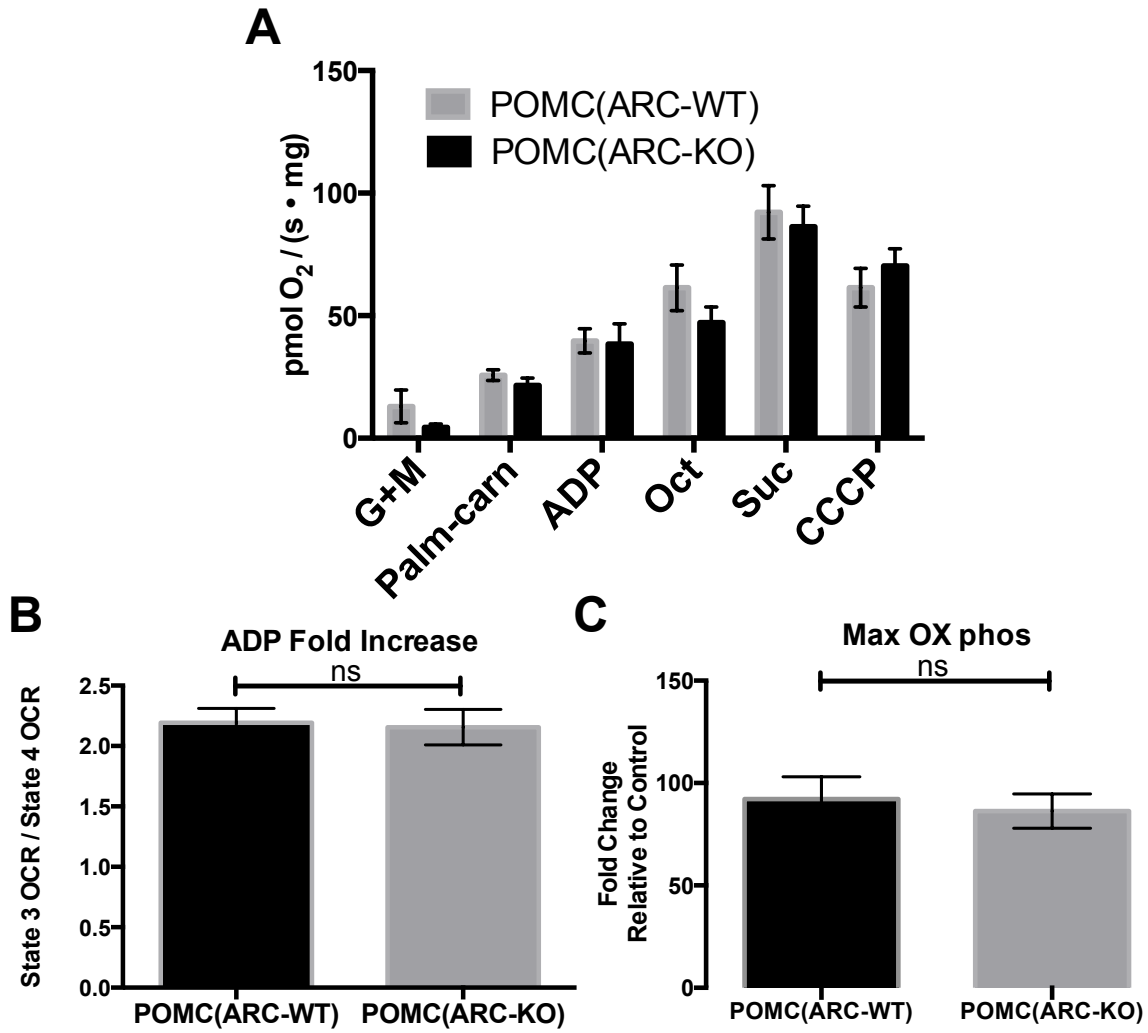

Figure 21 High-resolution respirometry analysis of permeabilized tissue preparations from obese ARC$^{POMC-KO}$ myocardium fails to show an increase in oxidative capacity.

A) O_2 consumption rate comparison between permeabilized WT and *Mc4r-/-* myocardial tissue from 56-week-old ARC$^{POMC-KO}$ mice. (n=2) **B)** ADP dependent O_2 consumption ratio (n=5) **C)** Ratio O_2 consumption of *Mc4r-/-* tissue compared to WT (n=5)

assay). Once primed, DCFH can be oxidized by a free radial, which results in the generation of DCF. DCF is in the chemical family of fluorescein and is fluorescent (ex/em: 492–495/517–527 nm). When compared to WT tissue, an increase in DCF fluorescence was observed in both 12 week old ("young") *Mc4r-/-* (WT: 1±0.343 *Mc4r-/-* : 1.47±0.245, unpaired t-test, p=0.039, n=5)(Figure 22A) and 30 week old ("old") *Mc4r-/-* (WT: 1±0.148 *Mc4r-/-* : 1.83±0.454, unpaired t-test, p=0.0054, n=5)(Figure 22B) myocardial lysates. That the content of free radicals was higher in the older *Mc4r-/-* mice indicates that this process increases over time. Since ROS can be both physiological and pathophysiological, pathological intermediates and end products of ROS were then examined in old 30-week-old *Mc4r-/-* tissue samples. While no significant increase in malondialdehyde, an intermediate of lipid peroxidation, was observed (WT: $5.18e^{-9}$ ± $2.26e^{-10}$ *Mc4r-/-* : $5.78e^{-9}$ ± $3.23e^{-10}$, unpaired t-test, p=0.56, n=5)(Figure 22C), a significant increase in 4-hydroxynonenal protein adducts was observed (WT: 0.0187±0.0023 *Mc4r-/-* 0.0258±0.0063, unpaired t-test, p=0.0398, n=5)(Figure 22D). 4-HNE adducts are an irreversible lipid-protein covalent bond caused by excessive ROS and have been shown to be a causative mechanism for ROS mediated heart damage (Mali & Palaniyandi, 2014). Therefore, the observed increases in mitochondrial capacity and *Mc4r-/-* mediated increases in fatty acid utilization likely contribute to progressive heart failure through a pathological increase in ROS production.

After identifying ROS as a potential link between increased O_2 consumption and tissue damage, we next sought to examine the gene changes in *Mc4r-/-* mice that contribute, or compensate for this pathological insult. *Mc4r-/-* myocardium of 30-week-

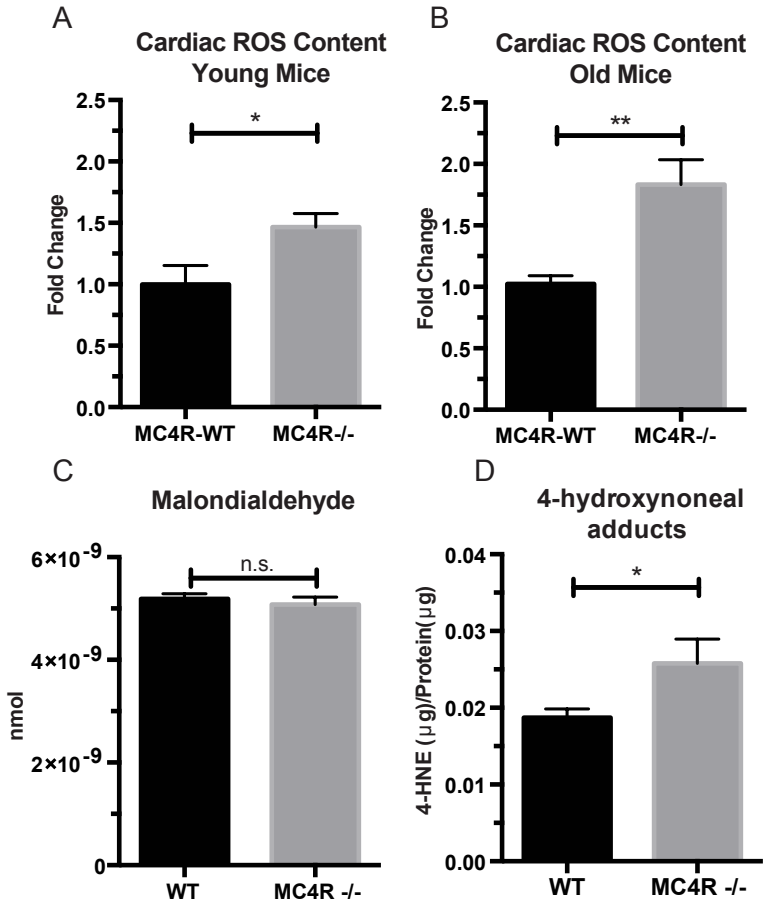

Figure 22 *Mc4r-/-* hearts display signs of increase ROS production

A) DCF assay comparing myocardial lysates from 6-12 week old *Mc4r-/-* and WT mice (ratio paired t-test, $p<0.05$, n=5). **B)** DCF assay comparing myocardial lysates from 30-33 week old *Mc4r-/-* and WT mice (ratio paired t-test, $p<0.05$, n=5). **C)** Malondialdehyde content in 30 week old *Mc4r-/-* and WT myocardium (student's t-test, $p>0.05$,n=5) **D)** 4-HNE protein content per mg total protein (student's t-test, $p>0.05$,n=5)

old mice was compared to age matched controls using RNA-seq. Similar to the qRT-PCR and western blot data, MC4R expression in the myocardium was undetectable (GEO accession number: GSE98439). However, 247 transcripts were identified that were significantly different from WT controls (Figure 23A). Differential expression of select genes was confirmed using qRT-PCR including increased expression of MYL7 and reduced expression of PGC-1α (Figure 23B). Further analysis of this data set reveals a collection of genes important in cardiac energetic homeostasis (Figure 23C). Of particular note were genes involved in myocyte structure (*Myl7, Myl4, Mylk2, Aacta2*), mitochondrial function (*Phd3, Nhe-1, Pgc1α, Hmgcs2*), calcium homeostasis (*Atp2a3/SERCA, Casq1, Camk2b*), and cellular membrane potential (*Kcnk1, Kcnj14, Scn4b, Chrna2*). Pathway ontology analysis of all significantly different transcripts was then used to identify a potential mechanism responsible for heart failure. This analysis revealed a contribution of 45 known signaling pathways and protein classes (Figure 24A) including growth factor signaling, GPCR signaling, cytoskeleton regulation, glycolysis and inflammation. Furthermore, protein class analysis (Figure 24B) reveals enrichment of receptor signaling, extracellular matrix proteins, cytoskeleton proteins and oxidoreductase enzymes. To understand the functional consequence of this network change, gene set enrichment analysis (GSEA) was performed. This algorithm compares the magnitude and direction of identified transcripts to a database of previous experiments. Of note, GSEA revealed signatures similar to that seen with H34K methylation and doxorubicin (DOX) treatment (Figure 24A-B). While both are associated with heart failure, the doxorubicin was particularly intriguing as it is a known to promote

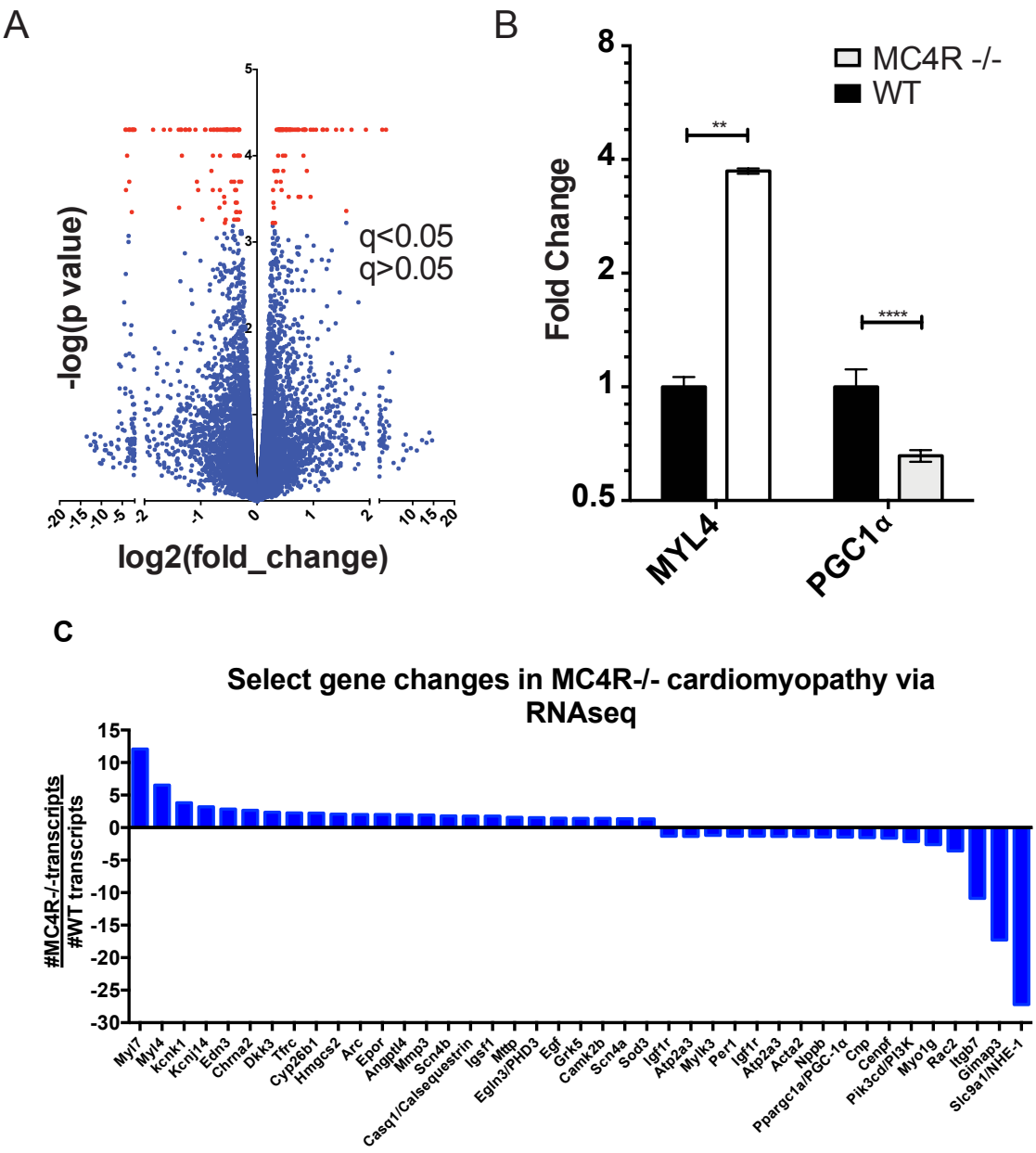

Figure 23 RNA-seq identified gene changes in MC4R -/- myocardium

A) Volcano plot of RNA-seq results. Red points indicate gene changes that reached statistical significance. (n=4 WT, n=6 *Mc4r-/-*). B) qRT-PCR confirmation of select gene changes found with RNA-seq (student's t-test, p<0.01, n=4 WT, n=6 *Mc4r-/-*) C) Select genes found to be dysregulated in *Mc4r-/-* myocardium. This list includes genes involved in contractility (Myl7, Myl4, Mylk2, Aacta2), mitochondrial function (Phd3, Nhe-1, Pgc1α, Hmgcs2, Gpd1, Slc22a33), calcium homeostasis (Atp2a3/SERCA, Casq1, Camk2b), and membrane potential (Kcnk1, Kcnj14, Scn4b, Chrna2).

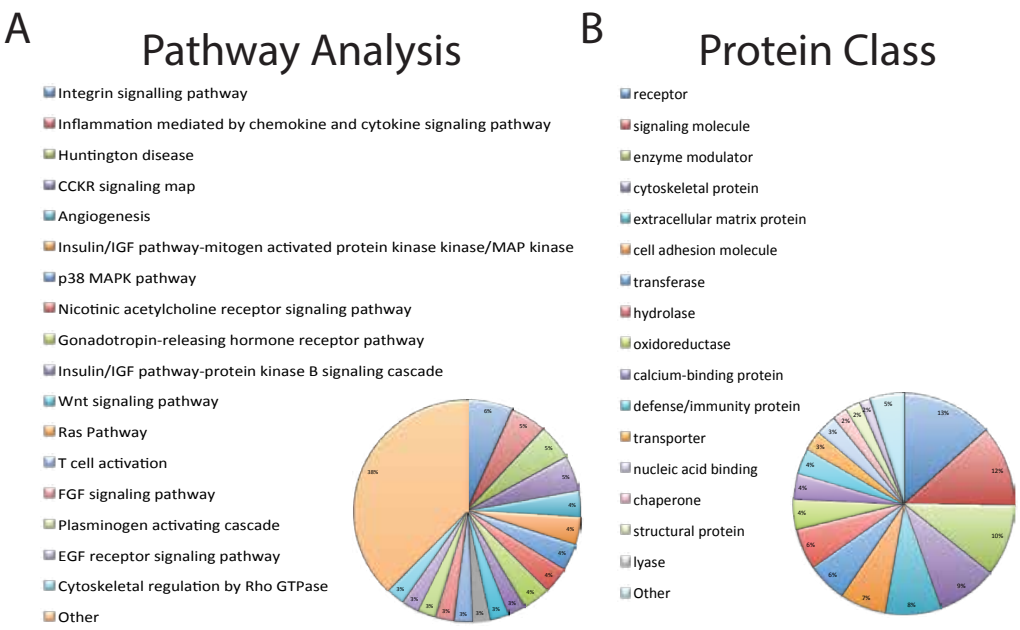

Figure 24 Pathway and Protein Class ontology of *Mc4r-/-* transcript changes

A) Gene ontology pathway analysis of significantly unregulated genes using PANTHER Pathways Overrepresentation test. Pathway changes relevant to heart failure include integrin signaling, inflammatory signaling, insulin signaling and acetylcholine signaling. **B)** Gene ontology pathway analysis of significantly unregulated genes using PANTHER Protein Class Overrepresentation test.

ROS mediated apoptosis. This finding was further validated by identification of DOX within the top 10 drugs found using LINCS cloud (Figure 24C). Similar to GSEA, this software compares the entered data set data with that from a library of microarray data from cells treated with a library of biologically active chemicals. Thus, while the pathway changes associated with MC4R deficiency appear to affect multiple nodes of cardiac tissue function, these changes are consistent with oxidative stress.

In order to determine the degree to which MC4R was playing a protective role in cardiac ROS stress, Mc4r+/- animals and their WT siblings were injected with a sub-cardiotoxic dose of DOX (2x5mg/kg IP injections) and examined by echocardiography (Figure 26A). Body weight measurements reveal that DOX injected Mc4r+/- mice lost twice as much weight as their DOX injected WT controls (Two way ANOVA, adjusted $p<0.0001$, n=6-17)(Figure 26B). When compared to WT animals injected with DOX, Mc4r+/- mice injected with DOX displayed reduced measures of contractility including fractional shortening and ejection fraction when compared to DOX injected WTs but not their saline controls (One way ANOVA, vs. WT-DOX adjusted $p<0.01$, vs. Mc4r+/- DOX adjusted p=0.17-0.12, n=6-17) (Figure 26C-D). DOX injected Mc4r+/- mice also had increased chamber size when compared to DOX injected WTs (One way ANOVA, vs. WT-DOX adjusted $p<0.05$, n=6-17) (Figure 26E). However, this parameter was not significantly different than their saline treated Mc4r+/- controls (One way ANOVA, vs. WT-DOX adjusted p=0.21, n=6-17). Similar to previous experiments, there was no appreciable change in wall thickness at this stage (LVPWd) (One way ANOVA, n=6-17) (Figure 26F). While there was no significant reduction in heart rate (Figure 26G), a few

A

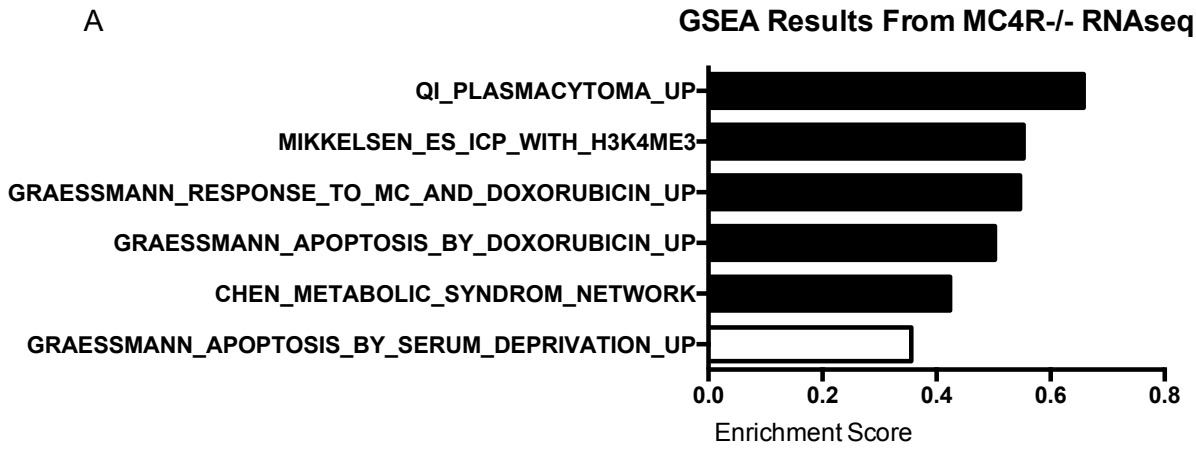

B

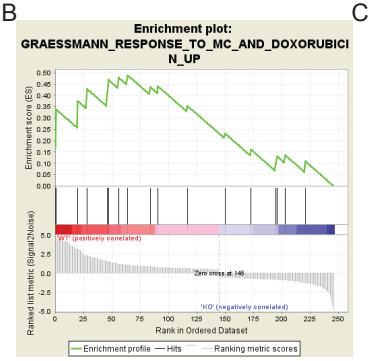

C

	cmap_id	cmap_name	score_best2
1	BRD-K70161581	BRD-K70161581	99.199
2	BRD-K85985071	ellipticine	99.727
3	BRD-K23149109	BRD-K23149109	98.634
4	BRD-A24021119	BRD-A24021119	99.306
5	BRD-K19894101	MST-312	97.437
6	BRD-K53792571	inhibitor-BEC	98.667
7	BRD-K92093830	doxorubicin	98.995
8	BRD-K50836978	purvalanol-a	97.732
9	BRD-K59184148	SB-216763	99.29
10	BRD-K04546108	JAK3-inhibitor-VI	98.579

Figure 25 *In silico* analysis of *Mc4r-/-* myocardial transcript changes using GSEA and LINCS cloud.

A) Gene set enrichment analysis (GSEA) results from a different gene transcripts found using RNA-seq reveals 5 networks similar to that seen in *Mc4r-/-* mice (nominal p<0.001). **B)** Enrichment plot comparing *Mc4r-/-* gene changes to those induced by doxorubicin. **C)** LINCS cloud results generated using significantly up regulated and down regulated genes. The results are a class of drugs able to induce gene changes similar to *Mc4r-/-* cardiomyopathy that includes doxorubicin.

Mc4r+/- mice were extremely bradycardic. However, when bradycardic mice from all groups are excluded, the statistical analysis described above still holds up (data not shown). It is important to note that this data on doxorubicin sensitivity resulted from analysis of one cohort of animals; additional studies will need to be performed to validate these findings.

Summary and Conclusions

In this chapter, myocardial fibers were examined by high-resolution respirometry to see if *Mc4r-/-* mice had alterations in mitochondrial function. Using this assay, 30-week-old *Mc4r-/-* mice were found to have increased myocardial oxidative capacity as compared to WT controls. This was despite having no increase in mitochondrial DNA or protein content. This increase in oxidative capacity was present in mice prior to the onset of heart failure suggesting that this alteration in mitochondrial function plays a role in development of *Mc4r-/-* cardiomyopathy or is a compensatory response to chronic chamber dilation. Furthermore, *Mc4r-/-* mice displayed increased myocardial ROS content and ROS mediated tissue damage, both of which are known to be harmful to tissue health.

The effect of MC4R deletion on muscle mitochondrial function was also examined. Unlike the heart, increased in mitochondrial function was not found in the red gastrocnemius muscle of *Mc4r-/-* mice. This suggests that effect was specific to the heart. $ARC^{POMC\text{-}KO}$ mice were also examined to see if hypothalamic MC4R signaling was critical in the development of these changes. However, this mouse line did not show any increase in oxygen consumption capacity. This finding suggests that this change is due

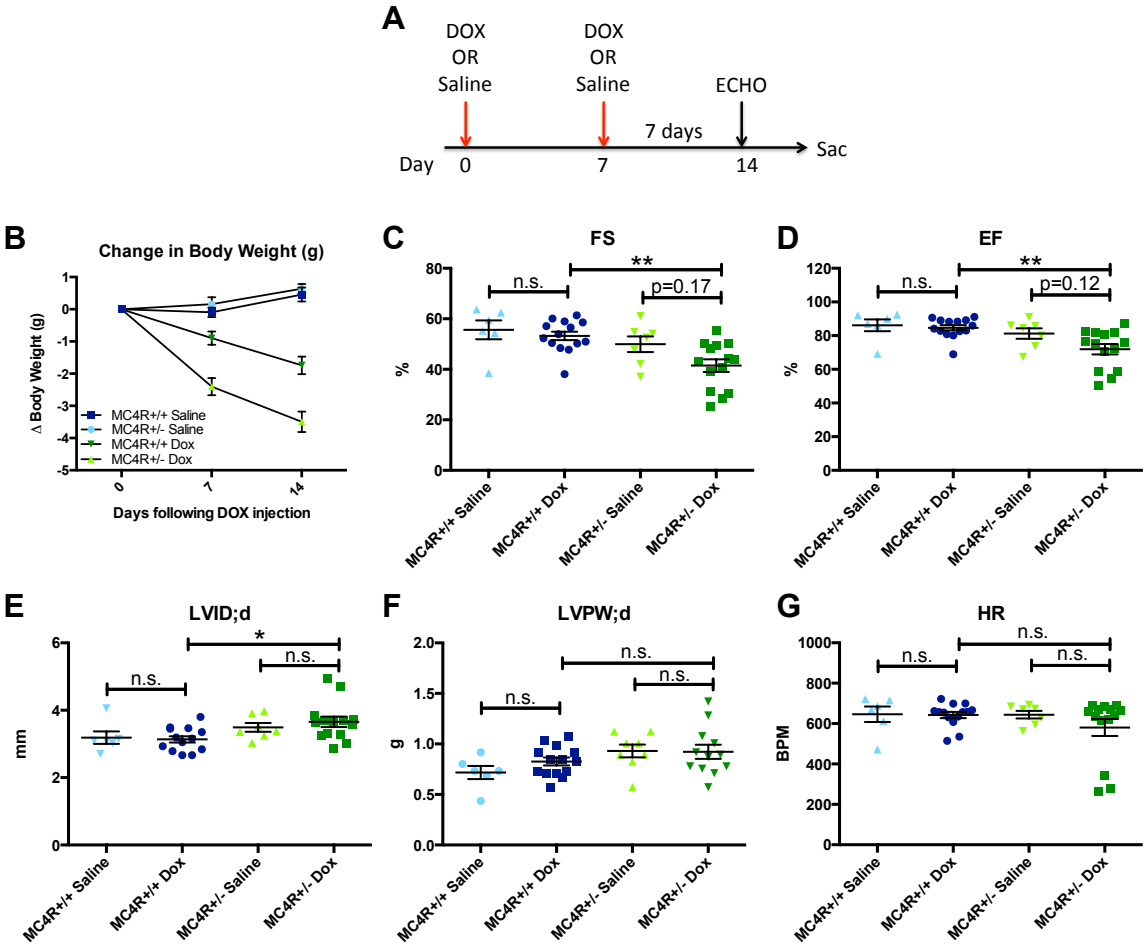

Figure 26 *Mc4r+/-* mice are sensitive to doxorubicin.

A) Treatment strategy to subclinical cardiac dysfunction in WT C57B6/J mice. Mice were given 5mg/kg doxorubicin over the course of 2 weeks during which time their bodyweights were recorded. After 2 weeks, mice were characterized by echocardiography. **B)** Body weights of *Mc4r+/-* and WT during the course of the treatment paradigm. *Mc4r+/-* mice almost twice as much weight as their WT controls. (One Way ANOVA, $p<0.05$, n=6-14) **C)** Fractional shortening of *Mc4r+/-* mice is significantly lower that both saline treated *Mc4r+/-* controls and DOX treated WT controls. (One Way ANOVA, $p<0.05$, n=6-14) **D)** Ejection Fraction of MC4R mice is significantly lower in both saline treated *Mc4r+/-* controls and DOX treated WT controls. (One Way ANOVA, $p<0.05$, n=6-14) **E)** *Mc4r+/-* DOX treated mice are significantly dilated when compared to DOX treated controls but not when compared to *Mc4r+/-* saline treated controls. (One Way ANOVA, $p<0.05$, n=6-14) **F)** There was no change in myocardial thickness between all groups. (One Way ANOVA, $p>0.05$, n=6-14) **G)** There was no change in heart between all groups, however some *Mc4r+/-* mice were extremely bradycardic (One Way ANOVA, $p>0.05$, n=6-14).

to a reduction in hindbrain MC4R function.

In order to gain further mechanistic insight into the *Mc4r-/-* cardiomyopathy syndrome, myocardial RNA was then analyzed by RNA-seq. The hearts of *Mc4r-/-* mice were found to have altered expression of 247 genes that span a wide variety of gene classes. Gene changes included those important in myocyte contractility, mitochondrial function, calcium homeostasis, and membrane potential maintenance. Subsequent *in silico* analyses revealed gene set similarities to those see in doxorubicin treated cells. Based on these findings, *Mc4r+/-* and mice were treated with a low dose doxorubicin treatment. These studies suggested that *Mc4r+/-* were more sensitive to doxorubicin than their WT controls. This finding further indicates the possibility that *Mc4r+/-* humans may be more sensitive to cardiotoxic drugs.

When compared to the literature, these results are rather unexpected. Mice with end stage heart failure typically display reduced mitochondrial function (Brown et al., 2017). This is thought to result from excessive adrenergic tone and tissue fibrosis (Brown et al., 2017). Since *Mc4r-/-* mice have reduced adrenergic tone (Sayk et al., 2010), it is possible that that the observed effect is a maladaptive compensatory response. It is also possible that *Mc4r-/-* mice have enhanced ability to oxidize fatty acid substrates due to chronic hyperinsulinemia (Fan et al., 2000). In these studies, oxidative capacity of *Mc4r-/-* mitochondria is examined using a combination of fatty acids, glutamate and succinate. Future studies are needed to determine if *Mc4r-/-* mitochondria have an increased ability to oxidize a specific substrate. The results obtained by *ex vivo* cardiac respirometry also stand in contrast to the reduction in O_2

consumption described using indirect calorimetry (Ste Marie et al., 2000). However, permeabilized tissue preparations are not a true measurement of true oxygen consumption rate. Rather, these studies measure of how much capacity for oxidation a tissue has when given a set amount of substrate. *In vivo*, cells must take up substrates before they can be oxidized. It is also possible that such changes are due to changes in hormones other than insulin. Recent studies have also shown that *Mc4r-/-* mice have altered GLP-1 homeostasis (Brandon L. Panaro et al., 2014). However, the effect that this change in substrate and hormonal milieu has on myocardial mitochondrial function remains to be determined. Furthermore, patients with heterozygous loss of MC4R display reduced suppression of the growth hormone axis. Overexpression or overproduction of growth hormone is deleterious to both heart structure and function. Thus, a growth hormone mechanism provides a plausible link between reduced MC4R expression in the brain and reduced cardiac function.

CHAPTER 4

DISCUSSION AND FUTURE DIRECTIONS

Through the course of this work, a new understanding of MC4R's role in heart health has been elucidated. Previous studies have examined how MC4R deficiency protects against obesity-associated hypertension in both mice and humans (A. A. da Silva et al., 2015) (Greenfield et al., 2009). This work shows that *Mc4r-/-* mice develop dilated cardiomyopathy as they get older. 30 week old *Mc4r-/-* mice display reduced contractility, cardiac dilatation, bradycardic arrhythmias and cardiomegaly. Ultrastructural imaging further demonstrates structural abnormalities within the heart. High-resolution respirometry of these tissue demonstrates an increased O2 consumption capacity. The cardiac abnormalities and mitochondrial dysfunction of *Mc4r-/-* mice described in this dissertation provides a foundation for future studies to determine the molecular mechanism(s) that underlies this phenotype. These findings also have putative clinical implications. Patients with MC4R deficiency and MC4R heterozygosity should be followed for cardiomyopathy, ECG abnormalities, and potentially chemotherapy-associated cardiotoxicity.

Hyperinsulinemia and Cardiomegaly

In the *Mc4r-/-* mouse, cardiomegaly is proportional to increased lean mass at 30-weeks of age (Figure 13A-C). This finding is suggestive of an endocrine mediator. One possible explanation for this finding is chronic hyperinsulinemia. The MC4R obesity

syndrome is characterized by both an early onset normoglycemic hyperinsulinemia and increased linear growth in both mice (Fan. W et al., 2000) and humans (Martinelli, C. et al. 2011). Hyperinsulinemia is associated with myocyte hypertrophy (Paternostro, Pagano, Gnecchi-Ruscone, Bonser, & Camici, 1999) and can promote a cardiomegalic phenotype (Susa et al., 1984). In this study, the heart weights of *Mc4r-/-* mice are no different than lean controls at 6 of age despite early this onset hyperinsulinemia (Figure 13B). However, there is a trend towards increased heart weight in 12-week-old *Mc4r-/-* mice which is in proportion to the slight increase in lean mass seen at this age (Figure 13B). Indeed, increased heart weight (Figure 13D) is not found in weight matched high fat fed controls. Therefore, there is possibly a difference between the insulin signaling in *Mc4r-/-* mice and DIO mice that could explain why *Mc4r-/-* have a disproportionately larger heart and lean mass component.

Impairment of insulin sensitivity and glucose tolerance has been shown to play a role in the development of cardiomegaly and heart failure through a variety of mechanisms including oxidative stress, mitochondrial dysfunction, altered substrate utilization, ER stress and impaired Ca2+ handling (Boudina S & Abel E. 2007, Guanghong J et al., 2016) Therefore, we characterized the glucose tolerance by GTT and insulin sensitivity of *Mc4r-/-* and DIO controls using a phospho-specific pAKT-T308 antibody. In these experiments, no difference in glucose tolerance or myocardial insulin sensitivity was observed between *Mc4r-/-* and DIO mice (Figure 9C). This is consistent with clinical studies that find no difference in insulin sensitivity between MC4R deficient subjects and weight matched controls using hyperinsulinemic euglycemic clamps

(Greenfield J et al., 2009). These findings suggest that *Mc4r-/-* mice develop increased cardiac mass by 30 weeks of age that is independent of insulin sensitivity and indicates that other factors may also be involved.

One possibility is alterations in the growth hormone-> IGF1 pathway. Supraphysiological growth hormone and IGF1 levels are a known cause of cardiomegaly and heart failure (Rajasoorya, Holdaway, Wrightson, Scott, & Ibbertson, 1994). Obesity is associated with a suppression of this pathway through increased insulin signaling on GHRH neurons in the hypothalamus (Israel et al., 2012). Humans with MC4R deficiency display reduced suppression of this neuroendocrine axis in response to obesity (Martinelli et al., 2011). While this has been challenged by a recent study in the mouse (Tan et al., 2016), obese weight matched controls were not examined. In our studies, we find an increased signature of Insulin/IGF signaling in our RNAseq pathway analysis (Figure 24A). Since insulin signaling does not appear to be causal in this disease, it is possible that both hyperinsulinemia, and incomplete suppression of the GH-> IGF1 signaling both contribute to cardiomegaly. A combined role of hyperinsulinemia and excessive GH->IGF1 signaling could be examined through the chronic administration of the somatostatin analog octreotide. This peptide suppresses both hormone pathways and has been shown to improve cardiac function in patients with acromegaly (Akaza et al., 2009; Hwang et al., 2007).

Role of Mitochondrial Dysfunction in MC4R associated cardiomyopathy

According to the Frank Starling Mechanism (Tewari et al., 2016), increased end

diastolic volume (a measure of pre-load) results in an increased ejection fraction on the following beat. However, any reduction in contractility seen during systolic failure prevents this physiological response. This failure to normalize end diastolic volume is further impaired by an increase in wall tension due to Laplace's Law (Hill & Olson 2008).

Equation 1

$$T = \frac{P \times r}{2h}$$

Where: T=wall tension, P=transmural pressure, r=chamber radius, h=wall thickness

Normally, this precipitates an increase in sympathetic tone. Since the hearts of *Mc4r-/-* animals do not display increased wall thickness, the observed increase in chamber size results in increased in wall tension. Why *Mc4r-/-* hearts do not hypertrophy appropriately may be due to chronically reduced sympathetic tone (Triposkiadis et al., 2009). Increased wall tension requires more force to be generated for each subsequent contraction. Since *Mc4r-/-* hearts are 33% more dilated (Figure 4E) this would mean a proportional increase in surface tension. The force needed to counteract this surface tension results from ATP cleavage of myosin heads running along actin filaments. Therefore, it would make sense that *Mc4r-/-* hearts require more ATP generation per unit area. This can be accomplished by either increasing mitochondrial number (a precarious option in the space limited myocardium) or by increasing the capacity to generate ATP through oxidative phosphorylation. This appears to be the case in the *Mc4r-/-* mouse. While we do not note increased ATP content, this method is simply a

snap shot of basal ATP levels and does not represent the ATP flux through the cell. Furthermore, the exact mechanism that increases mitochondrial respiration, such as increased super complex formation, increased proton motive force, or allosteric modulation, remains unknown. Each of these possibilities could be respectively examined experimentally by 2D-Blue native gel electrophoresis (Acín-Pérez, Fernández-Silva, Peleato, Pérez-Martos, & Enriquez), mitochondrial membrane potential dyes (Perry, Norman, Barbieri, Brown, & Gelbard, 2011), and shotgun proteomics (Kruse & Hojlund, 2017). No matter the underlying cause, this increase in respiration appears maladaptive over the long run.

Reactive oxygen species production in the heart is byproduct of mitochondrial respiratory activity by complex III & I and can result in heart damage and failure (Brown D. et al., 2017). An increase in heart ROS production that is proportional to the increase in respiratory capacity and increases with age was found in *Mc4r-/-* hearts. Older *Mc4r-/-* mice have a 2 fold increase in tissue ROS (Figure 22B) and a 2 fold increased maximal respiratory activity (Figure 17C). Younger *Mc4r-/-* mice have a 1.5 fold increased in ROS (Figure 22C) and a 1.5 fold increase in maximal respiratory activity (Figure 19C). The link between these two findings remains untested. However, both ROS formation and measured state 3 respiratory activity go up in response to increased mitochondrial membrane potential (Nicholls D, 2004) and contributes to age associated tissue damage. While an increase in mitochondrial membrane potential is a possible source of ROS production in these animals, this hypothesis remains to be tested. Since we observed mitochondrial abnormalities by respirometry in young lean *Mc4r-/-* mice

(Figure 19A-C) not yet exhibiting significant cardiac dysfunction, it is possible that defective development and/or regulation of cardiomyocyte function contributes to the defective cardiac function seen by 26 weeks of age.

Understanding the mechanism of *Mc4r-/-* cardiomyopathy.

For this dissertation, the aim has been to ensure that the MC4R cardiomyopathy phenotype is robust and not due to other confounders such as obesity or carrier mutations. Now that the MC4R phenotype is established, the next step is to determine the molecular mechanism that links the loss of MC4R with the development of cardiomyopathy. The work presented in this dissertation has provided some clues for studies that seek to address this question. The fact that MC4R is not expressed in the adult heart (Figure 11A-C) highlights the unlikelihood of a cell autonomous mechanism. However, the expression studies presented here have only examined the MC4R in healthy adult mouse heart. It is possible that MC4R expression in the developing heart plays a role in cardiomyocyte development or during disease process stimuli (e.g. hypertension or insulin resistance). Developmentally restricted expression of the MC4R has been observed in E14 through E18 rat heart (Mountjoy, Jenny Wu, Dumont, & Wild, 2003) but the development relevance of this finding remains unexplored. Examination of the Gene Expression Omnibus (GEO) reveals that MC4R expression is low in control hearts but becomes increased 4 fold following the development of hypertension associated heart failure (Figure 27) (Brooks, Shen, Conrad, Goldstein, & Bing, 2010). It is unclear if this change is adaptive, maladaptive, present in humans/mice or even

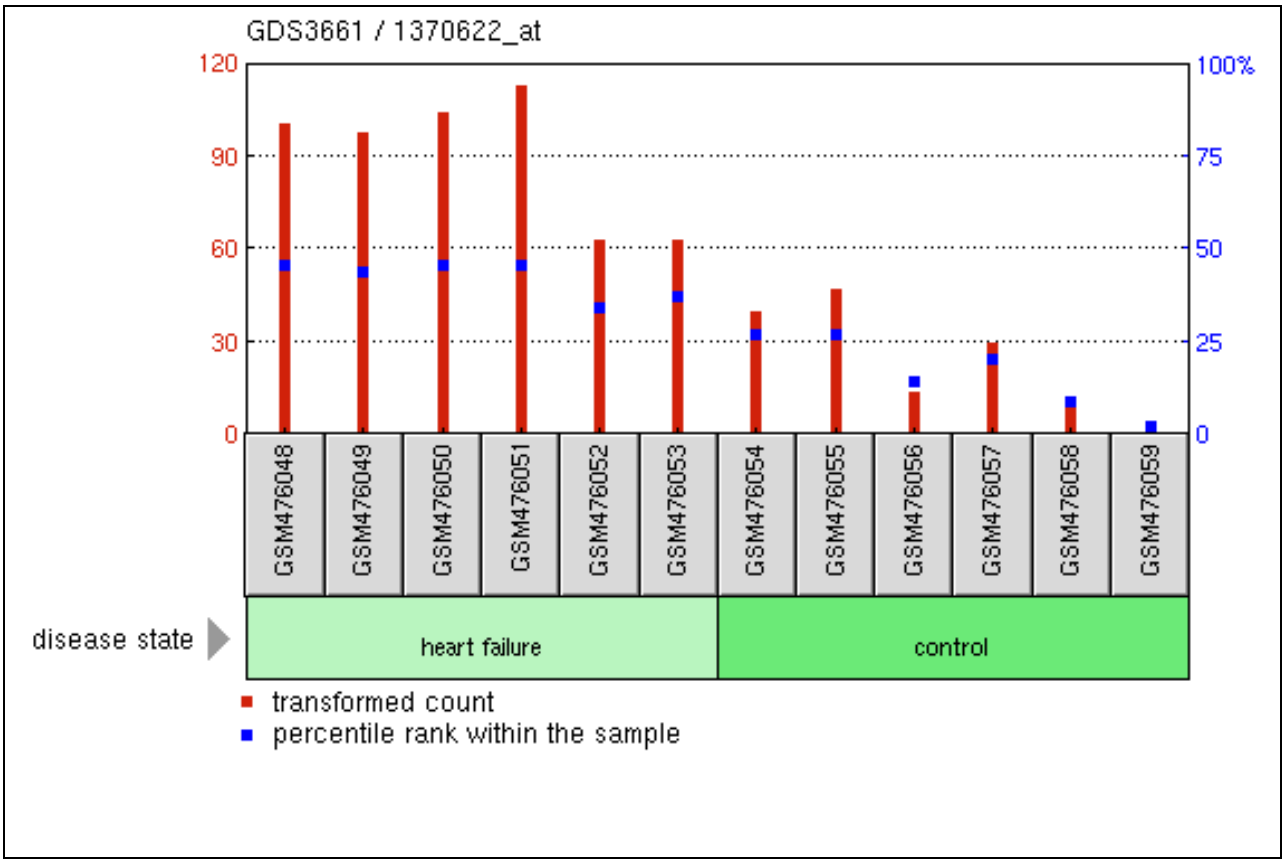

Figure 27 MC4R expression in the heart following the onset of hypertension-associated heart failure in rats.

Data from the GEO database indicates that MC4R mRNA may be up regulated during times of heart failure. Lack of this process is one reason why DIO mice are protected from heart failure.

physiologically relevant. However, serum levels of ACTH are increased during heart failure and would provide the MC4R with an endogenous agonist (Yamaji et al., 2009).

Site-specific MC4R knockout and rescue studies would be invaluable in addressing possibility of a developmental or adaptive cell autonomous function. Heart specific MC4R knockout and rescue could be generated to directly test the developmental and adaptive hypothesis. $MC4R^{flox/flox}$ and MC4R-$loxTB^{+/+}$ mice crossed the Myh6-Cre (Sohn et al., 2013) (Agah et al., 1997) would respectively delete or rescue MC4R expression throughout development. Absent any positive results from these mice, additional studies may necessary to determine if MC4R cardiomyopathy operates via a two hit paradigm. For instance, it is possible that MC4R deficiency alone is not sufficient for heart failure. Rather, MC4R may simply sensitize the animal to cardiac dysfunction. This would necessitate an event to precipitate dysfunction such as obesity, doxorubicin administration or trans-aortic banding. Therefore, all negative studies should be followed up with a cardiotoxic stimulus to ensure that any phenotype has not been masked.

Absent a role for early developmental or adaptive expression in mouse cardiomyocytes, the prominent expression of the MC4R in the central and peripheral nervous system implicates an autonomic mechanism. An echocardiographic characterization of $ARC^{POMC-KO}$ mice was a first attempt to localize the source of this pathology to central MC4R signaling. These studies should be interpreted cautiously and must be performed on conscious mice before any strong conclusions can be drawn. However, these mice appear to have normal cardiovascular function when examined

under anesthesia (Figure 12) and have normal mitochondrial function in the Oroboros system (Figure 21). An ideal approach to the role of central MC4R in disease pathogenesis is to knockout MC4R in the brain early in development. This can be performed by crossing the $MC4R^{flox/flox}$ mouse with the Nestin-Cre mouse (Tronche et al., 1999). Identification of cardiomyopathy in these animals would spurn the investigation into site-specific MC4R knockout by way of Phox2b-Cre (for the DMV and NTS), DBH-Cre (for sympathetic neurons), and SIM1-Cre (for PVN MC4R neurons) mice. While autonomic derangement is likely based on the observed bradycardic arrhythmias (Figure 5), endocrinological mechanisms such as the hyperinsulinemia or abnormal obesity associated growth factor suppression may also need to be considered. Once a population of neurons is identified, the use of chemogenetics would be a powerful tool with which to investigate how acute changes in the activity of these neurons leads to changes in heart function/metabolism.

The notion that this phenotype may be reversible is also compelling line of inquiry. This possibility can be examined by crossing the MC4R-loxTB mouse with the Rosa26-Cre2-ERT2 mouse (Ventura et al., 2007). Tamoxifen could be injected in young mice or after the development of cardiomyopathy to see if MC4R rescue can protect against or reverse heart failure respectively. Again, any negative results from such studies will need to be contextualized by the rescue efficiency and any other unchanged negative metabolic adaptation such as obesity or insulin resistance. A positive result to such a study would also lend credence to the use of MC4R agonists for the treatment of heart failure.

MC4R heterozygosity and personalized medicine

Homozygous loss of MC4R function, and homozygous loss of proopiomelanocortin gene function, a preprohormone precursor of the endogenous MC4R agonist, have both been reported in patients with early onset obesity (Farooqi et al., 2003; Krude et al., 1998). Based on our findings, these patients, though rare, should be followed for cardiomyopathy. Although most of these studies were conducted on *Mc4r-/-* mice, it is important to note that a trend towards reduced cardiac function was seen in *Mc4r+/-* mice, as demonstrated by reduced fractional shortening in both our aging study (Figure 4C) and in our doxorubicin sensitivity study (Figure 26). Heterozygous hypomorphic/null alleles of the MC4R are common, with an allele frequency of 1/1500 (I. Sadaf Farooqi et al., 2000). Since most phenotypes characterized in *Mc4r+/-* mice have translated to *Mc4r+/-* patients (Greenfield et al., 2009; van der Klaauw et al., 2016), patients with heterozygous MC4R mutations should also be followed as they may have an increased risk for the development of heart failure.

Patients with dominant negative MC4R mutations should also be identified and followed as they more closely reflect the *Mc4r-/-* syndrome (Biebermann et al., 2003; Y. X. Tao, 2005; Tarnow et al., 2008). The doxorubicin results (Figure 26) also suggests that common mutations in the MC4R may be an important risk factor for the development of heart failure in the context of another cardiac stressor such as doxorubicin (Singal & Iliskovic, 1998).

CHAPTER 5

METHODS

Mouse Husbandry

Unless otherwise noted, mice were bred within the barrier facility of the Vanderbilt University mouse vivarium. Heterozygous male mice older than 8 weeks of age were crossed with similarly aged heterozygous female mice to generate litters with knockout, heterozygous and wild type genotypes. 3 weeks after birth, pups were weaned in to new cages, 5 mice per cage, segregated by sex. Mice were maintained on a 12 hour light-dark cycle and housed at ambient temperature (~23C) on corn cob bedding within the non-barrier facility of the Vanderbilt University mouse vivarium. Unless other wise noted, mice were fed a chow diet (Lab Diet; St. Louis, MO; S-5LOD - 13.5 kcal% fat, 32.98 kcal% Protein, 56.7 kcal% Carbohydrate). For high fat diet studies (Research Diets; New Brunswick, NJ; D12492 - 60 kcal% fat, 20 kcal% Protein, 20 kcal% Carbohydrate), food was administered starting at 4 weeks of age and continued throughout the study. For all post mortem studies, v. Tissues were rapidly collected and snap frozen in liquid nitrogen.

Mice were then genotyped using tissue samples from ear punches and tagged with a unique identifier (National Brand and Tag). Ear punches were then digested (Sigma) in 25µL digestion buffer (E7526) with 6.5µL tissue prep solution (T3073) for 15 minutes at room temperature and then 3 minutes at 95C. Samples were then cooled on ice and 25uL of neutralization buffer was added (N3910). 1uL of template was then

added to a PCR reaction mixture and ran as outlined in Table 2 Genotyping Primers and Protocols. Once the reaction was complete, products were separated by gel electrophoresis using a 2% agarose gel in TAE and visualized with ethidium bromide (1:10,000). The genotype was determined in band size comparison to positive/negative controls and recorded for future experiments. All mouse lines were maintained on a C57BL/6J background with yearly backcrosses to wild type C57 mice (Jackson Laboratory; Sacramento, California - Jax Stock No: 000664).

Mouse Lines

Mc4r-/- mice were generated by Huszar et al. (1997). A 4.5kb targeting vector with a Neomycin cassette vector was transfected into mouse embryonic stem cells (RF-8 ES cell line) by electroporation. Neomycin resistant cells were selected for with G418 and resistant colonies were picked and injected into C57BL/6J mice to generate chimeras that were then were bred with C57BL/6J females. This mouse has since been backcrossed >20 times to C57BL/6J. LoxTB MC4R mice (Jax Stock No: 006414) were generated using similar strategy to the *Mc4r-/-* mice. A *loxp* flanked transcriptional blocker (loxTB) was inserted between the transcriptional start site and the start codon of MC4R to create the targeting vector (Balthasar et al., 2005). MC4R-Tau-Sapphire transgenic animals (Jax Stock No: 008323) were generated by H. Liu et al. (2003). A blue shifted GFP variant was fused with the tau coding sequence followed by a polyA signal. This vector was then inserted into the ATG start site of bacterial artificial chromosome (BAC) of MC4R flanking regions (+2.5kb -1.7kb). This BAC was then transformed into recombination deficient *E. Coli* using a shuttle vector (PSV1) with a

temperature sensitive ORI, a tetracycline resistance gene and a recombination gene (*RecA*). *E. coli* harboring the MC4R-tau-Sapphire BAC was then selected using temperature and tetracycline. The BAC was then purified, linearized and injected into the pronuclei of CBA/C57Bl6J mice. ARC^{POMC} deficient mice were generated by Lam et al. (2015). This mouse contains insertion of a neomycin resistance gene within the 5' neural enhancer region of POMC. Phenotypically, this results in loss of POMC expression within the ARC but retained expression in the pituitary and NTS.

Echocardiography

Echocardiography was performed using the VEVO® 2100 digital ultrasound system (Visual Sonics; Toronto, Ontario). Studies were performed using a MS400 18–38 MHz transducer on conscious mice. Conscious echocardiography has several benefits when compared to using anesthesia. The primary benefit is the lack of anesthesia mediated cardiac depression (Janssen, Debets, Leenders, & Smits, 2002). Mice were restrained on a heated platform in the supine position using tape and given 2% oxygen throughout the procedure. Fur was then removed using a chemical depilatory (Ca^{2+}-thioglyoic acid with $CaOH_2$). Initial images are taken with transducer oriented to obtain a parasternal long axis image in Brightness-Mode (B-Mode). After obtaining this image, the transducer was rotated to obtain a short axis image at the level of the mid-papillary muscle. Simultaneous one lead ECGs were preformed on the heated platform. Once in position, Motion-Mode (M-Mode) images were taken for further processing. M-mode images were then processed using the Visual Sonics Software ver2.2. Left ventricular internal dimension at diastole (LVIDd), Left ventricular internal

dimension at systole (LVIDs) and heart rate (HR) measurements were made in a blinded manner using the LV trace function while the left ventricular posterior wall at diastole (LVPWd) measurement was obtained using the ruler function. Fractional shortening (FS) and ejection fraction (EF) were calculated according using the following set of equations:

Equation 2

FS = 100 * ((LVIDd – LVIDs) / LVIDd)

Equation 3

LV Vol d = [7.0 / (2.4 + LVIDd) * $LVIDd^3$]

LV Vol s = [7.0 / (2.4 + LVIDs) * $LVIDs^3$]

EF = 100 * (LV Vol d – LV Vol s) / LV Vol d

Glucose tolerance testing

In order to assess insulin action, glucose tolerance tests were performed (Ayala et al., 2010). Two weeks prior to glucose tolerance test. Mice were housed individually and handled by scruffing and injecting .1mL saline for three times each week. One week prior to the experiment, body composition was obtained by NMR (mq10 Minispec; Bruker; Billericia, Massachusetts). Following habituation, mice were fasted for 4 hours from 2pm-6pm. Two hours prior to the experiment, the distal 1mm of the tail was removed with scissors. A basal glucose reading was obtained using a hand held glucometer (OneTouch Ultra) and mice were then injected with a 2mg/kg lean mass dose of glucose in PBS. Glucose readings were then obtained at 15, 30,60, and 120 minutes following glucose injection for each mouse at 1-minute intervals. Blood glucose

was obtained and mice were then injected with a 2mg/kg lean mass dose of glucose in sterile PBS.

Transmission Electron Microscopy

Samples were fixed with 2.5% glutaraldehyde in a 0.1M sodium cacodylate buffer. Following fixation, the samples were washed in 0.1M sodium cacodylate buffer. After washing, the samples were postfixed with 1% osmium tetroxide in 0.1M cacodylate buffer and then further washed in a 0.1M cacodylate buffer. The samples were then dehydrated through a graded series of increasing ethanol concentrations and infiltrated with epoxy resin. The samples were oriented and the epoxy resin cured in flat-embed molds. Thick sections of the embedded tissue were cut, stained with 1% Toluidine blue, and reviewed to determine location. When the correct structure was identified in thick sections, a region of interest was selected for thin sections. Thin sections were stained with 2% aqueous uranyl acetate and Reynolds' lead citrate. Samples were viewed using a FEI Tencai T-12 electron microscope (FEI Tencai; Hillsboro, Oregon) operating at 100 keV.

Mouse genotypes were blinded during imaging to avoid sampling bias. Images were obtained from 3 random EM grids per sample at 4400x. Additional images were taken at 11,000x, 15,000x, 21,000x and 42,000x. Additional features, such as myocyte nuclei and endothelial cells were also imaged. A trained pathologist analyzed all images in a blinded manner.

Histology

Mice were deeply anesthetized with 5mg/kg tribromoethanol and then sacrificed

by decapitation. Heart dissection was performed using an inferior approach through the diaphragm. The inferior vena cava was localized and clamped with hemostats. A cut was then made distal to the clamp and the heart was elevated to localize and cut the superior vena cava. By gently elevating the heart, the pulmonary veins could be visualized and severed. After a further elevation the outflow tracts are visualized and cut proximal to the right subclavian artery. Once isolated, the hearts were moved into a PBS solution to wash away any remaining blood, blotted dry, weighted, and then placed into a 10% formalin solution for 48 hours. After 48 hours, hearts were removed from the formalin and apical chunks were removed for Oil Red O staining. These sections were cryopreserved in a 15% sucrose-PBS solution for 24 hours and then transferred to a 30% sucrose solution for 48 hours. After cryopreservation, samples were moved into a block with OCT and frozen on dry ice.

For paraffin embedding, samples were dehydrated in increasing concentrations of ethanol. Samples were dehydrated using the following gradient: 70% ethanol solution – 1 hour, 95% ethanol solution – 1 hour, 100% ethanol solution – 4x1 hour, Xylene –2x1 hour Paraffin wax – 2x 1 hour at 58C with gentle agitation. 5µm sections were then cut using a microtome and tissue was bonded to slides at 65C for 20 minutes. For Oil Red O sections a freezing microtome was used and sections were mounted onto permafrost slides. H&E slides were dehydrated using the inverse gradient to that described above for embedding and stained using standard protocols. Oil Red O frozen sections were also stained using a standard protocol.

Western Blotting

Tissue samples were snap frozen in Liquid N_2 and then transferred to -80 ^{O}C. Tissue was lysed in Radio Immune Assay Buffer (50mM Tris, 150mM NaCl, 1% Triton X-100, 0.5% Na-Deoxycholate, 0.1% SDS, cOmplete^{TM} EDTA-Free Protease Inhibitor (Roche) Phos Stop (Roche) using a tissue homogenizer (Pro-Scientific 200; Oxford, Connecticut). Following lysis, protein samples were kept on ice for 30 minutes, spun at max speed for 30 minutes and then quantified by Bradford assay (BioRad; Hercules, California). Sample protein content was adjusted to 2mg/mL and then diluted with 2x Laemmli buffer with 2% BME (1% final). Sampled were then run on a Mini-Protean gel, transferred to PVDF membranes, blocked for 1hour in TBS-T 5%BSA solution and incubated with respective antibodies overnight (Total OX-Phos Rodent WB Cocktail, 1:1000; Abcam; Cambridge, United Kingdom) (GAPDH, 1:5000; Cell Signaling; Boston, Massachusetts) (GFP, 1:1000; Abcam). After washes in TBST, membranes were incubated with 2^{O} antibodies conjugated (1:10,000; Promega; Madison, Wisconsin) with HRP for one hour. After this incubation, membranes were again washed with TBST, exposed to ECL and imaged (ChemiDoc MP; BioRad; Hercules, California).

High Resolution Respirometry

After sacrifice, samples were rapidly placed in ice-cold MiR05 buffer (0.5mM EGTA, 3mM $MgCl_2$-6 H_2O, 60mM Lactobionic acid, 20mM Taurine, 10mM KH_2PO_4, 20mM HEPES, 110mM D-Sucrose, 1g/L Essentially Fatty Acid Free BSA) with an additional 2mM EGTA to chelate extracellular calcium. Samples were permeabilized as

previously described (Talati et al., 2016). Briefly, samples were separated into fiber bundles using forceps under a dissecting scope. Samples were then moved into a MiR05 + 2mM EGTA + 50µg/mL saponin solution and incubated for 30 minutes on ice. Samples were then washed twice by incubation in MiR05 buffer with 2mM EGTA for 15 minutes. Samples were then blotted dry and weighed so that a 2-4 mg sample was obtained. This sample was then placed in a pre-equilibrated chamber of an O2k Oxygraph (Oroboros Instruments; Innsbruck, Austria) that contained MiR05 buffer without additional 2mM EGTA. Chambers were then closed and O_2 consumption rate was measured in response to sequential additions of 10mM glutamate and 2 mM malate, 0.05 mM Palmitoylcarnitine, 2.5 mM ADP, 0.25 mM Octanoylcarnitine, 10 mM Succinate and 500 nM CCCP.

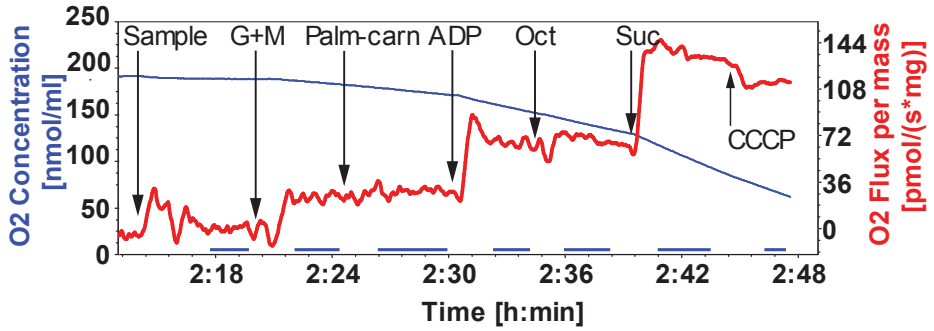

Figure 28 Representative high-resolution respirometry trace

ROS assays

All ROS assays were conducted according to the manufacturer's directions. For ROS (OxiSelect™ *In Vitro* ROS/RNS Assay Kit; Cell Biolabs, Inc.; San Diego, California) assays were conducted on tissue lysates from frozen tissue samples. Samples were weighted (10mg/sample), homogenized in PBS and centrifuged (10,000g, 5 minutes,

4^{O}C). Following sample preparation, assays were conducted according to the manufacturer's directions. MDA content was obtained using MDA lipid peroxidation assay (Abcam) according to the manufacturer's directions. For 4-HNE, the OxiSelect^{TM} 4-HNE Assay Kit (Cell Biolabs, Inc.) was used. Samples were homogenized in RIPA buffer with inhibitors and analyzed according to the manufacturer's directions.

RNA Isolation

RNA was isolated using TRIzol® (Thermo Fisher Scientific; Waltham, Massachusetts). 1mL of Trizol was added to 10mg tissue samples from the posterior wall of the left ventricle. Samples were homogenized using the TissueLyser II (Qiagen; Venlo, Netherlands) at max speed for 3 minutes. Samples were then centrifuged for 10 minutes at 4 ^{O}C at 10,000g to eliminate debris. After a 5-minute incubation at room temperature, 200µL of chloroform was added and the samples were shaken vigorously. After an additional 3-minute incubation at room temperature, samples were centrifuged at 4^{O}C and 12,000g to separate phase layers. The upper phase was then mixed with 100% EtOH and added directly onto RNeasy (Qiagen) columns. Columns were used as instructed by the manufacturer and included an on column DNase (Quiagen).

RNA-seq

Total RNA quality was assessed using the 2100 Bioanalyzer (Agilent; Santa Clara, California). 200ng of DNase-treated total RNA with a RNA integrity number greater than 7 was used to generate polyA-enriched mRNA libraries using KAPA Stranded mRNA sample kits with indexed adaptors (Roche; Basel, Switzerland). Library

quality was assessed using the 2100 Bioanalyzer (Agilent) and libraries were quantitated using KAPA Library Quantification Kits (Roche). Pooled libraries were subjected to 75 bp paired-end sequencing according to the manufacturer's protocol (HiSeq3000; Illumina; San Diego, California). Bcl2fastq2 Conversion Software (Illumina; San Diego, California) was used to generate de-multiplexed Fastq files. Read quality was checked using FastQCv0.11.5 (Babraham Institute, Cambridge, UK). Fastq data files were then imported into Galaxy (Afgan et al., 2016) and converted to a fastsanger file. A quality control was run and reads were then mapped to the mm10 mouse reference genome with *Tophat* v2.1.0 (Trapnell et al., 2012). Reads were then assembled into transcripts using *Cufflinks* v2.2.1 and merged using *Cuffmerge* v2.2.1. RMPK values were then quantified using *CuffQuant* v2.2.1. *Cuffnorm* v2.2.1.1 was then used to normalize counts for transcript length. Differential expression of transcripts was determined using the *Cuffdiff* v2.2.1.3 program and filtered for significance $q>0.05$. Once differential gene expression was determined, Gene Set Enrichment Analysis (GSEA; Broad Institute; Cambridge, Massachusetts) was used for pathway analysis and to determine enriched gene sets as previously described (Subramanian et al., 2005) (Mootha et al., 2003). Pathway analysis was conducted using PANTHER Pathway analysis on significantly different transcripts identified by RNA-seq (Mi & Thomas, 2009). Lincs cloud analysis was run as previously described (J. Liu, Lee, Salazar Hernandez, Mazitschek, & Ozcan).

qRT-PCR

cDNA was generated with iScript™ (BioRad; Hercules, California) according to the manufacturer's instructions. qRT-PCR was performed using POWER Syber® master mix (Thermo Fisher Scientific) with the following primers:

Primer	Sequence
mMC4R F	CCCGGACGGAGGATGCTAT
mMC4R R	TCGCCACGATCACTAGAATGT
mPGC1-a F	GCCGTGACCACTGACAACGAGGC
mPGC1-a R	GCCTCCTGAGGGGGAGGGGTGC
mMyl4 F	CGGACTCCAACGGGAGAGAT
mMyl4 R	GCTCCTTGTTGCGGGAGAT
mH19 F	GTACCCACCTGTCGTCC
mH19 R	GTCCACGAGACCAATGACTG
mCytB F	GTCCACGAGACCAATGACTG
mCytB R	ACTGAGAAGCCCCCTCAAAT

Table 1 qPCR primers

All PCR was performed on using standard cycling conditions on a Quantstudio 12k Flex Real Time PCR system (Thermo Fisher Scientific). Data was analyzed using the ΔΔCT method. All statistics were performed by comparing ΔCT values between groups and plotted as Fold Change+/- SEM ($2^{\Delta\Delta CT}$).

ATP assay

Fresh tissue was isolated from posterior left ventricular wall, weighted and placed into a 2N perchloric acid solution, homogenized and then incubated on ice for 30 minutes. Samples were then centrifuged (13,000g for 2 minutes at $4^{O}C$) and 100µL of supernatant was added to 500µL of assay buffer. Samples were then neutralized with 2M KOH, vortexed and centrifuged (13,000g for 15 minutes at $4^{O}C$) to remove PCA.

The resulting supernatant was then used in the Fluorometric ATP Assay Kit (Abcam) according to the manufacturer's instructions.

Doxorubicin Studies

Doxorubicin (Cayman Chemicals #15007) was solubilized in isotonic saline at a concentration of 1mg/mL. 28 week old *Mc4r+/-* and WT mice received two intraperitoneal injections of 5mg/kg doxorubicin or vehicle separated by 7days (cumulative dose of 10mg/kg). Body weights were measured prior to injection. One week following the second injection, mice were examined by echocardiography as previously described.

Statistics

Sample size estimation for echocardiography studies was conducted using the power equation ($\alpha<0.05$, $\beta=0.1$, $\Delta\mu=25\%$ $\sigma=5$). Remaining sample sizes were estimated based on previous publications. All statistical tests were conducted on the GraphPad Prism 6 software (Scientific Software; La Jolla, California). Data is presented as mean +/- standard error of the mean. All data with $p<0.05$ was considered statistically significant. Statistical nomenclature: * OR ^ = $p<0.05$; ** = $p<0.01$; *** = $p<0.001$; **** = $p<0.0001$.

MC4R-tau-Saphire Genotyping					
1: 115 GFP Fwd	GAT GCC ACC TAC GGC AAG CTG		**Temp (°C)**	**Time (min)**	**# of Cycles**
2: 116 GFP Rev	ACA GCT CGT CCA TGC CGA GAG		94	5:00	1
3: IC 210 Fwd oIMR 0015	CAA ATG TTG CTT GTC TGG TG		94	0:45	39
4: IC 210 Rev oIMR0016	GTC AGT CGA GTG CAC AGT TT		60	0:45	39
Primer combination	**Band (kB)**	**genotype**	72	0:45	39
1&2	~600	GFP positive	72	7:00	1
3&4	~210	Internal Control	10	n/a	n/a

MC4R-loxTB Genotyping					
1 - LoxTB MC4R WT Fwd	GCA GTA CAG CGA GTC TCA GG		**Temp (°C)**	**Time (min)**	**# of Cycles**
2 - LoxTB MC4R WT Rev	CTC CAA CAG GCT TAT GAC ACC		94	5:00	1
3 - LoxTB MC4R Mut Fwd	GTG CAA GTG CAG GTG CCA G		94	0:30	35
Primer combination	**Band (kB)**	**genotype**	62	0:30	35
1 + 2	500	KO	72	0:45	35
1 +2, 3 + 2	400 & 500	Het	72	5:00	1
3 + 2	400	WT	10	n/a	n/a

MC4R-neo Genotyping					
1 -MC4R Fwd	CAC TCG GAG CTT CCC TGA CCC AG		**Temp (°C)**	**Time (min)**	**# of Cycles**
2 –MC4R Rev	GAC CAT GGT TTC CGA CCC ATT		94	5:00	1
3 –Neo Rev	TTC CAA GCC TCT GAG CCC AGA		94	0:45	40
Primer combination	**Band (bp)**	**genotype**	66	0:45	40
1& 3	~540	KO	72	0:45	40
1& 3 + 1 & 2	~540 + ~400	Het	72	7:00	1
1 & 2	~400	WT	10	n/a	n/a

**** All genotyping for ARC POMC Knockout mice was performed by the Low lab.**

Table 2 Genotyping Primers and Protocols

APPENDIX A

[3]CHARACTERIZATION OF MC4R REGULATION OF THE KIR7.1 CHANNEL USING THE Tl^+ FLUX ASSAY

Abstract

The family of inward rectifying potassium channels (Kir channels) plays crucial roles in regulation of heart rhythms, renal excretion, insulin release and neuronal activity. Their dysfunction has been attributed to numerous diseases such as cardiac arrhythmia, kidney failure and electrolyte imbalance, diabetes mellitus, epilepsy, retinal degeneration, and other neuronal disorders. We have recently demonstrated that the melanocortin-4 receptor (MC4R), a $G\alpha_s$-coupled GPCR, regulates Kir7.1 activity through a mechanism independent of $G\alpha_s$ and cAMP. In contrast to the many other members of the Kir channel family, less is known about the biophysical properties, regulation, and physiological functions of Kir7.1. In addition to using conventional patch clamp techniques, we have employed a high throughput Tl^+ flux assay to further investigate the kinetics of MC4R-Kir7.1 signaling *in vitro*. Here, we discuss the employment of the Tl^+ flux assay to study MC4R -mediated regulation of Kir7.1 activity and to screen compounds for drug discovery.

[3] Text and figures are from Litt et al. 2017 *Mol. Methods*

Introduction

Inward rectifying K^+ currents (Kir) were first identified more than a half a century ago (Katz, 1949). Since their discovery, seven subfamilies of Kir channels have been characterized (Hibino et al., 2010). Kir channels regulate critical cellular parameters including resting membrane potential, action potential duration and hormone release. Due to their role in regulating these processes, Kir channels are critical for the proper function of cardiac myocytes, neurons, pancreatic b-cells, renal epithelial cells, glia and epithelial cells. Thus, a better understanding of how Kir channels are regulated holds great potential for future drug discovery.

Invariably, Kir channels are commonly regulated by the signaling lipid PIP_2 that enables channel opening through direct binding (Furst, Mondou, & D'Avanzo, 2014; Hilgemann & Ball, 1996). Besides PIP_2, factors that gate Kir channel conductance are unique to each sub-family. For instance, the G protein-coupled inward-rectifying channels (GIRK, Kir3.x) are opened by the βγ subunits of heterotrimeric G proteins (Pfaffinger, Martin, Hunter, Nathanson, & Hille, 1985), while Kir6.2 (K_{ATP}) is sensitive to intracellular ATP levels (S. J. Tucker et al., 1998). Despite extensive understanding of some Kir channels, the regulatory mechanisms of other Kir channels, including Kir7.1 remain largely uncharacterized.

Recently, our group used patch clamp electrophysiology to describe how Kir7.1, a low conductance weakly rectifying Kir subtype, is regulated by the Melanocortin 4 Receptor (MC4R)– Gs coupled GPCR (Ghamari-Langroudi et al., 2015). We observed

that MC4R activation decreases Kir7.1 opening even in the presence of G_s inhibitors. In order to understand the molecular mechanisms underlying this interaction, we created a heterologous expression system in HEK293 cells and adapted a thallium (Tl^+) based screening platform for quantification of channel opening (Weaver, Harden, Dworetzky, Robertson, & Knox, 2004).

The use of Tl^+– an equally permeant ion for K^+ channels – and an intracellular Tl^+ sensitive dye enables determination of potassium channel opening in a 384-well format (Weaver et al., 2004). Cells are loaded with the thallium sensitive dye, exposed to ligands or vehicle for 20 minutes and given a bolus of thallium Tl^+. The specific techniques below have been employed to characterize MC4R-Kir7.1 signaling and its modulators. However, these techniques can be used to characterize the nature of any Kir-GPCR interaction.

Materials

2.1 Assay Buffers:

1. Hanks Buffered Salt Solution (HBSS) with Ca^{2+} and Mg^{2+} (Thermo Scientific cat #14025076): 140 mg/L $CaCl_2$, 100 mg/L $MgCl_2 \cdot 6H_2O$, 100 mg/L $MgSO_4 \cdot 7H_2O$, 400 mg/L KCl, 60mg/L KH_2PO_4, 350 mg/L $NaHCO_3$, 8 g/L NaCl, 48 mg/L Na_2HPO4 (anhydrous), 1 g/L D-Glucose.
2. 1 M HEPES solution: Dissolve 119.15 g HEPES (free acid) in 400 mL ddH_2O. Add 5 M NaOH drop wise to achieve a pH of 7.0. Add ddH_2O until the solution reaches a final volume of 500 mL. Filter sterilize.

3. Assay Buffer: Add 10 mL of a 1 M HEPES solution to 500 mL of HBSS w/ Ca^{2+} & Mg^{2+}. pH solution to 7.4 with 5 M NaOH.
4. 6.7% w/v pluronic acid solution in DMSO: Dilute 200mL of a 20% Pluronic acid solution (Thermo Scientific cat #P3000MP) with 400uL anhydrous DMSO to obtain a 6.7% pluronic acid solution.
5. Thallos Stock: Add 60 μL of a 6.7% w/v pluronic acid solution into 100 μg of the cell-permeable Thallos-AM (VU053734-1) dye (TEFlabs cat # 0901sp, actual MW 841). Thallos-AM stock can be stored in aliquots at -20^{o}C for one month.
6. Dye Buffer: Add 6 μL of the Thallos-AM stock to 10 mL Assay Buffer. This volume is sufficient for one 384-well plate..
7. Thallium Sulfate Stock solution: Prepare 100 mM Thallium sulfate (Tl_2SO_4) solution by dissolving 2.52 g into 50 mL of ddH2O. CAUTION: Thallium is extremely toxic and should be handled with care. Always wear gloves when handling thallium buffers and ensure proper waste disposal with local environmental health and safety representatives.
8. 5x Thallium Working Solution: Add 0.2 mL of 100 mM Thallium Sulfate to 10mL Assay Buffer for a final working solution of 2 mM Tl^{+}. This solution is a 5x concentrated stock that will be added during the assay.
9. Peptide Ligand Buffer: Assay Buffer containing 0.1% w/v Bovine Serum Albumin (BSA). Filter sterilize.
10. Small Molecule Ligand Buffer: Assay Buffer containing 0.1% DMSO.

2.2 Cell Culture Materials

1. Culture Media: 10% FBS supplemented DMEM containing 4.5 g/L Glucose and 50 U/mL Penicillin-Streptomycin.
2. T-REx^{TM} selection media (B-Media): Culture Media containing 0.5 mg/L Blastocidin.
3. Kir channel selection media (BH-Media): B-media containing 200 μg/mL Hygromycin.
4. Double Selection Media (BGH-Media): BH-Media containing 500 μg/mL Geneticin.
5. Plating media: 10% FBS supplemented DMEM containing 4.5 g/L Glucose and 1 μg/mL Tetracycline-HCl.
6. Assay plates: Cell Plate: BD BioCoat Poly-D-Lysine 384-well small volume black microplate.

2.3-Robotics:

1. FDSS plate reader with integrated liquid handling head and kinetic fluorescence detector (Flo3).
2. 384 head automated liquid dispensing platform.
3. Automatic cell plate washer (Optional – see note 1).

2.4-Ligands (peptides)

1. All neuropeptides are diluted in Peptide Ligand Buffer at a 2x final concentration.
2. All small molecules are diluted in Small Molecule Ligand Buffer a 2x final concentration.

3. Compound Plate: Greiner 384-well polypropylene plate, V-bottom (cat # 781280)

Method

3-1 Generation of cell lines expressing different Kir subunits and melanocortin receptors.

3-1A Generation of polyclonal cell lines:

1. Tetracycline-Regulated Expression HEK293T cells (T-REx™) expressing a tetracycline regulatory element are transfected (Lipofectamine 2000) with a plasmid containing the desired Kir coding sequence (Kir7.1, Kir4.2 etc.) in a pcDNA5/TO plasmid backbone. (See note 2)
2. Two days following transfection, a polyclonal population of Kir expressing cells is selected using BH media.
3. After 30 days, stable Kir cells are then transfected with the desired GPCR (MC4R, MC3R, etc.) or a mock vector in a pcDNA3 backbone.
4. Two days following transfection, cells are selected for GPCR expression using BGH media.
5. 30 days following this second selection, a Kir-GPCR polyclonal cell line is now ready for clonal selection.
6. If characterizing the presence of a Kir-GPCR interaction, polyclonal cell lines can be used. However, if a known Kir-GPCR interaction will be examined in a HTS format, selecting monoclones using the process below is highly recommended.

3-1B Generation of monoclonal cell lines (see notes 3 & 4):

1. Single cell clones are selected for by diluting polyclonal cell lines to 0.8 cells/20 μL in BGH media and then plating them on a poly-D-lysine coated 384 well culture plate.
2. Wells are examined for the presence of single cell colonies over the next 30 days. Wells that contain more than one clone are noted and excluded.
3. BGH Media is added weekly until cells become confluent.
4. Once confluent, monoclone cells are transferred to progressively larger culture vessels to ensure sufficient cell number for clonal screening.
5. HEK293T monoclones stably expressing a Kir channel and a GPCR can now be screened for using the protocol described in section 3-2.

3-2 Assay Protocol

3-2A Cell plating:

1. Grow cells in BGH media in a 150 mm cell culture dish until 70-90% confluent.
2. Wash cells with DMEM and then disassociate using 5 mL 0.05% trypsin in DMEM.
3. Collect cells in a 15 mL conical tube and add 10 mL plating media.
4. Pellet cells in a swinging bucket centrifuge at 250 g for 5 minutes.
5. Aspirate supernatant and resuspend the cell pellet in 10 mL plating media containing Tetracycline to induce channel expression. Tetracycline concentration must be optimized empirically but we have found that 1 μg/mL is sufficient.

6. Count cells on a hemocytometer and dilute to 10^6 cells/mL with plating media containing Tetracycline. A final 75-90% confluency is optimum.
7. Pour the cell suspension into a sterile reservoir. Using an electronic multichannel repeat pipettor, immediately dispense 20 μL into each well of a black wall, clear-bottom, 384 well poly-D-lysine coated assay plate (BD Biosciences, Bedford, MA).
8. Lightly tap the corner of the plate to ensure that the cell suspension reaches the bottom of each well. Bubbles should be avoided as they prevent a uniform cell distribution.
9. Place the cell plate in a 37^{o}C 5% CO_2 incubator for 20-24 hours to ensure cell adherence and protein (receptor and channel) expression.
10. If running an assay that requires 24-hour incubation with a ligand, add compounds at this time.

3-2B Assay Procedure:

1. 20-24 hours following cell plating, check the assay plate to make sure that the cells are uniformly distributed within each well. If certain wells appear non-uniform, note them in a lab notebook so that they can be excluded from the final analysis.
2. Prior to beginning the assay, prepare all buffers described in section 2-1.
3. Remove the plating media by flicking the plate. Remove any residual media by slamming the plate on a set of clean laboratory napkins (see Note 1).

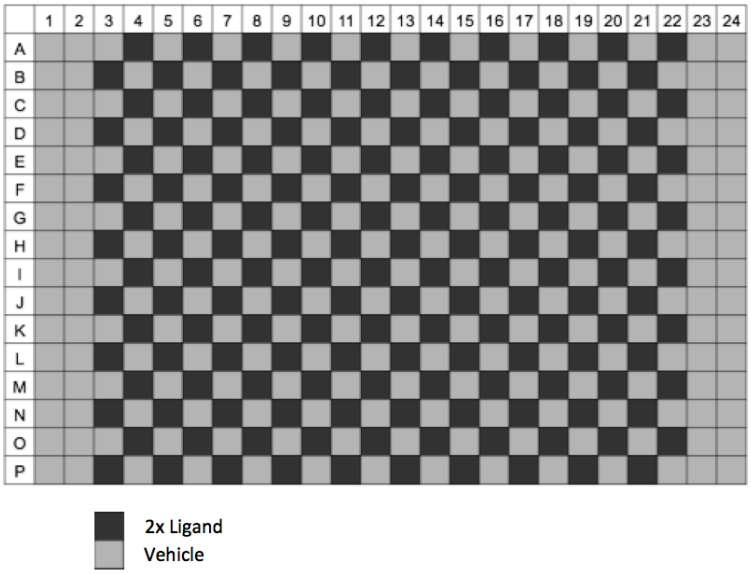

Figure 29 – Sample Plate Map

Calculation of the ΔF_{Ratio} necessitates the use of a checkerboard plate map. F_{Ratio} traces from agonist treated well traces are subtracted from the vehicle treated trace directly above (odd columns) or below (even columns) to obtain ΔF_{Ratio}. We have found that 12-16 compound well/vehicle subtractions, or two columns, are necessary to detect significant differences in Kir7.1 flux.

4. Add 20 μL of Dye Buffer to each well using an electronic multichannel repeat pipettor (see note 1).
5. Incubate cells in the dark for 30-60 minutes at room temperature. This incubation allows for intracellular esterases to cleave the acetoxymethyl-ester group from the Thallos-AM dye. This ensures intracellular accumulation of the dye and prevents dye efflux.
6. During this incubation, prepare the compound plate. Compound plates containing a ligand compound and the vehicle should be made in a checkerboard pattern (Figure 30& Note 5). Prepare the ligands at 2x the final desired concentration.
7. Once the incubation is complete, the dye buffer is removed by again flicking the plate and then slamming on a set of clean laboratory napkins. Then, add 20 μL of Assay Buffer to each well using an electronic multichannel repeat pipettor.
8. Using a 384 head automated liquid handling robot, transfer 20 μL of ligand solution from the compound plate to the corresponding well in the assay plate. This step can be done inside the plate reader or on a separate machine depending on the specific assay design.
9. If using α-MSH, incubate the Assay plate for 20 minutes (Figure 30 & note 6).
10. During this incubation, prepare a compound plate containing 25 μL of Thallium buffer in every well.
11. Following the ligand incubation, place the assay plate in a 384 well kinetic plate reader with liquid handling capabilities. Record in the fluorescence mode with an

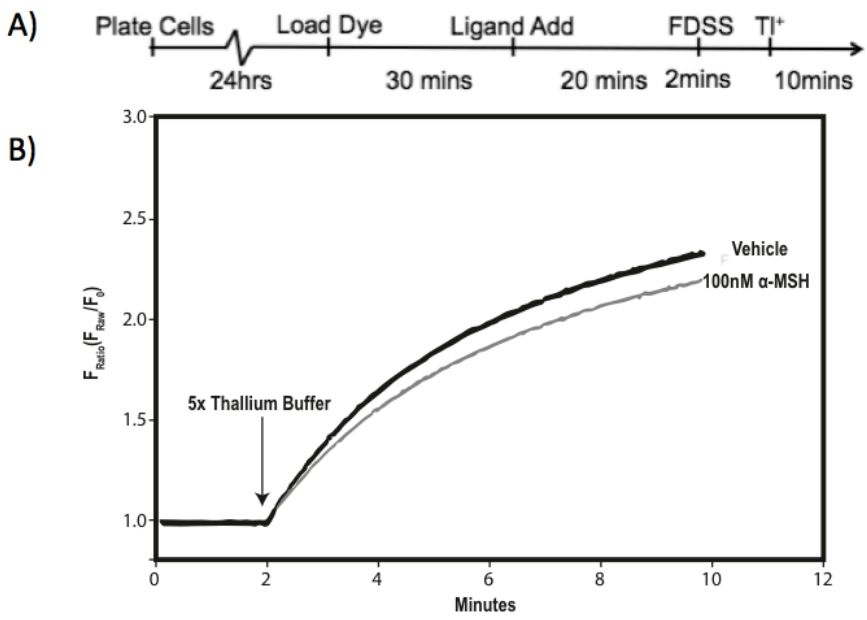

Figure 30 – Experimental protocol and sample traces

A) A cell plate is prepared with $2x10^4$ cells/well in a 384 well plate and incubated for 24 hours. Cells are then washed with assay buffer, loaded with dye buffer and incubated for 30 minutes. After another wash with assay buffer, the ligand is added using a 384 well robotic pipettor to ensure that every well receives agonist at the same time. After 20 minutes, the plate is now ready to be read in the FDSS kinetic plate reader. **B**) Once placed in the FDSS reader, a two-minute baseline reading (F_0) is obtained. Using the FDSS automated liquid handler, 10µL of a 5x Thallium buffer is added to each well of the assay plate. Fluorescence is read for 10 minutes following this addition. ΔF_{Ratio} is then calculated using the method described in section 3-3.

excitation at 470 nm using an argon laser. Emission was filtered using a 530 ± 30 nm band pass filter. The protocol is as follows:

a. 12 minute total recording time with sampling at 1-2 Hz.
b. While recording, add 10 μL of 5x thallium buffer into all wells using the 384 well liquid handling module after 2 minutes of baseline recording.

3-3 Data Analysis

1. Data from individual assay wells are exported as normalized fluorescence responses (F_{ratio}), obtained by dividing each data point (F_{raw}) by the average of the fluorescence signal during the two-minute period of baseline recording (F_0) (Figure 31A):

   $F_{ratio}=F_{raw}/F_0$

2. Effects of a ligand on Kir channel opening ($F_{Net\_Response}$) are quantified and displayed by subtracting the fluorescence response of a well treated with the ligand ($F_{ratio\_Compound}$) from that of a well treated with the vehicle directly below or above ($F_{ratio\_Vehicle}$). This gives the net effect of a ligand on the channel opening ($F_{Net\_Response}$) and is also referred to as the "ratio subtracted" measurement (ΔF_{ratio}) (Figure 31A&B):

Equation 4

$$F_{Net\_Response} = \Delta F_{Ratio} = F_{Ratio(Compound)} - F_{Ratio(Vehicle)}$$

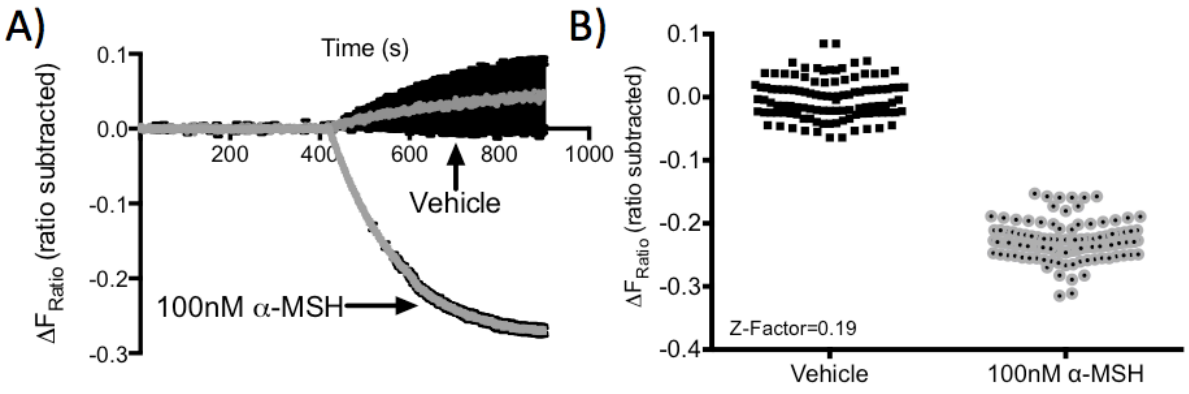
A)
Time (s)
0.1
0.0
-0.1
-0.2
-0.3
200
400
600
800
1000
Vehicle
100nM α-MSH
ΔF Ratio (ratio subtracted)
B)
0.1
0.0
-0.1
-0.2
-0.3
-0.4
ΔF Ratio (ratio subtracted)
Z-Factor=0.19
Vehicle
100nM α-MSH

3. Once the ΔF_{Ratio} for a ligand has been determined, the maximum or minimum ΔF_{Ratio} (ΔF_{Ratio} Max) of each replicate can be determined and used to statistically compare between groups.
4. Z-factor, a measure of statistical effect size and variability, is used to investigate the high throughput screening viability of an assay. A Z-factor>0.5 is considered acceptable for high throughput screening. The Z-factor can be calculated using the following formula:

Equation 5

$$\text{Z-factor} = 1 - \frac{3(\sigma_c + \sigma_v)}{|\mu_c - \mu_v|}$$

μ_c = Average ΔF_{Ratio} Compound -Vehicle
μ_v = Average ΔF_{Ratio} Vehicle -Vehicle
σ_c = Standard Deviation ΔF_{Ratio} Compound -Vehicle
σ_v = Standard Deviation ΔF_{Ratio} Vehicle -Vehicle

3-4 Results

We have employed the thallium flux assay to characterize the MC4R-Kir7.1 signaling pathway in HEK293 cells stably expressing MC4R and Kir7.1-M125R. The use of the Kir7.1M125R mutation is critical as wild-type Kir7.1 has an extremely low single channel conductance (~50 fS), which reduces the assay signal. As reported previously, a 20-minute exposure of the MC4R agonist α-MSH reduces Kir7.1 mediated thallium flux by up to 20%, indicating decreases in channel opening (Figure 32A). Investigating the viability of the α-MSH response for a high throughput screening using a

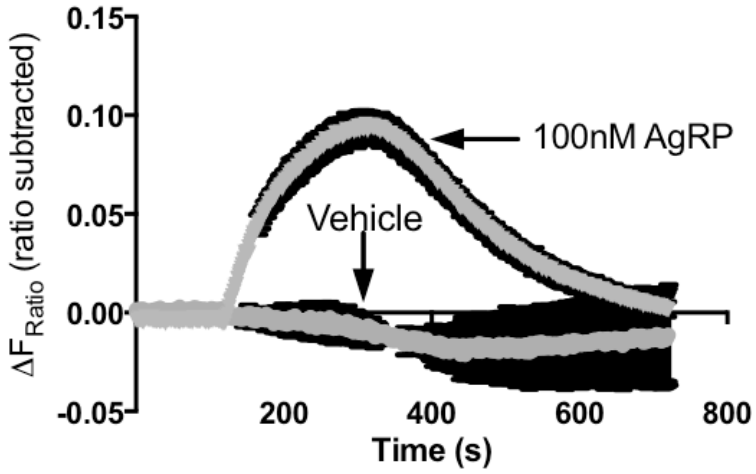

Figure 32 – AgRP increases Kir7.1 mediated thallium flux.

100nM AgRP increases thallium flux in HEK293 cells expressing MC4R and Kir7.1. Grey=average of ΔF_{Ratio} measurements, Error bars +/-SEM. n=36

checkerboard plate format (Figure 30) and the analysis method described in section 3-3, an assay Z-Factor of 0.19 was obtained for 100nM α-MSH (Figure 32B). Under these given circumstances, this assay of MC4R-Kir7.1 signaling classifies as “medium throughput” assay.

In addition to studying the effects of α-MSH, we have also used the thallium flux assay to characterize the effects of the MC4R inverse agonist AgRP on MC4R-Kir7.1 signaling. Using a checkerboard format as depicted in Figure 29, 100nM AgRP was found to increase thallium flux relative to vehicle control indicating increases in channel opening (Figure 33). Together as previously reported, these results indicate that the thallium assay can be employed to study molecular pathways involved in MC4R-Kir7.1 signaling.

Given the regulation of Kir7.1 by MC4R ligands, we sought to devise an experimental protocol to investigate the molecular signaling pathways that mediate this interaction. Previous electrophysiology experiments have shown that MC4R regulates Kir7.1 through a G-protein-independent manner. Using the strategy outlined in Figure 33, we first examined a role of cAMP-dependent activation of Protein Kinase A (PKA) in this signaling pathway. After flicking off the Thallos-AM dye, 10uL of a 3x Rp-cAMP solution, a potent competitive inhibitor of the activation of cAMP-dependent protein kinases, was added to the cell plate. Following a two-minute incubation, 10uL of a 4x α-MSH buffer was then added to the assay plate. Using the analysis described in section 3-3, we found that Rp-cAMP was unable to block MC4R-Kir7.1 signaling (Figure 34A). Examining directly a role of G_{sa} next, we employed a dominant negative G_s construct

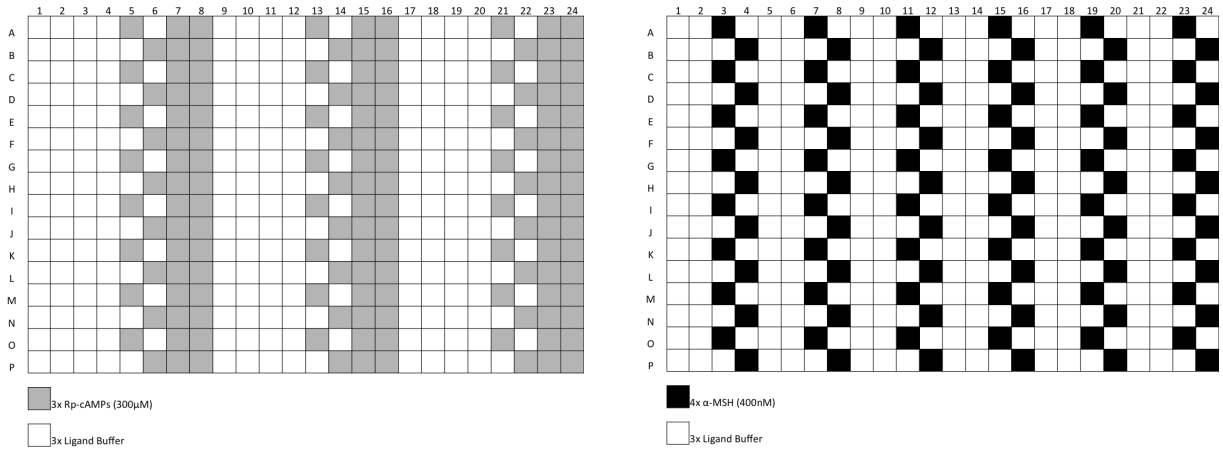

Figure 33 – Plate map strategy for analyzing compounds that modulate MC4R-Kir7.1 signaling.

This plate map format allows the study of pharmocological probes in the thallium flux assay. In this example, Rp-cAMPs, a potent competitive inhibitor of the activation of cAMP-dependent protein kinases, is dispensed in a checkerboad format on colulmns 5&6 but in every well of columns 7&8. Following a 10µL addition of this compound to the assay plate, a second 10µL stimulus of 400nM (4x) α-MSH is then added. This plate is designed in a checkerboard format on columns 3&4 for a positive control and 7&8 to determine the ability of Rp-cAMPs to block the effect of α-MSH.

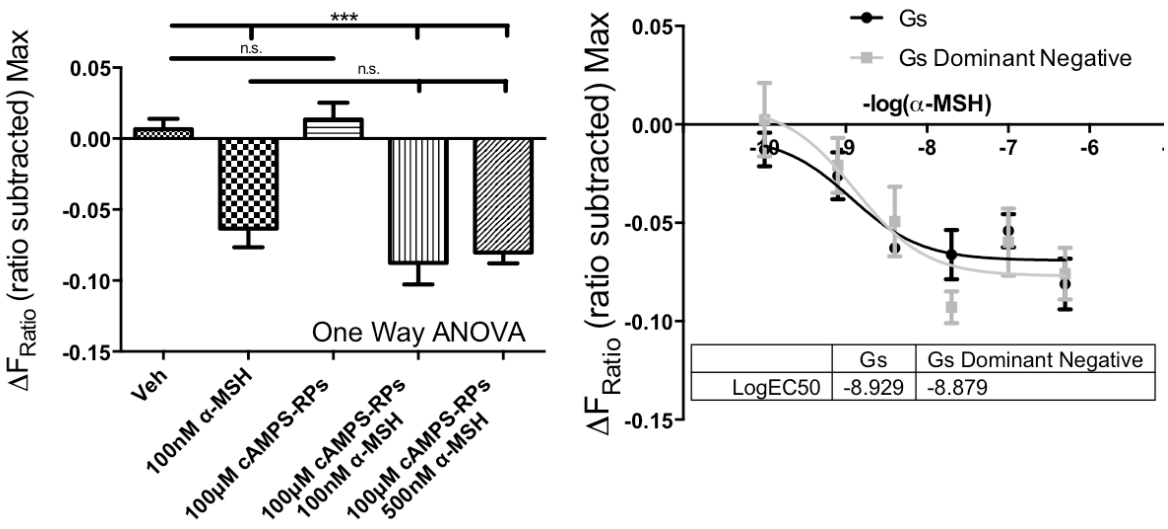

Figure 34 – MC4R-Kir7.1 signaling is not regulated by G_s

A) 100μM Rp-cAMPs does not block the effect of α-MSH on Kir7.1 conductance. n=36 ΔF_{Ratio} measurements/group; Error bars +/-SEM; One Way ANOVA $p<0.001$. **B**) In this experiment, a dominant negative G_s plasmid or a wild type G_s plasmid is transfected into HEK293 cells expressing MC4R and Kir7.1. 48 hours later, cells are exposed to a dose response curve of α-MSH. Expression of a dominant negative G_s plasmid in MC4R-Kir7.1 cells does not right shift the α-MSH dose response curve as indicated by the lack of an effect on the EC_{50} of α-MSH. n=12 ΔF_{Ratio} measurements/group; Error bars +/-SEM; One Way ANOVA $p<0.001$.

that has been shown to completely block the canonical G_{sa}-AC-cAMP signaling pathway. Co-expression of this construct in HEK293 cells was not able to affect EC_{50} of the α-MSH concentration response curve when compared to transfection with a control G_{sa} plasmid (Figure 34B). Together, these results support our earlier findings (Ghamari-Langroudi et al., 2015) that the MC4R-Kir7.1 signaling is independent of G_s-AC-cAMP signaling pathway. Furthermore, these data suggest that a non-canonical GPCR signaling pathway may be essential for this interaction.

Notes

1. Removing the media and assay buffers in a consistent manner is critical for this assay. In the past we have used several expensive plate washing robots for these purposes. However, the most consistent and cost effective manner is the "flick and slam" method:
    a. Using your dominant hand, hold the plate with your palm facing (but not touching) the bottom of the plate.
    b. Next, bend your arm and wrist so that top of the plate faces your chest.
    c. Finally, rapidly adduct your arm and wrist in a single fluid movement to expel the buffer contained in the plate into a sink. Wash the media down the drain with 10% bleach.
    d. Finally, invert the plate onto a set of clean laboratory napkins and repeatedly slam the plate down until all of the remaining media is removed.

2. Stable cell lines are critical when performing the thallium assay to characterize GPCR-Kir interactions. Using a tetracycline regulatory system enables the generation of stable cell lines with constructs that may prove toxic when constitutively expressed. Channels that are not toxic when overexpressed may not require this system. However, if you are unfamiliar with the channel you are studying, it is pragmatic to choose this approach.

3. Generation of mono-clones is not necessary when characterizing the presence or absence of a GPCR-Kir interaction. We have successfully employed polyclonal cell lines in this regard. However, when attempting to run this assay in a medium to high throughput manner, monoclones are essential. Clone selection should be determined empirically using the assay screening format employed in all future screening.

4. In an attempt to create cell lines more rapidly, our group has used other ways to rapidly generate monoclones. Our more recent studies on MC4R-Kir7.1 signaling were performed on a cell line using the Flp-In/T-REx 293 system (Thermo). This cell line contains a single FRT site that enables FLP recombinase mediated insertion of the pcDNA5/FRT/TO plasmid. This enables inducible expression of the vector contained in the ORF of the plasmid. Using this plasmid, we designed a biscistronic vector with hMC4R and hKir7.1(M125R) potassium channel using the cleavable peptide linker p2A. This method required a single round of

selection in BH media because recombination and transcription is only possible from the FRT locus.

5. Creating a compound plate is critical because it enables uniform addition to each well. In our experience, a minimum of 12 compound treated wells and 12 vehicle treated wells are necessary to observe changes in Tl^+ flux caused by melanocortin agonists. This is largely due to a small signal to noise ratio and intrinsic assay variance. If possible, do not use Row A,B,O,&P as they are subject to edge effect.

6. It may be necessary to optimize the incubation time for different ligands. This can be accomplished with a time course as depicted in Figure 5.

APPENDIX B

Characterization of *Mc4r-/-* energy metabolism using the sable system

In an attempt to determine if *Mc4r-/-* mice preferentially burn fatty acids or carbohydrates *Mc4r-/-* mice and their WT siblings were examined by indirect calorimetry. Mice were acclimatized to single housing for 2 weeks prior to the experiment. At 6-weeks-old, chow fed *Mc4r-/-* and WT mice were body weight matched, underwent body composition analysis (see above) and placed into Promethion metabolic cages (Sable Systems) with *ad libitum* access to 5LOD food and water. Throughout the study, mice experienced a 12 hour light cycle followed by a 12 hour dark cycle. The room was not entered throughout the study. Once in the chambers, VO_2 and VCO_2 measurements were obtained at 5-minute intervals. The Reparatory exchange ratio (RER) was calculated as follows:

Equation 6

$$RER = \frac{VCO_2}{VO_2}$$

Energy expenditure was calculated according to the Weir equation (Even & Nadkarni, 2012; Weir, 1949):

Equation 7

$$EE = 16.3VO_2 + 4.57VCO_2$$

While the *Mc4r-/-* mice were not heavier than their WT controls (WT: 20.02±1.116; *Mc4r-/-* : 20.95±1.70, Unpaired 2-tailed t-test p=0.2452, n=7)(Figure

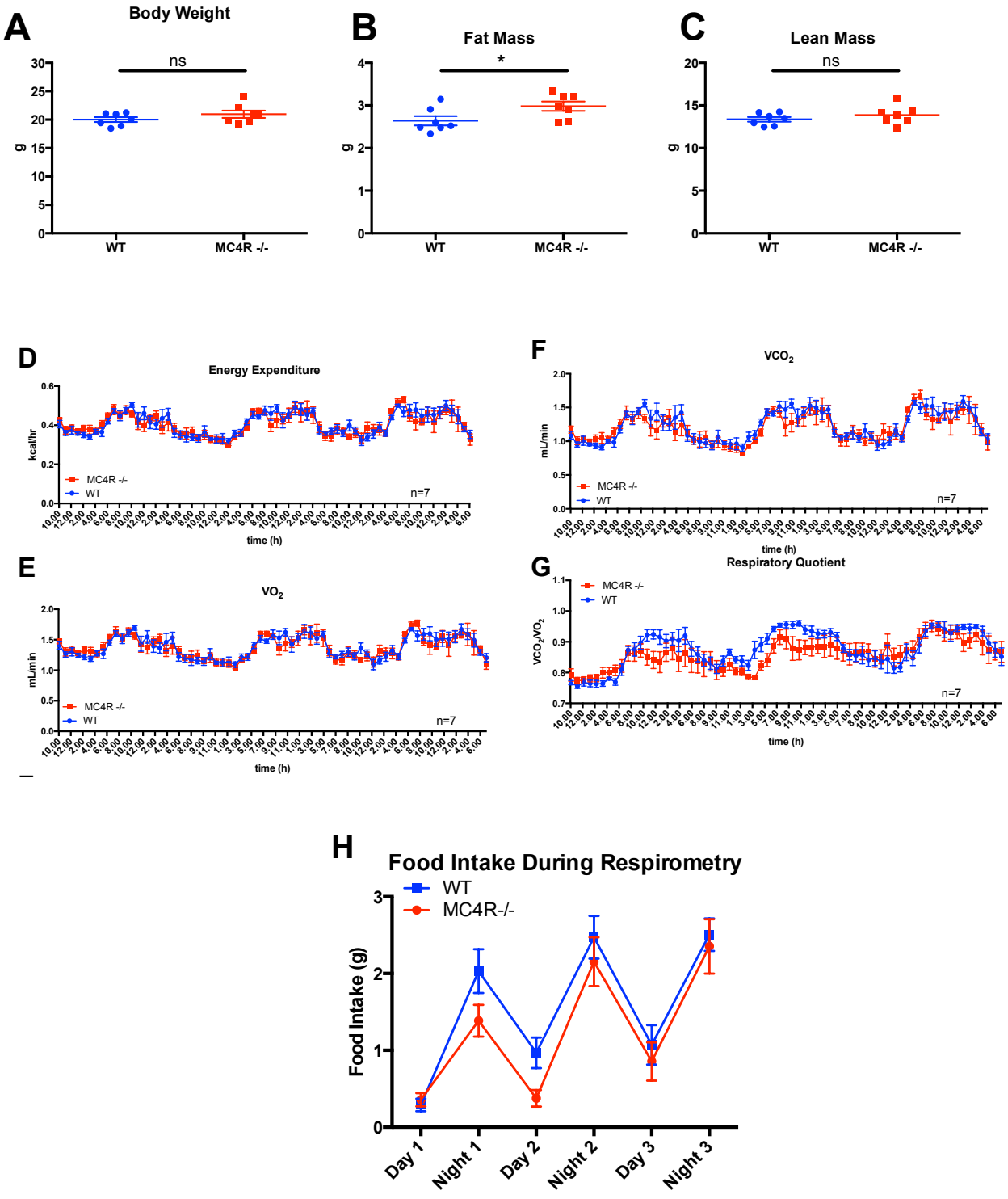

Figure 35 Indirect calorimetry measurements of 6-week-old, body weight matched *Mc4r-/-* and WT mice.

A) Body weights of *Mc4r-/-* and WT mice at 6 months of age (2 tailed student's t

test $p>0.05$ n=7). **B)** Fat mass of *Mc4r-/-* and WT mice at 6 months of age (2 tailed student's t test $p<0.05$ n=7). **C)** Lean mass of *Mc4r-/-* and WT mice at 6 months of age (2 tailed student's t test $p>0.05$ n=7). **D)** Energy expenditure of *Mc4r-/-* and WT mice (2 way ANOVA Sidak post test, $p>0.05$, n=7). **E)** Oxygen consumption of *Mc4r-/-* and WT mice 2 way ANOVA Sidak post test, $p>0.05$, n=7) **F)** Carbon dioxide production of *Mc4r-/-* and WT mice (2 way ANOVA Sidak post test, $p>0.05$, n=7) **G)** Respiratory quotient of *Mc4r-/-* and WT mice (2 way ANOVA Sidak post test, $p<0.01$, n=7) **H)** Food intake (2 way ANOVA Sidak post test, $p=0.181$, n=7)

35A), they did display a small, but statistically significant increase in body fat content (WT: 2.34±0.285; *Mc4r-/-* : 2.61±0.299, Unpaired 2-tailed t-test p=0.325, n=7) (Figure 35B) with no difference in lean mass (WT: 12.47±0.73; *Mc4r-/-* : 13.88±1.087, Unpaired 2-tailed t-test p=0.0464, n=7) (Figure 35C). Over a 3 day recording, there was no difference in energy expenditure, VO_2 and VCO_2 when compared to their wild type siblings (2 Way ANOVA, EE: p=0.97 VO_2: p=0.98,VCO_2: p=0.85, n=7) (Figure 35D-F). However, *Mc4r-/-* mice did display a slight, but significant reduction in the RER (2 Way ANOVA, p=0.0064, n=7) (Figure 35G). However, this reduction in RER was paralleled with a slight but statistically insignificant reduction in food intake by *Mc4r-/-* mice (Figure 35H).

This cohort was then examined again at 12 weeks to see if this phenotype became exaggerated with age. At this time point, *Mc4r-/-* mice were significantly heavier (WT: 22.57±0.785; *Mc4r-/-* : 27.21±2.03, Unpaired 2-tailed t-test p<0.0.0001, n=7) and had both increased lean (WT: 15.43±0.702; *Mc4r-/-* : 17.26±0.668, Unpaired 2-tailed t-test p=0.0.0003, n=7) and fat mass (WT: 2.55±0.409; *Mc4r-/-* : 5.41±1.19, Unpaired 2-tailed t-test p<0.0.0001, n=7) Figure 36A-C). At the 12 week time point, *Mc4r-/-* mice also began to show a drop in energy expenditure when compared to controls (2 Way ANOVA, p=0.011, n=7) (Figure 36D) as well as VO_2 and VCO_2 (2 Way ANOVA, VO_2: p=0.0169 or VCO_2: p=0.0005, n=7). Furthermore, the reduction in RER was further depressed indicating the use of fat as a primary fuel source (2 Way ANOVA, p<0.0001, n=7)(Figure 36E-G). At this time point, *Mc4r-/-* mice displayed a significant reduction in food intake compared to WT controls (2 Way ANOVA, p<0.01, n=7). Together, these

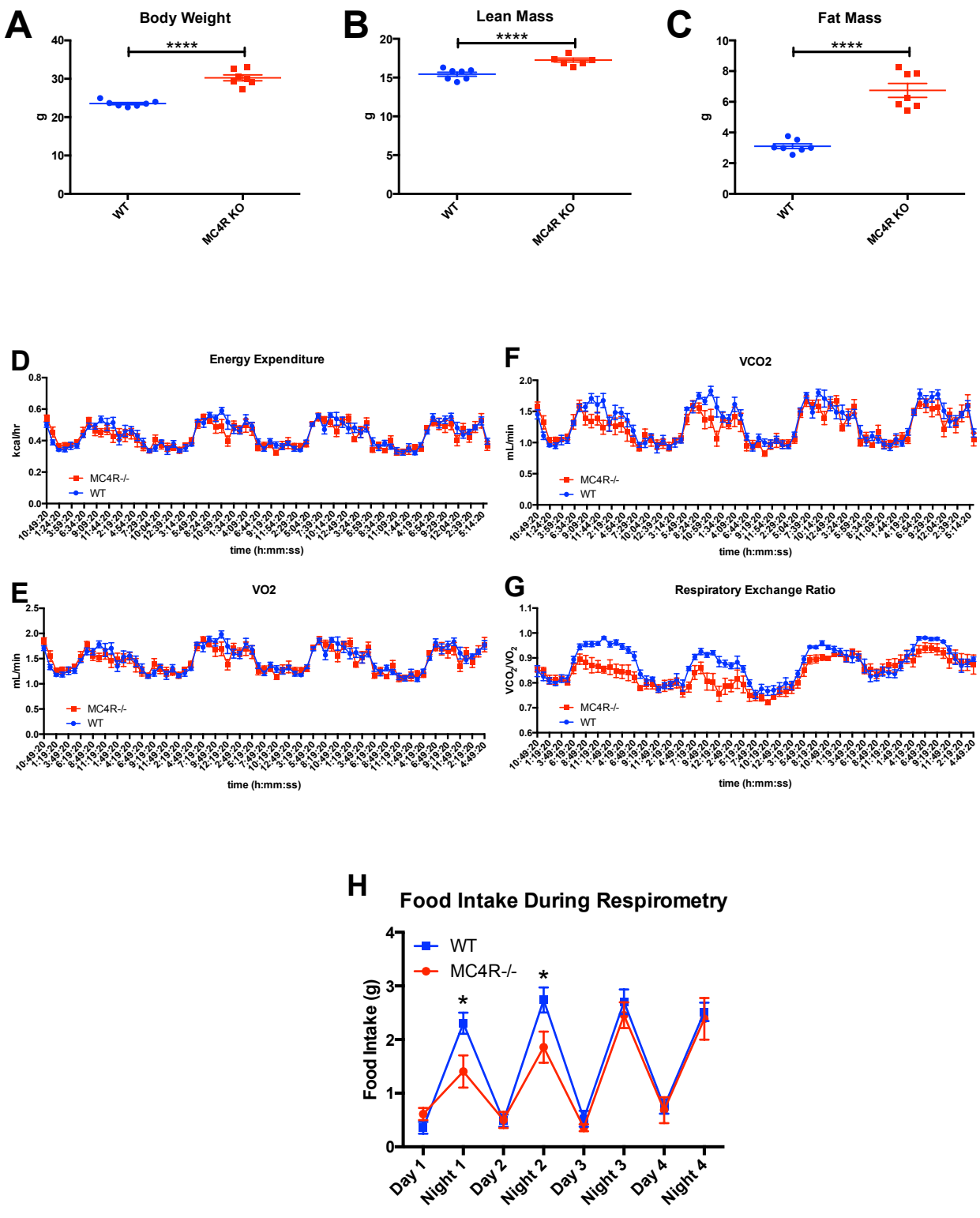

Figure 36 Indirect calorimetry measurements of 12 week old *Mc4r-/-* and WT mice.

A) Body weights of *Mc4r-/-* and WT mice at 6 months of age (2 tailed student's t test $p>0.0001$ n=7). **B)** Lean mass of *Mc4r-/-* and WT mice at 12 months of age (2 tailed student's t test $p>0.0001$ n=7). **C)** Fat mass of *Mc4r-/-* and WT mice at 12 months of age (2 tailed student's t test $p>0.0001$ n=7). **D)** Energy expenditure of *Mc4r-/-* and WT mice (2 way ANOVA Sidak post test, $p<0.05$, n=7). **E)** Oxygen consumption of *Mc4r-/-* and WT mice 2 way ANOVA Sidak post test, $p<0.05$, n=7) **F)** Carbon dioxide production of *Mc4r-/-* and WT mice (2 way ANOVA Sidak post test, $p<0.001$, n=7) **G)** Respiratory quotient of *Mc4r-/-* and WT mice (2 way ANOVA Sidak post test, $p>0.0001$, n=7) **H)** Food intake (2 way ANOVA Sidak post test, adjusted $p<0.05$, n=7)

findings suggests that loss of the *Mc4r-/-* results in delayed ability to cope with the novel environment of the metabolic chamber. However, over time the *Mc4r-/-* mice seem to adapt well. Based on these results, future studies into the basal metabolic rates of *Mc4r-/-* mice should be performed over longer periods of time so as to enable the *Mc4r-/-* mice to adapt and avoid artifacts of stress induced anorexia.

REFERENCES

Acín-Pérez, R., Fernández-Silva, P., Peleato, M. L., Pérez-Martos, A., & Enriquez, J. A. Respiratory Active Mitochondrial Supercomplexes. *Molecular Cell, 32*(4), 529-539. doi:10.1016/j.molcel.2008.10.021

Adamantidis, A. R., Zhang, F., Aravanis, A. M., Deisseroth, K., & de Lecea, L. (2007). Neural substrates of awakening probed with optogenetic control of hypocretin neurons. *Nature, 450*(7168), 420-424. doi:10.1038/nature06310

Afgan, E., Baker, D., van den Beek, M., Blankenberg, D., Bouvier, D., Čech, M., . . . Goecks, J. (2016). The Galaxy platform for accessible, reproducible and collaborative biomedical analyses: 2016 update. *Nucleic Acids Research, 44*(Web Server issue), W3-W10. doi:10.1093/nar/gkw343

Agah, R., Frenkel, P. A., French, B. A., Michael, L. H., Overbeek, P. A., & Schneider, M. D. (1997). Gene recombination in postmitotic cells. Targeted expression of Cre recombinase provokes cardiac-restricted, site-specific rearrangement in adult ventricular muscle in vivo. *J Clin Invest, 100*(1), 169-179. doi:10.1172/jci119509

Akaza, I., Tsuchiya, K., Akaza, M., Sugiyama, T., Izumiyama, H., Doi, M., . . . Hirata, Y. (2009). Improvement of congestive heart failure after octreotide and transsphenoidal surgery in a patient with acromegaly. *Intern Med, 48*(9), 697-700.

Alexander, G. M., Rogan, S. C., Abbas, A. I., Armbruster, B. N., Pei, Y., Allen, J. A., . . . Roth, B. L. (2009). Remote control of neuronal activity in transgenic mice expressing evolved G protein-coupled receptors. *Neuron, 63*(1), 27-39. doi:10.1016/j.neuron.2009.06.014

Almundarij, T. I., Smyers, M. E., Spriggs, A., Heemstra, L. A., Beltz, L., Dyne, E., . . . Novak, C. M. (2016). Physical Activity, Energy Expenditure, and Defense of Body Weight in Melanocortin 4 Receptor-Deficient Male Rats. *Sci Rep, 6*, 37435. doi:10.1038/srep37435

Anderson, E. J., Cakir, I., Carrington, S. J., Cone, R. D., Ghamari-Langroudi, M., Gillyard, T., . . . Litt, M. J. (2016). 60 YEARS OF POMC: Regulation of feeding and energy homeostasis by alpha-MSH. *J Mol Endocrinol, 56*(4), T157-174. doi:10.1530/jme-16-0014

Aponte, Y., Atasoy, D., & Sternson, S. M. (2011). AGRP neurons are sufficient to

orchestrate feeding behavior rapidly and without training. *Nat Neurosci, 14*(3), 351-355. doi:10.1038/nn.2739

Aravanis, A. M., Wang, L. P., Zhang, F., Meltzer, L. A., Mogri, M. Z., Schneider, M. B., & Deisseroth, K. (2007). An optical neural interface: in vivo control of rodent motor cortex with integrated fiberoptic and optogenetic technology. *J Neural Eng, 4*(3), S143-156. doi:10.1088/1741-2560/4/3/S02

Armbruster, B. N., Li, X., Pausch, M. H., Herlitze, S., & Roth, B. L. (2007). Evolving the lock to fit the key to create a family of G protein-coupled receptors potently activated by an inert ligand. *Proc Natl Acad Sci U S A, 104*(12), 5163-5168. doi:10.1073/pnas.0700293104

Ashrafian, H., & Frenneaux, M. P. (2007). Metabolic Modulation in Heart Failure: The Coming of Age. *Cardiovascular Drugs and Therapy, 21*(1), 5-7. doi:10.1007/s10557-007-6000-z

Atasoy, D., Aponte, Y., Su, H. H., & Sternson, S. M. (2008). A FLEX switch targets Channelrhodopsin-2 to multiple cell types for imaging and long-range circuit mapping. *J Neurosci, 28*(28), 7025-7030. doi:10.1523/JNEUROSCI.1954-08.2008

Atasoy, D., Betley, J. N., Su, H. H., & Sternson, S. M. (2012). Deconstruction of a neural circuit for hunger. *Nature, 488*(7410), 172-177. doi:10.1038/nature11270

Ayala, J. E., Samuel, V. T., Morton, G. J., Obici, S., Croniger, C. M., Shulman, G. I., . . . McGuinness, O. P. (2010). Standard operating procedures for describing and performing metabolic tests of glucose homeostasis in mice. *Disease Models & Mechanisms, 3*(9-10), 525-534. doi:10.1242/dmm.006239

Bäck, A. (2014). Parts of Animals *Aristotle's Theory of Abstraction* (pp. 243-270): Springer.

Bagnol, D., Lu, X. Y., Kaelin, C. B., Day, H. E., Ollmann, M., Gantz, I., . . . Watson, S. J. (1999). Anatomy of an endogenous antagonist: relationship between Agouti-related protein and proopiomelanocortin in brain. *J Neurosci, 19*(18), RC26.

Balthasar, N., Coppari, R., McMinn, J., Liu, S. M., Lee, C. E., Tang, V., . . . Lowell, B. B. (2004). Leptin receptor signaling in POMC neurons is required for normal body weight homeostasis. *Neuron, 42*(6), 983-991. doi:10.1016/j.neuron.2004.06.004

Balthasar, N., Dalgaard, L. T., Lee, C. E., Yu, J., Funahashi, H., Williams, T., . . . Lowell, B. B. (2005). Divergence of melanocortin pathways in the control of food intake and energy expenditure. *Cell, 123*(3), 493-505. doi:10.1016/j.cell.2005.08.035

Battiprolu, P. K., Hojayev, B., Jiang, N., Wang, Z. V., Luo, X., Iglewski, M., . . . Hill, J. A.

(2012). Metabolic stress-induced activation of FoxO1 triggers diabetic cardiomyopathy in mice. *J Clin Invest, 122*(3), 1109-1118. doi:10.1172/jci60329

BEDFORD, D., & KONSTAM, G. (1946). Obscure heart disease in West African troops. *Br Heart J, 8*, 236.

Betley, J. N., Cao, Z. F., Ritola, K. D., & Sternson, S. M. (2013). Parallel, redundant circuit organization for homeostatic control of feeding behavior. *Cell, 155*(6), 1337-1350. doi:10.1016/j.cell.2013.11.002

Betley, J. N., Xu, S., Cao, Z. F., Gong, R., Magnus, C. J., Yu, Y., & Sternson, S. M. (2015). Neurons for hunger and thirst transmit a negative-valence teaching signal. *Nature, 521*(7551), 180-185. doi:10.1038/nature14416

Biebermann, H., Krude, H., Elsner, A., Chubanov, V., Gudermann, T., & Gruters, A. (2003). Autosomal-dominant mode of inheritance of a melanocortin-4 receptor mutation in a patient with severe early-onset obesity is due to a dominant-negative effect caused by receptor dimerization. *Diabetes, 52*(12), 2984-2988.

Boudina, S., & Abel, E. D. (2007). Diabetic Cardiomyopathy Revisited. *Circulation, 115*(25), 3213-3223. doi:10.1161/circulationaha.106.679597

Bouyer, K., & Simerly, R. B. (2013). Neonatal leptin exposure specifies innervation of presympathetic hypothalamic neurons and improves the metabolic status of leptin-deficient mice. *J Neurosci, 33*(2), 840-851. doi:10.1523/JNEUROSCI.3215-12.2013

Boyden, E. S., Zhang, F., Bamberg, E., Nagel, G., & Deisseroth, K. (2005). Millisecond-timescale, genetically targeted optical control of neural activity. *Nat Neurosci, 8*(9), 1263-1268. doi:10.1038/nn1525

Brainard, R. E., Watson, L. J., Demartino, A. M., Brittian, K. R., Readnower, R. D., Boakye, A. A., . . . Jones, S. P. (2013). High fat feeding in mice is insufficient to induce cardiac dysfunction and does not exacerbate heart failure. *PLoS One, 8*(12), e83174. doi:10.1371/journal.pone.0083174

Braun, T. P., Orwoll, B., Zhu, X., Levasseur, P. R., Szumowski, M., Nguyen, M. L., . . . Marks, D. L. (2012). Regulation of lean mass, bone mass, and exercise tolerance by the central melanocortin system. *PLoS One, 7*(7), e42183. doi:10.1371/journal.pone.0042183

Broberger, C., Johansen, J., Johansson, C., Schalling, M., & Hökfelt, T. (1998). The neuropeptide Y/agouti gene-related protein (AGRP) brain circuitry in normal, anorectic, and monosodium glutamate-treated mice. *Proc Natl Acad Sci U S A, 95*(25), 15043-15048.

Bronstein, D. M., Schafer, M. K., Watson, S. J., & Akil, H. (1992). Evidence that beta-endorphin is synthesized in cells in the nucleus tractus solitarius: detection of POMC mRNA. *Brain Res, 587*(2), 269-275.

Brooks, W. W., Shen, S. S., Conrad, C. H., Goldstein, R. H., & Bing, O. H. (2010). Transition from compensated hypertrophy to systolic heart failure in the spontaneously hypertensive rat: Structure, function, and transcript analysis. *Genomics, 95*(2), 84-92. doi:10.1016/j.ygeno.2009.12.002

Brown, D. A., Perry, J. B., Allen, M. E., Sabbah, H. N., Stauffer, B. L., Shaikh, S. R., . . . Gheorghiade, M. (2017). Expert consensus document: Mitochondrial function as a therapeutic target in heart failure. *Nat Rev Cardiol, 14*(4), 238-250. doi:10.1038/nrcardio.2016.203

Buch, T. R., Heling, D., Damm, E., Gudermann, T., & Breit, A. (2009). Pertussis toxin-sensitive signaling of melanocortin-4 receptors in hypothalamic GT1-7 cells defines agouti-related protein as a biased agonist. *J Biol Chem, 284*(39), 26411-26420. doi:10.1074/jbc.M109.039339

Bugger, H., & Abel, E. D. (2014). Molecular mechanisms of diabetic cardiomyopathy. *Diabetologia, 57*(4), 660-671. doi:10.1007/s00125-014-3171-6

Butler, A. A., Kesterson, R. A., Khong, K., Cullen, M. J., Pelleymounter, M. A., Dekoning, J., . . . Cone, R. D. (2000). A unique metabolic syndrome causes obesity in the melanocortin-3 receptor-deficient mouse. *Endocrinology, 141*(9), 3518-3521. doi:10.1210/endo.141.9.7791

Butler, A. A., Marks, D. L., Fan, W., Kuhn, C. M., Bartolome, M., & Cone, R. D. (2001). Melanocortin-4 receptor is required for acute homeostatic responses to increased dietary fat. *Nat Neurosci, 4*(6), 605-611. doi:10.1038/88423

Calligaris, S. D., Lecanda, M., Solis, F., Ezquer, M., Gutierrez, J., Brandan, E., . . . Conget, P. (2013). Mice long-term high-fat diet feeding recapitulates human cardiovascular alterations: an animal model to study the early phases of diabetic cardiomyopathy. *PLoS One, 8*(4), e60931. doi:10.1371/journal.pone.0060931

Carpenter, B., Nehmé, R., Warne, T., Leslie, A. G. W., & Tate, C. G. (2016). Structure of the adenosine A2A receptor bound to an engineered G protein. *Nature, 536*(7614), 104-107. doi:10.1038/nature18966

http://www.nature.com/nature/journal/v536/n7614/abs/nature18966.html - supplementary-information

Caruso, V., Lagerstrom, M. C., Olszewski, P. K., Fredriksson, R., & Schioth, H. B. (2014). Synaptic changes induced by melanocortin signalling. *Nat Rev Neurosci,*

15(2), 98-110. doi:10.1038/nrn3657

Chai, B. X., Neubig, R. R., Millhauser, G. L., Thompson, D. A., Jackson, P. J., Barsh, G. S., . . . Gantz, I. (2003). Inverse agonist activity of agouti and agouti-related protein. *Peptides, 24*(4), 603-609.

Chen, A. S., Marsh, D. J., Trumbauer, M. E., Frazier, E. G., Guan, X. M., Yu, H., . . . Van der Ploeg, L. H. (2000). Inactivation of the mouse melanocortin-3 receptor results in increased fat mass and reduced lean body mass. *Nat Genet, 26*(1), 97-102. doi:10.1038/79254

Chen, K. Y., Muniyappa, R., Abel, B. S., Mullins, K. P., Staker, P., Brychta, R. J., . . . Skarulis, M. C. (2015). RM-493, a melanocortin-4 receptor (MC4R) agonist, increases resting energy expenditure in obese individuals. *J Clin Endocrinol Metab, 100*(4), 1639-1645. doi:10.1210/jc.2014-4024

Chen, K. Y., Muniyappa, R., Abel, B. S., Mullins, K. P., Staker, P., Brychta, R. J., . . . Skarulis, M. C. (2015). RM-493, a Melanocortin-4 Receptor (MC4R) Agonist, Increases Resting Energy Expenditure in Obese Individuals. *J Clin Endocrinol Metab, 100*(4), 1639-1645. doi:10.1210/jc.2014-4024

Chen, W., Kelly, M. A., Opitz-Araya, X., Thomas, R. E., Low, M. J., & Cone, R. D. (1997). Exocrine gland dysfunction in MC5-R-deficient mice: evidence for coordinated regulation of exocrine gland function by melanocortin peptides. *Cell, 91*(6), 789-798.

Christakis, N. A., & Fowler, J. H. (2007). The spread of obesity in a large social network over 32 years. *N Engl J Med, 357*(4), 370-379. doi:10.1056/NEJMsa066082

Christoffersen, C., Bollano, E., Lindegaard, M. L., Bartels, E. D., Goetze, J. P., Andersen, C. B., & Nielsen, L. B. (2003). Cardiac lipid accumulation associated with diastolic dysfunction in obese mice. *Endocrinology, 144*(8), 3483-3490. doi:10.1210/en.2003-0242

Civelli, O., Birnberg, N., Herbert, E. (1982). Detection and quantitation of pro-opiomelanocortin mRNA in pituitary and brain tissue from different species. *Journal of Biological Chemistry, 257*, 6783-6787.

Clark, A. J., Lavender, P. M., Coates, P., Johnson, M. R., & Rees, L. H. (1990). In vitro and in vivo analysis of the processing and fate of the peptide products of the short proopiomelanocortin mRNA. *Mol Endocrinol, 4*(11), 1737-1743. doi:10.1210/mend-4-11-1737

Cone, R. D. (2005). Anatomy and regulation of the central melanocortin system. *Nat Neurosci, 8*(5), 571-578. doi:10.1038/nn1455

Cowley, M. A., Smart, J. L., Rubinstein, M., Cerdan, M. G., Diano, S., Horvath, T. L., . . . Low, M. J. (2001). Leptin activates anorexigenic POMC neurons through a neural network in the arcuate nucleus. *Nature, 411*(6836), 480-484. doi:10.1038/35078085

Cui, H., Sohn, J. W., Gautron, L., Funahashi, H., Williams, K. W., Elmquist, J. K., & Lutter, M. (2012). Neuroanatomy of melanocortin-4 receptor pathway in the lateral hypothalamic area. *J Comp Neurol, 520*(18), 4168-4183. doi:10.1002/cne.23145

Czyzyk, T. A., Sikorski, M. A., Yang, L., & McKnight, G. S. (2008). Disruption of the RIIbeta subunit of PKA reverses the obesity syndrome of Agouti lethal yellow mice. *Proc Natl Acad Sci U S A, 105*(1), 276-281. doi:10.1073/pnas.0710607105

da Silva, A. A., do Carmo, J. M., Kanyicska, B., Dubinion, J., Brandon, E., & Hall, J. E. (2008). Endogenous Melanocortin System Activity Contributes to the Elevated Arterial Pressure in Spontaneously Hypertensive Rats. *Hypertension, 51*(4), 884-890. doi:10.1161/HYPERTENSIONAHA.107.100636

da Silva, A. A., Spradley, F. T., Granger, J. P., Hall, J. E., & do Carmo, J. M. (2015). Brain-mediated antidiabetic, anorexic, and cardiovascular actions of leptin require melanocortin-4 receptor signaling. *J Neurophysiol, 113*(7), 2786-2791. doi:10.1152/jn.00911.2014

Davies, J., & Ball, J. (1955). The pathology of endomyocardial fibrosis in Uganda. *Br Heart J, 17*(3), 337.

Dec, G. W., & Fuster, V. (1994). Idiopathic dilated cardiomyopathy. *N Engl J Med, 331*(23), 1564-1575. doi:10.1056/nejm199412083312307

Deisseroth, K. (2011). Optogenetics. *Nat Methods, 8*(1), 26-29. doi:10.1038/nmeth.f.324

Dhahri, W., Drolet, M.-C., Roussel, E., Couet, J., & Arsenault, M. (2014). Chronic high-fat diet-induced obesity decreased survival and increased hypertrophy of rats with experimental eccentric hypertrophy from chronic aortic regurgitation. *BMC Cardiovascular Disorders, 14*(1), 123. doi:10.1186/1471-2261-14-123

Dietrich, M. O., Zimmer, M. R., Bober, J., & Horvath, T. L. (2015). Hypothalamic Agrp neurons drive stereotypic behaviors beyond feeding. *Cell, 160*(6), 1222-1232. doi:10.1016/j.cell.2015.02.024

do Carmo, J. M., da Silva, A. A., Cai, Z., Lin, S., Dubinion, J. H., & Hall, J. E. (2011). Control of blood pressure, appetite, and glucose by leptin in mice lacking leptin receptors in proopiomelanocortin neurons. *Hypertension, 57*(5), 918-926. doi:10.1161/hypertensionaha.110.161349

do Carmo, J. M., da Silva, A. A., Rushing, J. S., & Hall, J. E. (2012). Activation of the central melanocortin system contributes to the increased arterial pressure in obese Zucker rats. *Am J Physiol Regul Integr Comp Physiol, 302*(5), R561-567. doi:10.1152/ajpregu.00392.2011

Dote, K., Sato, H., Tateishi, H., Uchida, T., & Ishihara, M. (1991). [Myocardial stunning due to simultaneous multivessel coronary spasms: a review of 5 cases]. *J Cardiol, 21*(2), 203-214.

Eerola, K., Rinne, P., Penttinen, A. M., Vahatalo, L., Savontaus, M., & Savontaus, E. (2014). alpha-MSH overexpression in the nucleus tractus solitarius decreases fat mass and elevates heart rate. *J Endocrinol, 222*(1), 123-136. doi:10.1530/joe-14-0064

Elliott, P., Andersson, B., Arbustini, E., Bilinska, Z., Cecchi, F., Charron, P., . . . Keren, A. (2008). Classification of the cardiomyopathies: a position statement from the European Society Of Cardiology Working Group on Myocardial and Pericardial Diseases. *Eur Heart J, 29*(2), 270-276. doi:10.1093/eurheartj/ehm342

Even, P. C., & Nadkarni, N. A. (2012). Indirect calorimetry in laboratory mice and rats: principles, practical considerations, interpretation and perspectives. *American Journal of Physiology - Regulatory, Integrative and Comparative Physiology, 303*(5), R459.

Fan, W., Boston, B. A., Kesterson, R. A., Hruby, V. J., & Cone, R. D. (1997). Role of melanocortinergic neurons in feeding and the agouti obesity syndrome. *Nature, 385*(6612), 165-168. doi:10.1038/385165a0

Fan, W., Dinulescu, D. M., Butler, A. A., Zhou, J., Marks, D. L., & Cone, R. D. (2000). The central melanocortin system can directly regulate serum insulin levels. *Endocrinology, 141*(9), 3072-3079. doi:10.1210/endo.141.9.7665

Farooqi, I. S., Keogh, J. M., Yeo, G. S., Lank, E. J., Cheetham, T., & O'Rahilly, S. (2003). Clinical spectrum of obesity and mutations in the melanocortin 4 receptor gene. *N Engl J Med, 348*(12), 1085-1095. doi:10.1056/NEJMoa022050

Farooqi, I. S., Yeo, G. S., Keogh, J. M., Aminian, S., Jebb, S. A., Butler, G., . . . O'Rahilly, S. (2000). Dominant and recessive inheritance of morbid obesity associated with melanocortin 4 receptor deficiency. *J Clin Invest, 106*(2), 271-279. doi:10.1172/jci9397

Farooqi, I. S., Yeo, G. S. H., Keogh, J. M., Aminian, S., Jebb, S. A., Butler, G., . . . O'Rahilly, S. (2000). Dominant and recessive inheritance of morbid obesity associated with melanocortin 4 receptor deficiency. *Journal of Clinical*

Investigation, 106(2), 271-279.

Felker, G. M., Thompson, R. E., Hare, J. M., Hruban, R. H., Clemetson, D. E., Howard, D. L., . . . Kasper, E. K. (2000). Underlying causes and long-term survival in patients with initially unexplained cardiomyopathy. *N Engl J Med, 342*(15), 1077-1084. doi:10.1056/nejm200004133421502

Ferrari, R., Censi, S., Mastrorilli, F., & Boraso, A. (2003). Prognostic benefits of heart rate reduction in cardiovascular disease. *European Heart Journal Supplements, 5*(suppl_G), G10-G14. doi:10.1016/S1520-765X(03)90002-2

Fong, T. M., Mao, C., MacNeil, T., Kalyani, R., Smith, T., Weinberg, D., . . . Van der Ploeg, L. H. (1997). ART (protein product of agouti-related transcript) as an antagonist of MC-3 and MC-4 receptors. *Biochem Biophys Res Commun, 237*(3), 629-631. doi:10.1006/bbrc.1997.7200

Fragasso, G., Salerno, A., Spoladore, R., Bassanelli, G., Arioli, F., & Margonato, A. (2008). Metabolic therapy of heart failure. *Curr Pharm Des, 14*(25), 2582-2591.

Francis, S. H., Turko, I. V., & Corbin, J. D. (2001). Cyclic nucleotide phosphodiesterases: relating structure and function. *Prog Nucleic Acid Res Mol Biol, 65*, 1-52.

Furst, O., Mondou, B., & D'Avanzo, N. (2014). Phosphoinositide regulation of inward rectifier potassium (Kir) channels. *Front Physiol, 4*, 404. doi:10.3389/fphys.2013.00404

Gantz, I., Konda, Y., Tashiro, T., Shimoto, Y., Miwa, H., Munzert, G., . . . Yamada, T. (1993). Molecular cloning of a novel melanocortin receptor. *J Biol Chem, 268*(11), 8246-8250.

Gantz, I., Miwa, H., Konda, Y., Shimoto, Y., Tashiro, T., Watson, S. J., . . . Yamada, T. (1993). Molecular cloning, expression, and gene localization of a fourth melanocortin receptor. *J Biol Chem, 268*(20), 15174-15179.

Garfield, A. S., Li, C., Madara, J. C., Shah, B. P., Webber, E., Steger, J. S., . . . Lowell, B. B. (2015). A neural basis for melanocortin-4 receptor-regulated appetite. *Nat Neurosci, 18*(6), 863-871. doi:10.1038/nn.4011

Gemayel, C., Pelliccia, A., & Thompson, P. D. (2001). Arrhythmogenic right ventricular cardiomyopathy. *J Am Coll Cardiol, 38*(7), 1773-1781.

Gersh, B. J., Maron, B. J., Bonow, R. O., Dearani, J. A., Fifer, M. A., Link, M. S., . . . Yancy, C. W. (2011). 2011 ACCF/AHA guideline for the diagnosis and treatment of hypertrophic cardiomyopathy: executive summary: a report of the American College of Cardiology Foundation/American Heart Association Task Force on

Practice Guidelines. *Circulation, 124*(24), 2761-2796. doi:10.1161/CIR.0b013e318223e230

Ghamari-Langroudi, M., Digby, G. J., Sebag, J. A., Millhauser, G. L., Palomino, R., Matthews, R., . . . Cone, R. D. (2015). G-protein-independent coupling of MC4R to Kir7.1 in hypothalamic neurons. *Nature, 520*(7545), 94-98. doi:10.1038/nature14051

Ghamari-Langroudi, M., Srisai, D., & Cone, R. D. (2011). Multinodal regulation of the arcuate/paraventricular nucleus circuit by leptin. *Proc Natl Acad Sci U S A, 108*(1), 355-360. doi:10.1073/pnas.1016785108

Ghamari-Langroudi, M., Vella, K. R., Srisai, D., Sugrue, M. L., Hollenberg, A. N., & Cone, R. D. (2010). Regulation of thyrotropin-releasing hormone-expressing neurons in paraventricular nucleus of the hypothalamus by signals of adiposity. *Mol Endocrinol, 24*(12), 2366-2381. doi:10.1210/me.2010-0203

Glas, E., Muckter, H., Gudermann, T., & Breit, A. (2016). Exchange factors directly activated by cAMP mediate melanocortin 4 receptor-induced gene expression. *Sci Rep, 6*, 32776. doi:10.1038/srep32776

Goetz, R., Rohman, M., Haller, J., Dee, R., & Rosenak, S. S. (1961). Internal mammary-coronary artery anastomosis. A nonsuture method employing tantalum rings. *The Journal of thoracic and cardiovascular surgery, 41*, 378.

Graham, M., Shutter, J. R., Sarmiento, U., Sarosi, I., & Stark, K. L. (1997). Overexpression of Agrt leads to obesity in transgenic mice. *Nat Genet, 17*(3), 273-274. doi:10.1038/ng1197-273

Granell, S., Serra-Juhe, C., Martos-Moreno, G. A., Diaz, F., Perez-Jurado, L. A., Baldini, G., & Argente, J. (2012). A novel melanocortin-4 receptor mutation MC4R-P272L associated with severe obesity has increased propensity to be ubiquitinated in the ER in the face of correct folding. *PLoS One, 7*(12), e50894. doi:10.1371/journal.pone.0050894

Greenfield, J. R., Miller, J. W., Keogh, J. M., Henning, E., Satterwhite, J. H., Cameron, G. S., . . . Farooqi, I. S. (2009). Modulation of blood pressure by central melanocortinergic pathways. *N Engl J Med, 360*(1), 44-52. doi:10.1056/NEJMoa0803085

Guertl, B., Noehammer, C., & Hoefler, G. (2000). Metabolic cardiomyopathies. *International Journal of Experimental Pathology, 81*(6), 349-372. doi:10.1046/j.1365-2613.2000.00186.x

Hachamovitch, R., Chang, J. D., Kuntz, R. E., Papageorgiou, P., Levin, M. S., &

Goldberger, A. L. (1995). Recurrent reversible cardiogenic shock triggered by emotional distress with no obstructive coronary disease. *Am Heart J, 129*(5), 1026-1028.

Hagan, M. M., Rushing, P. A., Pritchard, L. M., Schwartz, M. W., Strack, A. M., Van Der Ploeg, L. H., . . . Seeley, R. J. (2000). Long-term orexigenic effects of AgRP-(83--132) involve mechanisms other than melanocortin receptor blockade. *Am J Physiol Regul Integr Comp Physiol, 279*(1), R47-52.

Hall, M. E., Harmancey, R., & Stec, D. E. (2015). Lean heart: Role of leptin in cardiac hypertrophy and metabolism. *World Journal of Cardiology, 7*(9), 511-524. doi:10.4330/wjc.v7.i9.511

Harvey, W. (2006). *The circulation of the blood*: Cosimo, Inc.

Haskell-Luevano, C., Cone, R. D., Monck, E. K., & Wan, Y. P. (2001). Structure activity studies of the melanocortin-4 receptor by in vitro mutagenesis: identification of agouti-related protein (AGRP), melanocortin agonist and synthetic peptide antagonist interaction determinants. *Biochemistry, 40*(20), 6164-6179.

Heberden, W. (1816). *Commentaries on the History and Cure of Diseases*: Payne and Foss.

Heid, I. M., Vollmert, C., Kronenberg, F., Huth, C., Ankerst, D. P., Luchner, A., . . . Hebebrand, J. (2008). Association of the MC4R V103I polymorphism with the metabolic syndrome: the KORA Study. *Obesity (Silver Spring), 16*(2), 369-376. doi:10.1038/oby.2007.21

Heydemann, A. (2016). An Overview of Murine High Fat Diet as a Model for Type 2 Diabetes Mellitus. *J Diabetes Res, 2016*, 2902351. doi:10.1155/2016/2902351

Hibino, H., Inanobe, A., Furutani, K., Murakami, S., Findlay, I., & Kurachi, Y. (2010). Inwardly rectifying potassium channels: their structure, function, and physiological roles. *Physiol Rev, 90*(1), 291-366. doi:10.1152/physrev.00021.2009

Hilgemann, D. W., & Ball, R. (1996). Regulation of cardiac Na+,Ca2+ exchange and KATP potassium channels by PIP2. *Science, 273*(5277), 956-959.

Hill, C., & Dunbar, J. C. (2002). The effects of acute and chronic alpha melanocyte stimulating hormone (alphaMSH) on cardiovascular dynamics in conscious rats. *Peptides, 23*(9), 1625-1630.

Hill , J. A., & Olson , E. N. (2008). Cardiac Plasticity. *New England Journal of Medicine, 358*(13), 1370-1380. doi:10.1056/NEJMra072139

Hinney, A., Volckmar, A. L., & Knoll, N. (2013). Melanocortin-4 receptor in energy homeostasis and obesity pathogenesis. *Prog Mol Biol Transl Sci, 114*, 147-191. doi:10.1016/b978-0-12-386933-3.00005-4

Ho, R., & Sutherland, E. W. (1975). cAMP-mediated feedback regulation in target cells. *Adv Cyclic Nucleotide Res, 5*, 533-548.

Ho, R. J., & Sutherland, E. W. (1975). Action of feedback regulator on adenylate cyclase. *Proc Natl Acad Sci U S A, 72*(5), 1773-1777.

Hruby, V. J., Lu, D., Sharma, S. D., Castrucci, A. L., Kesterson, R. A., al-Obeidi, F. A., . . . Cone, R. D. (1995). Cyclic lactam alpha-melanotropin analogues of Ac-Nle4-cyclo[Asp5, D-Phe7,Lys10] alpha-melanocyte-stimulating hormone-(4-10)-NH2 with bulky aromatic amino acids at position 7 show high antagonist potency and selectivity at specific melanocortin receptors. *J Med Chem, 38*(18), 3454-3461.

Hufnagel, C. A., Harvey, W. P., Rabil, P. J., & Mc, D. T. (1954). Surgical correction of aortic insufficiency. *Surgery, 35*(5), 673-683.

Humphreys, M. H., Ni, X. P., & Pearce, D. (2011). Cardiovascular effects of melanocortins. *Eur J Pharmacol, 660*(1), 43-52. doi:10.1016/j.ejphar.2010.10.102

Huo, L., Grill, H. J., & Bjorbaek, C. (2006). Divergent regulation of proopiomelanocortin neurons by leptin in the nucleus of the solitary tract and in the arcuate hypothalamic nucleus. *Diabetes, 55*(3), 567-573.

Hurst, J. W. (1986). The first coronary angioplasty as described by Andreas Gruentzig. *Am J Cardiol, 57*(1), 185-186.

Huszar, D., Lynch, C. A., Fairchild-Huntress, V., Dunmore, J. H., Fang, Q., Berkemeier, L. R., . . . Lee, F. (1997). Targeted disruption of the melanocortin-4 receptor results in obesity in mice. *Cell, 88*(1), 131-141.

Huszar, D., Lynch, C. A., FairchildHuntress, V., Dunmore, J. H., Fang, Q., Berkemeier, L. R., . . . Lee, F. (1997). Targeted disruption of the melanocortin-4 receptor results in obesity in mice. *Cell, 88*(1), 131-141.

Hwa, J. J., Ghibaudi, L., Gao, J., & Parker, E. M. (2001). Central melanocortin system modulates energy intake and expenditure of obese and lean Zucker rats. *American Journal of Physiology - Regulatory, Integrative and Comparative Physiology, 281*(2), R444-R451.

Hwa, J. J., Ghibaudi, L., Gao, J., & Parker, E. M. (2001). Central melanocortin system modulates energy intake and expenditure of obese and lean Zucker rats. *Am J Physiol Regul Integr Comp Physiol, 281*(2), R444-451.

Hwang, M. W., Shimatsu, A., Sasaki, Y., Ayukawa, H., Inenaga, K., Takeoka, R., . . . Kawai, C. (2007). Resolution of acromegalic cardiomyopathy in mild acromegalic physical abnormality after short-term octreotide therapy. *Heart Vessels, 22*(3), 202-207. doi:10.1007/s00380-006-0960-y

Ingles, J., Burns, C., Barratt, A., & Semsarian, C. (2015). Application of Genetic Testing in Hypertrophic Cardiomyopathy for Preclinical Disease Detection. *Circ Cardiovasc Genet, 8*(6), 852-859. doi:10.1161/circgenetics.115.001093

Isfort, M., Stevens, S. C., Schaffer, S., Jong, C. J., & Wold, L. E. (2014). Metabolic dysfunction in diabetic cardiomyopathy. *Heart Fail Rev, 19*(1), 35-48. doi:10.1007/s10741-013-9377-8

Israel, D. D., Sheffer-Babila, S., de Luca, C., Jo, Y. H., Liu, S. M., Xia, Q., . . . Chua, S. C., Jr. (2012). Effects of leptin and melanocortin signaling interactions on pubertal development and reproduction. *Endocrinology, 153*(5), 2408-2419. doi:10.1210/en.2011-1822

Itoh, M., Kato, H., Suganami, T., Konuma, K., Marumoto, Y., Terai, S., . . . Ogawa, Y. (2013). Hepatic crown-like structure: a unique histological feature in non-alcoholic steatohepatitis in mice and humans. *PLoS One, 8*(12), e82163. doi:10.1371/journal.pone.0082163

Iwasa, M., Kawabe, K., & Sapru, H. N. (2013). Activation of melanocortin receptors in the intermediolateral cell column of the upper thoracic cord elicits tachycardia in the rat. *Am J Physiol Heart Circ Physiol, 305*(6), H885-893. doi:10.1152/ajpheart.00443.2013

Janssen, B., Debets, J., Leenders, P., & Smits, J. (2002). Chronic measurement of cardiac output in conscious mice. *Am J Physiol Regul Integr Comp Physiol, 282*(3), R928-935. doi:10.1152/ajpregu.00406.2001

Jia, G., DeMarco, V. G., & Sowers, J. R. (2016). Insulin resistance and hyperinsulinaemia in diabetic cardiomyopathy. *Nat Rev Endocrinol, 12*(3), 144-153. doi:10.1038/nrendo.2015.216

Jonsson, L., Skarphedinsson, J. O., Skuladottir, G. V., Atlason, P. T., Eiriksdottir, V. H., Franzson, L., & Schioth, H. B. (2001). Melanocortin receptor agonist transiently increases oxygen consumption in rats. *Neuroreport, 12*(17), 3703-3708.

Joseph, S. A., Pilcher, W. H., & Bennett-Clarke, C. (1983). Immunocytochemical localization of ACTH perikarya in nucleus tractus solitarius: evidence for a second opiocortin neuronal system. *Neurosci Lett, 38*(3), 221-225.

Kahn, A. R., Hixson, J. D., Puffer, J. E., & Bakken, E. E. (1973). Three-years' clinical

experience with radioisotope powered cardiac pacemakers. *IEEE Trans Biomed Eng, 20*(5), 326-331. doi:10.1109/tbme.1973.324283

Kaiyala, K. J., & Schwartz, M. W. (2011). Toward a More Complete (and Less Controversial) Understanding of Energy Expenditure and Its Role in Obesity Pathogenesis. *Diabetes, 60*(1), 17-23. doi:10.2337/db10-0909

Kalay, N., Ozdogru, I., Gul, A., Yucel, Y., Cetinkaya, Y., Inanc, M. T., . . . Eryol, N. K. (2008). Effects of intermittent and long-term glucose-insulin-potassium infusion in patients with systolic heart failure. *Experimental & Clinical Cardiology, 13*(2), 85-88.

Katz, B. (1949). Les constantes electriques de la membrane du muscle. . *Arch. Sci. Physiol., 3*, 285-299.

Kenchaiah, S., Evans, J. C., Levy, D., Wilson, P. W., Benjamin, E. J., Larson, M. G., . . . Vasan, R. S. (2002). Obesity and the risk of heart failure. *N Engl J Med, 347*(5), 305-313. doi:10.1056/NEJMoa020245

Kievit, P., Halem, H., Marks, D. L., Dong, J. Z., Glavas, M. M., Sinnayah, P., . . . Culler, M. D. (2013). Chronic treatment with a melanocortin-4 receptor agonist causes weight loss, reduces insulin resistance, and improves cardiovascular function in diet-induced obese rhesus macaques. *Diabetes, 62*(2), 490-497. doi:10.2337/db12-0598

Kim, C., Xuong, N. H., & Taylor, S. S. (2005). Crystal structure of a complex between the catalytic and regulatory (RIalpha) subunits of PKA. *Science, 307*(5710), 690-696. doi:10.1126/science.1104607

Kim, C. S., Lee, S. H., Kim, R. Y., Kim, B. J., Li, S. Z., Lee, I. H., . . . Baik, J. H. (2002). Identification of domains directing specificity of coupling to G-proteins for the melanocortin MC3 and MC4 receptors. *J Biol Chem, 277*(35), 31310-31317. doi:10.1074/jbc.M112085200

Kishi, T., Aschkenasi, C. J., Lee, C. E., Mountjoy, K. G., Saper, C. B., & Elmquist, J. K. (2003). Expression of melanocortin 4 receptor mRNA in the central nervous system of the rat. *J Comp Neurol, 457*(3), 213-235. doi:10.1002/cne.10454

Kleiber, M. (1932). Body size and metabolism. *ENE, 1*(9).

Kleuss, C., Raw, A. S., Lee, E., Sprang, S. R., & Gilman, A. G. (1994). Mechanism of GTP hydrolysis by G-protein alpha subunits. *Proc Natl Acad Sci U S A, 91*(21), 9828-9831.

Koch, M., Varela, L., Kim, J. G., Kim, J. D., Hernandez-Nuno, F., Simonds, S. E., . . . Horvath, T. L. (2015). Hypothalamic POMC neurons promote cannabinoid-

induced feeding. *Nature, 519*(7541), 45-50. doi:10.1038/nature14260

Konda, Y., Gantz, I., DelValle, J., Shimoto, Y., Miwa, H., & Yamada, T. (1994). Interaction of dual intracellular signaling pathways activated by the melanocortin-3 receptor. *J Biol Chem, 269*(18), 13162-13166.

Krashes, M. J., Koda, S., Ye, C., Rogan, S. C., Adams, A. C., Cusher, D. S., . . . Lowell, B. B. (2011). Rapid, reversible activation of AgRP neurons drives feeding behavior in mice. *J Clin Invest, 121*(4), 1424-1428. doi:10.1172/JCI46229

Krashes, M. J., Shah, B. P., Koda, S., & Lowell, B. B. (2013). Rapid versus delayed stimulation of feeding by the endogenously released AgRP neuron mediators GABA, NPY, and AgRP. *Cell Metab, 18*(4), 588-595. doi:10.1016/j.cmet.2013.09.009

Krashes, M. J., Shah, B. P., Koda, S., & Lowell, B. B. (2013). Rapid versus delayed stimulation of feeding by the endogenously released AgRP neuron mediators, GABA, NPY and AgRP. *Cell metabolism, 18*(4), 10.1016/j.cmet.2013.1009.1009. doi:10.1016/j.cmet.2013.09.009

Krude, H., Biebermann, H., Luck, W., Horn, R., Brabant, G., & Gruters, A. (1998). Severe early-onset obesity, adrenal insufficiency and red hair pigmentation caused by POMC mutations in humans. *Nat Genet, 19*(2), 155-157. doi:10.1038/509

Kruse, R., & Hojlund, K. (2017). Mitochondrial phosphoproteomics of mammalian tissues. *Mitochondrion, 33*, 45-57. doi:10.1016/j.mito.2016.08.004

Kuo, J. J., Silva, A. A., & Hall, J. E. (2003). Hypothalamic melanocortin receptors and chronic regulation of arterial pressure and renal function. *Hypertension, 41*(3 Pt 2), 768-774. doi:10.1161/01.hyp.0000048194.97428.1a

Labinskyy, V., Bellomo, M., Chandler, M. P., Young, M. E., Lionetti, V., Qanud, K., . . . Recchia, F. A. (2007). Chronic activation of peroxisome proliferator-activated receptor-alpha with fenofibrate prevents alterations in cardiac metabolic phenotype without changing the onset of decompensation in pacing-induced heart failure. *J Pharmacol Exp Ther, 321*(1), 165-171. doi:10.1124/jpet.106.116871

Lam, D. D., de Souza, F. S. J., Nasif, S., Yamashita, M., López-Leal, R., Otero-Corchon, V., . . . Low, M. J. (2015). Partially Redundant Enhancers Cooperatively Maintain Mammalian Pomc Expression Above a Critical Functional Threshold. *PLoS Genetics, 11*(2), e1004935. doi:10.1371/journal.pgen.1004935

Lei, Q., Jones, M. B., Talley, E. M., Schrier, A. D., McIntire, W. E., Garrison, J. C., &

Bayliss, D. A. (2000). Activation and inhibition of G protein-coupled inwardly rectifying potassium (Kir3) channels by G protein beta gamma subunits. *Proc Natl Acad Sci U S A, 97*(17), 9771-9776.

Lemus, M. B., Bayliss, J. A., Lockie, S. H., Santos, V. V., Reichenbach, A., Stark, R., & Andrews, Z. B. (2015). A stereological analysis of NPY, POMC, Orexin, GFAP astrocyte, and Iba1 microglia cell number and volume in diet-induced obese male mice. *Endocrinology, 156*(5), 1701-1713. doi:10.1210/en.2014-1961

Levitan, E. B., Yang, A. Z., Wolk, A., & Mittleman, M. A. (2009). Adiposity and incidence of heart failure hospitalization and mortality: a population-based prospective study. *Circ Heart Fail, 2*(3), 202-208. doi:10.1161/circheartfailure.108.794099

Lewis, T. (1919). *Clinical electrocardiography*: Hoeber.

Li, S. J., Varga, K., Archer, P., Hruby, V. J., Sharma, S. D., Kesterson, R. A., . . . Kunos, G. (1996). Melanocortin antagonists define two distinct pathways of cardiovascular control by alpha- and gamma-melanocyte-stimulating hormones. *J Neurosci, 16*(16), 5182-5188.

Lionetti, V., Linke, A., Chandler, M. P., Young, M. E., Penn, M. S., Gupte, S., . . . Recchia, F. A. (2005). Carnitine palmitoyl transferase-I inhibition prevents ventricular remodeling and delays decompensation in pacing-induced heart failure. *Cardiovasc Res, 66*(3), 454-461. doi:10.1016/j.cardiores.2005.02.004

Lionetti, V., Stanley, W. C., & Recchia, F. A. (2011). Modulating fatty acid oxidation in heart failure. *Cardiovasc Res, 90*(2), 202-209. doi:10.1093/cvr/cvr038

Liu, H., Kishi, T., Roseberry, A. G., Cai, X., Lee, C. E., Montez, J. M., . . . Elmquist, J. K. (2003). Transgenic mice expressing green fluorescent protein under the control of the melanocortin-4 receptor promoter. *J Neurosci, 23*(18), 7143-7154.

Liu, J., Lee, J., Salazar Hernandez, Mario A., Mazitschek, R., & Ozcan, U. Treatment of Obesity with Celastrol. *Cell, 161*(5), 999-1011. doi:10.1016/j.cell.2015.05.011

Lu, D., Willard, D., Patel, I. R., Kadwell, S., Overton, L., Kost, T., . . . et al. (1994). Agouti protein is an antagonist of the melanocyte-stimulating-hormone receptor. *Nature, 371*(6500), 799-802. doi:10.1038/371799a0

Luquet, S., Perez, F. A., Hnasko, T. S., & Palmiter, R. D. (2005). NPY/AgRP neurons are essential for feeding in adult mice but can be ablated in neonates. *Science, 310*(5748), 683-685. doi:10.1126/science.1115524

Lute, B., Jou, W., Lateef, D. M., Goldgof, M., Xiao, C., Piñol, R. A., . . . Reitman, M. L. (2014). Biphasic Effect of Melanocortin Agonists on Metabolic Rate and Body Temperature. *Cell metabolism, 20*(2), 333-345. doi:10.1016/j.cmet.2014.05.021

Magenis, R. E., Smith, L., Nadeau, J. H., Johnson, K. R., Mountjoy, K. G., & Cone, R. D. (1994). Mapping of the ACTH, MSH, and neural (MC3 and MC4) melanocortin receptors in the mouse and human. *Mamm Genome, 5*(8), 503-508.

Mali, V. R., & Palaniyandi, S. S. (2014). Regulation and therapeutic strategies of 4-hydroxy-2-nonenal metabolism in heart disease. *Free Radic Res, 48*(3), 251-263. doi:10.3109/10715762.2013.864761

Mansour, M., White, D., Wernette, C., Dennis, J., Tao, Y. X., Collins, R., . . . Morrison, E. (2010). Pancreatic neuronal melanocortin-4 receptor modulates serum insulin levels independent of leptin receptor. *Endocrine, 37*(1), 220-230. doi:10.1007/s12020-009-9289-5

Margulies, K. B., Anstrom, K. J., Hernandez, A. F., Redfield, M. M., Shah, M. R., Braunwald, E., & Cappola, T. P. (2014). GLP-1 Agonist Therapy for Advanced Heart Failure with Reduced Ejection Fraction: Design and Rationale for the Functional Impact of GLP-1 for Heart Failure Treatment (FIGHT) Study. *Circ Heart Fail, 7*(4), 673-679. doi:10.1161/CIRCHEARTFAILURE.114.000346

Maron, B. J. (2005). Distinguishing hypertrophic cardiomyopathy from athlete's heart: a clinical problem of increasing magnitude and significance. *Heart, 91*(11), 1380-1382. doi:10.1136/hrt.2005.060962

Maron, B. J., Olivotto, I., Spirito, P., Casey, S. A., Bellone, P., Gohman, T. E., . . . Cecchi, F. (2000). Epidemiology of hypertrophic cardiomyopathy-related death: revisited in a large non-referral-based patient population. *Circulation, 102*(8), 858-864.

Maron, B. J., Towbin, J. A., Thiene, G., Antzelevitch, C., Corrado, D., Arnett, D., . . . Young, J. B. (2006). Contemporary definitions and classification of the cardiomyopathies: an American Heart Association Scientific Statement from the Council on Clinical Cardiology, Heart Failure and Transplantation Committee; Quality of Care and Outcomes Research and Functional Genomics and Translational Biology Interdisciplinary Working Groups; and Council on Epidemiology and Prevention. *Circulation, 113*(14), 1807-1816. doi:10.1161/circulationaha.106.174287

Martinelli, C. E., Keogh, J. M., Greenfield, J. R., Henning, E., van der Klaauw, A. A., Blackwood, A., . . . Farooqi, I. S. (2011). Obesity due to melanocortin 4 receptor (MC4R) deficiency is associated with increased linear growth and final height, fasting hyperinsulinemia, and incompletely suppressed growth hormone secretion. *J Clin Endocrinol Metab, 96*(1), E181-188. doi:10.1210/jc.2010-1369

Marty, A. T. (1996). Atlas of Heart Disease: LWW.

Matsumura, K., Tsuchihashi, T., Abe, I., & Iida, M. (2002). Central alpha-melanocyte-stimulating hormone acts at melanocortin-4 receptor to activate sympathetic nervous system in conscious rabbits. *Brain Res, 948*(1-2), 145-148.

Mazumder, P. K., O'Neill, B. T., Roberts, M. W., Buchanan, J., Yun, U. J., Cooksey, R. C., . . . Abel, E. D. (2004). Impaired cardiac efficiency and increased fatty acid oxidation in insulin-resistant ob/ob mouse hearts. *Diabetes, 53*(9), 2366-2374.

Mazurek, S., & Kim, G. H. (2017). Genetic and Epigenetic Regulation of Arrhythmogenic Cardiomyopathy. *Biochim Biophys Acta*. doi:10.1016/j.bbadis.2017.04.020

McGaffin, K. R., Witham, W. G., Yester, K. A., Romano, L. C., O'Doherty, R. M., McTiernan, C. F., & O'Donnell, C. P. (2011). Cardiac-specific leptin receptor deletion exacerbates ischaemic heart failure in mice. *Cardiovasc Res, 89*(1), 60-71. doi:10.1093/cvr/cvq288

Mestroni, L., Rocco, C., Gregori, D., Sinagra, G., Di Lenarda, A., Miocic, S., . . . Camerini. (1999). Familial dilated cardiomyopathy: evidence for genetic and phenotypic heterogeneity. Heart Muscle Disease Study Group. *J Am Coll Cardiol, 34*(1), 181-190.

Metra, M., & Teerlink, J. R. (2017). Heart failure. *Lancet*. doi:10.1016/s0140-6736(17)31071-1

Mi, H., & Thomas, P. (2009). PANTHER Pathway: An Ontology-Based Pathway Database Coupled with Data Analysis Tools. In Y. Nikolsky & J. Bryant (Eds.), *Protein Networks and Pathway Analysis* (pp. 123-140). Totowa, NJ: Humana Press.

Montague, C. T., Farooqi, I. S., Whitehead, J. P., Soos, M. A., Rau, H., Wareham, N. J., . . . O'Rahilly, S. (1997). Congenital leptin deficiency is associated with severe early-onset obesity in humans. *Nature, 387*(6636), 903-908. doi:10.1038/43185

Mootha, V. K., Lindgren, C. M., Eriksson, K.-F., Subramanian, A., Sihag, S., Lehar, J., . . . Groop, L. C. (2003). PGC-1[alpha]-responsive genes involved in oxidative phosphorylation are coordinately downregulated in human diabetes. *Nat Genet, 34*(3), 267-273. doi:http://www.nature.com/ng/journal/v34/n3/suppinfo/ng1180_S1.html

Morgan, C., & Cone, R. D. (2006). Melanocortin-5 receptor deficiency in mice blocks a novel pathway influencing pheromone-induced aggression. *Behav Genet, 36*(2), 291-300. doi:10.1007/s10519-005-9024-9

Morita, H., Larson, M. G., Barr, S. C., Vasan, R. S., O'Donnell, C. J., Hirschhorn, J. N., . . . Benjamin, E. J. (2006). Single-gene mutations and increased left ventricular

wall thickness in the community: the Framingham Heart Study. *Circulation, 113*(23), 2697-2705. doi:10.1161/circulationaha.105.593558

Mountjoy, K. G. (2015). Pro-Opiomelanocortin (POMC) Neurones, POMC-Derived Peptides, Melanocortin Receptors and Obesity: How Understanding of this System has Changed Over the Last Decade. *J Neuroendocrinol, 27*(6), 406-418. doi:10.1111/jne.12285

Mountjoy, K. G., Jenny Wu, C. S., Dumont, L. M., & Wild, J. M. (2003). Melanocortin-4 receptor messenger ribonucleic acid expression in rat cardiorespiratory, musculoskeletal, and integumentary systems. *Endocrinology, 144*(12), 5488-5496. doi:10.1210/en.2003-0570

en.2003-0570 [pii]

Mountjoy, K. G., Kong, P. L., Taylor, J. A., Willard, D. H., & Wilkison, W. O. (2001). Melanocortin receptor-mediated mobilization of intracellular free calcium in HEK293 cells. *Physiol Genomics, 5*(1), 11-19.

Mountjoy, K. G., Mortrud, M. T., Low, M. J., Simerly, R. B., & Cone, R. D. (1994). Localization of the melanocortin-4 receptor (MC4-R) in neuroendocrine and autonomic control circuits in the brain. *Mol Endocrinol, 8*(10), 1298-1308. doi:10.1210/mend.8.10.7854347

Mountjoy, K. G., Robbins, L. S., Mortrud, M. T., & Cone, R. D. (1992). The cloning of a family of genes that encode the melanocortin receptors. *Science, 257*(5074), 1248-1251.

Mudhar, H., Wagner, B., & Suvarna, S. (2001). Electron microscopy of myocardial tissue. A nine year review. *Journal of Clinical Pathology, 54*(4), 321-325. doi:10.1136/jcp.54.4.321

Munusamy, S., do Carmo, J. M., Hosler, J. P., & Hall, J. E. (2015). Obesity-induced changes in kidney mitochondria and endoplasmic reticulum in the presence or absence of leptin. *American Journal of Physiology - Renal Physiology, 309*(8), F731.

National Heart, L. a. B. I. (1998). *Morbidity & mortality: 1998 chartbook on cardiovascular, lung, and blood diseases.* Retrieved from

Ni, X. P., Butler, A. A., Cone, R. D., & Humphreys, M. H. (2006). Central receptors mediating the cardiovascular actions of melanocyte stimulating hormones. *J Hypertens, 24*(11), 2239-2246. doi:10.1097/01.hjh.0000249702.49854.fa

Nicholls, D. G., Ferguson, S. J., & Ferguson, S. (2002). *Bioenergetics*. Oxford, UNKNOWN: Elsevier Science.

Nijenhuis, W. A., Oosterom, J., & Adan, R. A. (2001). AgRP(83-132) acts as an inverse agonist on the human-melanocortin-4 receptor. *Mol Endocrinol, 15*(1), 164-171. doi:10.1210/mend.15.1.0578

Nogueiras, R., Wiedmer, P., Perez-Tilve, D., Veyrat-Durebex, C., Keogh, J. M., Sutton, G. M., . . . Tschöp, M. H. (2007). The central melanocortin system directly controls peripheral lipid metabolism. *J Clin Invest, 117*(11), 3475-3488. doi:10.1172/JCI31743

Ogden, C. L., Carroll, M. D., Kit, B. K., & Flegal, K. M. (2014). Prevalence of childhood and adult obesity in the United States, 2011-2012. *Jama, 311*(8), 806-814. doi:10.1001/jama.2014.732

Ollmann, M. M., Wilson, B. D., Yang, Y. K., Kerns, J. A., Chen, Y., Gantz, I., & Barsh, G. S. (1997). Antagonism of central melanocortin receptors in vitro and in vivo by agouti-related protein. *Science, 278*(5335), 135-138.

Owen, D. R., MacAllister, R., & Sofat, R. (2015). Intravenous Furosemide for Acute Decompensated Congestive Heart Failure: What Is the Evidence? *Clin Pharmacol Ther, 98*(2), 119-121. doi:10.1002/cpt.120

Padilla, S. L., Carmody, J. S., & Zeltser, L. M. (2010). Pomc-expressing progenitors give rise to antagonistic neuronal populations in hypothalamic feeding circuits. *Nat Med, 16*(4), 403-405. doi:10.1038/nm.2126

Padilla, S. L., Reef, D., & Zeltser, L. M. (2012). Defining POMC neurons using transgenic reagents: impact of transient Pomc expression in diverse immature neuronal populations. *Endocrinology, 153*(3), 1219-1231. doi:10.1210/en.2011-1665

Panaro, B. L., & Cone, R. D. (2013). Melanocortin-4 receptor mutations paradoxically reduce preference for palatable foods. *Proc Natl Acad Sci U S A, 110*(17), 7050-7055. doi:10.1073/pnas.1304707110

Panaro, B. L., Tough, I. R., Engelstoft, M. S., Matthews, R. T., Digby, G. J., Moller, C. L., . . . Cone, R. D. (2014). The melanocortin-4 receptor is expressed in enteroendocrine L cells and regulates the release of peptide YY and glucagon-like peptide 1 in vivo. *Cell Metab, 20*(6), 1018-1029. doi:10.1016/j.cmet.2014.10.004

Panaro, B. L., Tough, I. R., Engelstoft, M. S., Matthews, R. T., Digby, G. J., Møller, C. L., . . . Cone, R. D. (2014). The Melanocortin-4 Receptor is Expressed in Enteroendocrine L Cells and Regulates the Release of Peptide YY and Glucagon-Like Peptide 1 In Vivo. *Cell metabolism, 20*(6), 1018-1029.

doi:10.1016/j.cmet.2014.10.004

Paolisso, G., Gambardella, A., Galzerano, D., D'Amore, A., Rubino, P., Verza, M., . . . D'Onofrio, F. (1994). Total-body and myocardial substrate oxidation in congestive heart failure. *Metabolism, 43*(2), 174-179.

Paternostro, G., Pagano, D., Gnecchi-Ruscone, T., Bonser, R. S., & Camici, P. G. (1999). Insulin resistance in patients with cardiac hypertrophy. *Cardiovasc Res, 42*(1), 246-253.

Pavia, J. M., Schioth, H. B., & Morris, M. J. (2003). Role of MC4 receptors in the depressor and bradycardic effects of alpha-MSH in the nucleus tractus solitarii of the rat. *Neuroreport, 14*(5), 703-707. doi:10.1097/01.wnr.0000065510.53896.35

Peltier, L. F. (2003). On the Usefulness of the Parts of the Body.

Perello, M., Stuart, R. C., & Nillni, E. A. (2007). Differential effects of fasting and leptin on proopiomelanocortin peptides in the arcuate nucleus and in the nucleus of the solitary tract. *Am J Physiol Endocrinol Metab, 292*(5), E1348-1357. doi:10.1152/ajpendo.00466.2006

Perry, S. W., Norman, J. P., Barbieri, J., Brown, E. B., & Gelbard, H. A. (2011). Mitochondrial membrane potential probes and the proton gradient: a practical usage guide. *BioTechniques, 50*(2), 98-115. doi:10.2144/000113610

Pfaffinger, P. J., Martin, J. M., Hunter, D. D., Nathanson, N. M., & Hille, B. (1985). GTP-binding proteins couple cardiac muscarinic receptors to a K channel. *Nature, 317*(6037), 536-538.

Pinto, S., Roseberry, A. G., Liu, H., Diano, S., Shanabrough, M., Cai, X., . . . Horvath, T. L. (2004). Rapid rewiring of arcuate nucleus feeding circuits by leptin. *Science, 304*(5667), 110-115. doi:10.1126/science.1089459

Poggioli, R., Vergoni, A. V., & Bertolini, A. (1986). ACTH-(1-24) and alpha-MSH antagonize feeding behavior stimulated by kappa opiate agonists. *Peptides, 7*(5), 843-848.

Prasad, A., Dangas, G., Srinivasan, M., Yu, J., Gersh, B. J., Mehran, R., & Stone, G. W. (2014). Incidence and angiographic characteristics of patients with apical ballooning syndrome (takotsubo/stress cardiomyopathy) in the HORIZONS-AMI trial: an analysis from a multicenter, international study of ST-elevation myocardial infarction. *Catheter Cardiovasc Interv, 83*(3), 343-348. doi:10.1002/ccd.23441

Qian, S., Chen, H., Weingarth, D., Trumbauer, M. E., Novi, D. E., Guan, X., . . . Marsh, D. J. (2002). Neither Agouti-Related Protein nor Neuropeptide Y Is Critically

Required for the Regulation of Energy Homeostasis in Mice. *Molecular and Cellular Biology, 22*(14), 5027-5035. doi:10.1128/mcb.22.14.5027-5035.2002

Raher, M. J., Thibault, H. B., Buys, E. S., Kuruppu, D., Shimizu, N., Brownell, A. L., . . . Scherrer-Crosbie, M. (2008). A short duration of high-fat diet induces insulin resistance and predisposes to adverse left ventricular remodeling after pressure overload. *Am J Physiol Heart Circ Physiol, 295*(6), H2495-2502. doi:10.1152/ajpheart.00139.2008

Rajasoorya, C., Holdaway, I. M., Wrightson, P., Scott, D. J., & Ibbertson, H. K. (1994). Determinants of clinical outcome and survival in acromegaly. *Clin Endocrinol (Oxf), 41*(1), 95-102.

Rasmussen, S. G. F., DeVree, B. T., Zou, Y., Kruse, A. C., Chung, K. Y., Kobilka, T. S., . . . Kobilka, B. K. (2011). Crystal Structure of the β(2)Adrenergic Receptor-Gs protein complex. *Nature, 477*(7366), 549-555. doi:10.1038/nature10361

Richardson, P., McKenna, W., Bristow, M., Maisch, B., Mautner, B., O'Connell, J., . . . Nordet, P. (1996). Report of the 1995 World Health Organization/International Society and Federation of Cardiology Task Force on the Definition and Classification of cardiomyopathies. *Circulation, 93*(5), 841-842.

Rosca, M. G., Tandler, B., & Hoppel, C. L. (2013). Mitochondria in cardiac hypertrophy and heart failure. *Journal of molecular and cellular cardiology, 55*, 31-41. doi:10.1016/j.yjmcc.2012.09.002

Roselli-Rehfuss, L., Mountjoy, K. G., Robbins, L. S., Mortrud, M. T., Low, M. J., Tatro, J. B., . . . Cone, R. D. (1993). Identification of a receptor for gamma melanotropin and other proopiomelanocortin peptides in the hypothalamus and limbic system. *Proc Natl Acad Sci U S A, 90*(19), 8856-8860.

Rossi, J., Balthasar, N., Olson, D., Scott, M., Berglund, E., Lee, C. E., . . . Elmquist, J. K. (2011). Melanocortin-4 receptors expressed by cholinergic neurons regulate energy balance and glucose homeostasis. *Cell Metab, 13*(2), 195-204. doi:10.1016/j.cmet.2011.01.010

Royalty, J. E., Konradsen, G., Eskerod, O., Wulff, B. S., & Hansen, B. S. (2014). Investigation of Safety, Tolerability, Pharmacokinetics, and Pharmacodynamics of Single and Multiple Doses of a Long-Acting α-MSH Analog in Healthy Overweight and Obese Subjects. *Journal of Clinical Pharmacology, 54*(4), 394-404. doi:10.1002/jcph.211

Rubler, S., Dlugash, J., Yuceoglu, Y. Z., Kumral, T., Branwood, A. W., & Grishman, A. (1972). New type of cardiomyopathy associated with diabetic glomerulosclerosis.

Am J Cardiol, 30(6), 595-602.

Salie, R., Huisamen, B., & Lochner, A. (2014). High carbohydrate and high fat diets protect the heart against ischaemia/reperfusion injury. *Cardiovasc Diabetol, 13*, 109-109. doi:10.1186/s12933-014-0109-8

Sayk, F., Heutling, D., Dodt, C., Iwen, K. A., Wellhoner, J. P., Scherag, S., . . . Lehnert, H. (2010). Sympathetic function in human carriers of melanocortin-4 receptor gene mutations. *J Clin Endocrinol Metab, 95*(4), 1998-2002. doi:10.1210/jc.2009-2297

Schwartzberg, D. G., & Nakane, P. K. (1983). ACTH-related peptide containing neurons within the medulla oblongata of the rat. *Brain Res, 276*(2), 351-356.

Semeniuk, L. M., Kryski, A. J., & Severson, D. L. (2002). Echocardiographic assessment of cardiac function in diabetic db/db and transgenic db/db-hGLUT4 mice. *Am J Physiol Heart Circ Physiol, 283*(3), H976-982. doi:10.1152/ajpheart.00088.2002

Semsarian, C., Ingles, J., Maron, M. S., & Maron, B. J. (2015). New perspectives on the prevalence of hypertrophic cardiomyopathy. *J Am Coll Cardiol, 65*(12), 1249-1254. doi:10.1016/j.jacc.2015.01.019

Sénac, J. B. (1777). *Traité de la structure du coeur, de son action et de ses maladies* (Vol. 1): chez Joseph Barbou.

Shek, E. W., Brands, M. W., & Hall, J. E. (1998). Chronic leptin infusion increases arterial pressure. *Hypertension, 31*(1 Pt 2), 409-414.

Shen, Y., Fu, W. Y., Cheng, E. Y., Fu, A. K., & Ip, N. Y. (2013). Melanocortin-4 receptor regulates hippocampal synaptic plasticity through a protein kinase A-dependent mechanism. *J Neurosci, 33*(2), 464-472. doi:10.1523/jneurosci.3282-12.2013

Shinyama, H., Masuzaki, H., Fang, H., & Flier, J. S. (2003). Regulation of melanocortin-4 receptor signaling: agonist-mediated desensitization and internalization. *Endocrinology, 144*(4), 1301-1314. doi:10.1210/en.2002-220931

Shirani, J., Pick, R., Roberts, W. C., & Maron, B. J. (2000). Morphology and significance of the left ventricular collagen network in young patients with hypertrophic cardiomyopathy and sudden cardiac death. *J Am Coll Cardiol, 35*(1), 36-44.

Shukla, C., Koch, L. G., Britton, S. L., Cai, M., Hruby, V. J., Bednarek, M., & Novak, C. M. (2015). Contribution of regional brain melanocortin receptor subtypes to elevated activity energy expenditure in lean, active rats. *Neuroscience, 310*, 252-267. doi:10.1016/j.neuroscience.2015.09.035

Shutter, J. R., Graham, M., Kinsey, A. C., Scully, S., Luthy, R., & Stark, K. L. (1997). Hypothalamic expression of ART, a novel gene related to agouti, is up-regulated in obese and diabetic mutant mice. *Genes Dev, 11*(5), 593-602.

Siljee, J. E., Unmehopa, U. A., Kalsbeek, A., Swaab, D. F., Fliers, E., & Alkemade, A. (2013). Melanocortin 4 receptor distribution in the human hypothalamus. *Eur J Endocrinol, 168*(3), 361-369. doi:10.1530/EJE-12-0750

Singal, P. K., & Iliskovic, N. (1998). Doxorubicin-Induced Cardiomyopathy. *New England Journal of Medicine, 339*(13), 900-905. doi:10.1056/NEJM199809243391307

Small, C., Liu, Y., Stanley, S., Connoley, I., Kennedy, A., Stock, M., & Bloom, S. (2003). Chronic CNS administration of Agouti-related protein (Agrp) reduces energy expenditure. *International journal of obesity, 27*(4), 530-533.

Small, C. J., Liu, Y. L., Stanley, S. A., Connoley, I. P., Kennedy, A., Stock, M. J., & Bloom, S. R. (2003). Chronic CNS administration of Agouti-related protein (Agrp) reduces energy expenditure. *Int J Obes Relat Metab Disord, 27*(4), 530-533. doi:10.1038/sj.ijo.0802253

Sohal, V. S., Zhang, F., Yizhar, O., & Deisseroth, K. (2009). Parvalbumin neurons and gamma rhythms enhance cortical circuit performance. *Nature, 459*(7247), 698-702. doi:10.1038/nature07991

Sohn, J.-W., Harris, L. E., Berglund, E. D., Liu, T., Vong, L., Lowell, B. B., . . . Elmquist, J. K. (2013). Melanocortin 4 Receptors Reciprocally Regulate Sympathetic and Parasympathetic - Preganglionic Neurons. *Cell, 152*(3), 612-619. doi:10.1016/j.cell.2012.12.022

Srinivasan, S., Lubrano-Berthelier, C., Govaerts, C., Picard, F., Santiago, P., Conklin, B. R., & Vaisse, C. (2004). Constitutive activity of the melanocortin-4 receptor is maintained by its N-terminal domain and plays a role in energy homeostasis in humans. *Journal of Clinical Investigation, 114*(8), 1158-1164. doi:10.1172/JCI200421927

Srinivasan, S., Lubrano-Berthelier, C., Govaerts, C., Picard, F., Santiago, P., Conklin, B. R., & Vaisse, C. (2004). Constitutive activity of the melanocortin-4 receptor is maintained by its N-terminal domain and plays a role in energy homeostasis in humans. *J Clin Invest, 114*(8), 1158-1164. doi:10.1172/jci21927

Srisai, D., Gillum, M. P., Panaro, B. L., Zhang, X. M., Kotchabhakdi, N., Shulman, G. I., . . . Cone, R. D. (2011). Characterization of the hyperphagic response to dietary fat in the MC4R knockout mouse. *Endocrinology, 152*(3), 890-902. doi:10.1210/en.2010-0716

Stampfer, M., Epstein, S. E., Beiser, G. D., & Braunwald, E. (1968). Hemodynamic effects of diuresis at rest and during intense upright exercise in patients with impaired cardiac function. *Circulation, 37*(6), 900-911.

Stanley, W. C., Recchia, F. A., & Lopaschuk, G. D. (2005). Myocardial substrate metabolism in the normal and failing heart. *Physiol Rev, 85*(3), 1093-1129. doi:10.1152/physrev.00006.2004

Statistics, N. C. f. H. (2016). *Health, United States, 2015: With Special Feature on Racial and Ethnic Health Disparities*. Retrieved from Hyattsville, MD:

Ste Marie, L., Miura, G. I., Marsh, D. J., Yagaloff, K., & Palmiter, R. D. (2000). A metabolic defect promotes obesity in mice lacking melanocortin-4 receptors. *Proc Natl Acad Sci U S A, 97*(22), 12339-12344. doi:10.1073/pnas.220409497

Stepp, D. W., Osakwe, C. C., Belin de Chantemele, E. J., & Mintz, J. D. (2013). Vascular effects of deletion of melanocortin-4 receptors in rats. *Physiol Rep, 1*(6), e00146. doi:10.1002/phy2.146

Sternson, S. M., & Roth, B. L. (2014). Chemogenetic tools to interrogate brain functions. *Annu Rev Neurosci, 37*, 387-407. doi:10.1146/annurev-neuro-071013-014048

Stutzmann, F., Tan, K., Vatin, V., Dina, C., Jouret, B. a., Tichet, J., . . . Meyre, D. (2008). Prevalence of Melanocortin-4 Receptor Deficiency in Europeans and Their Age-Dependent Penetrance in Multigenerational Pedigrees. *Diabetes, 57*(9), 2511-2518. doi:10.2337/db08-0153

Subramanian, A., Tamayo, P., Mootha, V. K., Mukherjee, S., Ebert, B. L., Gillette, M. A., . . . Mesirov, J. P. (2005). Gene set enrichment analysis: A knowledge-based approach for interpreting genome-wide expression profiles. *Proceedings of the National Academy of Sciences, 102*(43), 15545-15550. doi:10.1073/pnas.0506580102

Susa, J. B., Neave, C., Sehgal, P., Singer, D. B., Zeller, W. P., & Schwartz, R. (1984). Chronic hyperinsulinemia in the fetal rhesus monkey. Effects of physiologic hyperinsulinemia on fetal growth and composition. *Diabetes, 33*(7), 656-660.

Sutton, A. K., Pei, H., Burnett, K. H., Myers, M. G., Jr., Rhodes, C. J., & Olson, D. P. (2014). Control of food intake and energy expenditure by Nos1 neurons of the paraventricular hypothalamus. *J Neurosci, 34*(46), 15306-15318. doi:10.1523/JNEUROSCI.0226-14.2014

Sweeney, G. (2010). Cardiovascular effects of leptin. *Nat Rev Cardiol, 7*(1), 22-29. doi:10.1038/nrcardio.2009.224

Talati, M. H., Brittain, E. L., Fessel, J. P., Penner, N., Atkinson, J., Funke, M., . . .

Hemnes, A. R. (2016). Mechanisms of Lipid Accumulation in the Bone Morphogenetic Protein Receptor Type 2 Mutant Right Ventricle. *Am J Respir Crit Care Med, 194*(6), 719-728. doi:10.1164/rccm.201507-1444OC

Tallam, L. S., da Silva, A. A., & Hall, J. E. (2006). Melanocortin-4 receptor mediates chronic cardiovascular and metabolic actions of leptin. *Hypertension, 48*(1), 58-64. doi:10.1161/01.HYP.0000227966.36744.d9

Tallam, L. S., Kuo, J. J., da Silva, A. A., & Hall, J. E. (2004). Cardiovascular, renal, and metabolic responses to chronic central administration of agouti-related peptide. *Hypertension, 44*(6), 853-858. doi:10.1161/01.HYP.0000148993.47498.b2

Tallam, L. S., Stec, D. E., Willis, M. A., da Silva, A. A., & Hall, J. E. (2005). Melanocortin-4 receptor-deficient mice are not hypertensive or salt-sensitive despite obesity, hyperinsulinemia, and hyperleptinemia. *Hypertension, 46*(2), 326-332. doi:10.1161/01.HYP.0000175474.99326.bf

Tan, H. Y., Steyn, F. J., Huang, L., Cowley, M., Veldhuis, J. D., & Chen, C. (2016). Hyperphagia in male melanocortin 4 receptor deficient mice promotes growth independently of growth hormone. *The Journal of Physiology, 594*(24), 7309-7326. doi:10.1113/JP272770

Tao, Y.-X., & Huang, H. (2014). Ipsen 5i is a Novel Potent Pharmacoperone for Intracellularly Retained Melanocortin-4 Receptor Mutants. *Frontiers in Endocrinology, 5*, 131. doi:10.3389/fendo.2014.00131

Tao, Y. X. (2005). Molecular mechanisms of the neural melanocortin receptor dysfunction in severe early onset obesity. *Mol Cell Endocrinol, 239*(1-2), 1-14. doi:10.1016/j.mce.2005.04.012

Tao, Y. X. (2010). The melanocortin-4 receptor: physiology, pharmacology, and pathophysiology. *Endocr Rev, 31*(4), 506-543. doi:10.1210/er.2009-0037

Tarnow, P., Rediger, A., Brumm, H., Ambrugger, P., Rettenbacher, E., Widhalm, K., . . . Biebermann, H. (2008). A heterozygous mutation in the third transmembrane domain causes a dominant-negative effect on signalling capability of the MC4R. *Obes Facts, 1*(3), 155-162. doi:10.1159/000138251

Tayal, U., Prasad, S., & Cook, S. A. (2017). Genetics and genomics of dilated cardiomyopathy and systolic heart failure. *Genome Medicine, 9*, 20. doi:10.1186/s13073-017-0410-8

Teare, D. (1958). Asymmetrical hypertrophy of the heart in young adults. *Br Heart J, 20*(1), 1-8.

Tewari, S. G., Bugenhagen, S. M., Vinnakota, K. C., Rice, J. J., Janssen, P. M., &

Beard, D. A. (2016). Influence of metabolic dysfunction on cardiac mechanics in decompensated hypertrophy and heart failure. *J Mol Cell Cardiol, 94*, 162-175. doi:10.1016/j.yjmcc.2016.04.003

TOSHIOINUI, G. K., FUJINO, M. A., MEGUID, M. M., & KASUGA, M. (2002). Effects of agouti-related protein, orexin and melanin-concentrating hormone on oxygen consumption in mice. *International journal of molecular medicine, 10*, 523-525.

Trapnell, C., Roberts, A., Goff, L., Pertea, G., Kim, D., Kelley, D. R., . . . Pachter, L. (2012). Differential gene and transcript expression analysis of RNA-seq experiments with TopHat and Cufflinks. *Nat. Protocols, 7*(3), 562-578.

Triposkiadis, F., Karayannis, G., Giamouzis, G., Skoularigis, J., Louridas, G., & Butler, J. (2009). The Sympathetic Nervous System in Heart Failure. *J Am Coll Cardiol, 54*(19), 1747-1762. doi:http://dx.doi.org/10.1016/j.jacc.2009.05.015

Tronche, F., Kellendonk, C., Kretz, O., Gass, P., Anlag, K., Orban, P. C., . . . Schutz, G. (1999). Disruption of the glucocorticoid receptor gene in the nervous system results in reduced anxiety. *Nat Genet, 23*(1), 99-103. doi:10.1038/12703

Tsai, H. C., Zhang, F., Adamantidis, A., Stuber, G. D., Bonci, A., de Lecea, L., & Deisseroth, K. (2009). Phasic firing in dopaminergic neurons is sufficient for behavioral conditioning. *Science, 324*(5930), 1080-1084. doi:10.1126/science.1168878

Tucker, K. R., Godbey, S. J., Thiebaud, N., & Fadool, D. A. (2012). Olfactory ability and object memory in three mouse models of varying body weight, metabolic hormones, and adiposity. *Physiology & behavior, 107*(3), 424-432. doi:10.1016/j.physbeh.2012.09.007

Tucker, S. J., Gribble, F. M., Proks, P., Trapp, S., Ryder, T. J., Haug, T., . . . Ashcroft, F. M. (1998). Molecular determinants of KATP channel inhibition by ATP. *Embo j, 17*(12), 3290-3296. doi:10.1093/emboj/17.12.3290

Vaisse, C., Clement, K., Guy-Grand, B., & Froguel, P. (1998). A frameshift mutation in human MC4R is associated with a dominant form of obesity. *Nat Genet, 20*(2), 113-114. doi:10.1038/2407

van de Wall, E., Leshan, R., Xu, A. W., Balthasar, N., Coppari, R., Liu, S. M., . . . Chua, S. C., Jr. (2008). Collective and individual functions of leptin receptor modulated neurons controlling metabolism and ingestion. *Endocrinology, 149*(4), 1773-1785. doi:10.1210/en.2007-1132

van der Klaauw, A. A., Keogh, J. M., Henning, E., Stephenson, C., Kelway, S., Trowse, V. M., . . . Farooqi, I. S. (2016). Divergent effects of central melanocortin

signalling on fat and sucrose preference in humans. *Nat Commun, 7*, 13055. doi:10.1038/ncomms13055

van der Vusse, G. J., Glatz, J. F., Stam, H. C., & Reneman, R. S. (1992). Fatty acid homeostasis in the normoxic and ischemic heart. *Physiol Rev, 72*(4), 881-940.

Ventura, A., Kirsch, D. G., McLaughlin, M. E., Tuveson, D. A., Grimm, J., Lintault, L., . . . Jacks, T. (2007). Restoration of p53 function leads to tumour regression in vivo. *Nature, 445*(7128), 661-665. doi:10.1038/nature05541

Vergoni, A. V., Poggioli, R., & Bertolini, A. (1986). Corticotropin inhibits food intake in rats. *Neuropeptides, 7*(2), 153-158.

Voss-Andreae, A., Murphy, J. G., Ellacott, K. L., Stuart, R. C., Nillni, E. A., Cone, R. D., & Fan, W. (2007). Role of the central melanocortin circuitry in adaptive thermogenesis of brown adipose tissue. *Endocrinology, 148*(4), 1550-1560. doi:10.1210/en.2006-1389

Wang, D., He, X., Zhao, Z., Feng, Q., Lin, R., Sun, Y., . . . Zhan, C. (2015). Whole-brain mapping of the direct inputs and axonal projections of POMC and AgRP neurons. *Front Neuroanat, 9*, 40. doi:10.3389/fnana.2015.00040

Wang, D., Ma, J., Zhang, S., Hinney, A., Hebebrand, J., Wang, Y., & Wang, H. J. (2010). Association of the MC4R V103I polymorphism with obesity: a Chinese case-control study and meta-analysis in 55,195 individuals. *Obesity (Silver Spring), 18*(3), 573-579. doi:10.1038/oby.2009.268

Wang, Q., Liu, Y., Fu, Q., Xu, B., Zhang, Y., Kim, S., . . . Xiang, Y. K. (2017). Inhibiting Insulin-Mediated beta2-Adrenergic Receptor Activation Prevents Diabetes-Associated Cardiac Dysfunction. *Circulation, 135*(1), 73-88. doi:10.1161/circulationaha.116.022281

Wang, X. H., Wang, H. M., Zhao, B. L., Yu, P., & Fan, Z. C. (2014). Rescue of defective MC4R cell-surface expression and signaling by a novel pharmacoperone Ipsen 17. *J Mol Endocrinol, 53*(1), 17-29. doi:10.1530/jme-14-0005

Wang, Z. V., Li, D. L., & Hill, J. A. (2014). Heart Failure and Loss of Metabolic Control. *Journal of cardiovascular pharmacology, 63*(4), 302-313. doi:10.1097/FJC.0000000000000054

Ward, K. R., Bardgett, J. F., Wolfgang, L., & Stocker, S. D. (2011). Sympathetic response to insulin is mediated by melanocortin 3/4 receptors in the hypothalamic paraventricular nucleus. *Hypertension, 57*(3), 435-441. doi:10.1161/hypertensionaha.110.160671

Weaver, C. D., Harden, D., Dworetzky, S. I., Robertson, B., & Knox, R. J. (2004). A

thallium-sensitive, fluorescence-based assay for detecting and characterizing potassium channel modulators in mammalian cells. *J Biomol Screen, 9*(8), 671-677. doi:10.1177/1087057104268749

Weir, J. B. (1949). New methods for calculating metabolic rate with special reference to protein metabolism. *J Physiol, 109*(1-2), 1-9.

Wittstein, I. S., Thiemann, D. R., Lima, J. A., Baughman, K. L., Schulman, S. P., Gerstenblith, G., . . . Champion, H. C. (2005). Neurohumoral features of myocardial stunning due to sudden emotional stress. *N Engl J Med, 352*(6), 539-548. doi:10.1056/NEJMoa043046

Wortley, K. E., Anderson, K. D., Yasenchak, J., Murphy, A., Valenzuela, D., Diano, S., . . . Sleeman, M. W. (2005). Agouti-related protein-deficient mice display an age-related lean phenotype. *Cell Metab, 2*(6), 421-427. doi:10.1016/j.cmet.2005.11.004

Wu, Q., & Palmiter, R. D. (2011). GABAergic signaling by AgRP neurons prevents anorexia via a melanocortin-independent mechanism. *Eur J Pharmacol, 660*(1), 21-27. doi:10.1016/j.ejphar.2010.10.110

Wu, W., Lu, C. X., Wang, Y. N., Liu, F., Chen, W., Liu, Y. T., . . . Zhang, X. (2015). Novel Phenotype-Genotype Correlations of Restrictive Cardiomyopathy With Myosin-Binding Protein C (MYBPC3) Gene Mutations Tested by Next-Generation Sequencing. *J Am Heart Assoc, 4*(7). doi:10.1161/jaha.115.001879

Wu, Z., Xu, Y., Zhu, Y., Sutton, A. K., Zhao, R., Lowell, B. B., . . . Tong, Q. (2012). An obligate role of oxytocin neurons in diet induced energy expenditure. *PLoS One, 7*(9), e45167. doi:10.1371/journal.pone.0045167

Xiang, Z., Proneth, B., Dirain, M. L., Litherland, S. A., & Haskell-Luevano, C. (2010). Pharmacological characterization of 30 human melanocortin-4 receptor polymorphisms with the endogenous proopiomelanocortin-derived agonists, synthetic agonists, and the endogenous agouti-related protein antagonist. *Biochemistry, 49*(22), 4583-4600. doi:10.1021/bi100068u

Yamaji, M., Tsutamoto, T., Kawahara, C., Nishiyama, K., Yamamoto, T., Fujii, M., & Horie, M. (2009). Serum Cortisol as a Useful Predictor of Cardiac Events in Patients with Chronic Heart Failure: the Impact of Oxidative Stress. *Circulation: Heart Failure*.

Yen, T. T., Gill, A. M., Frigeri, L. G., Barsh, G. S., & Wolff, G. L. (1994). Obesity, Diabetes, and Neoplasia in Yellow a(Vy)/- Mice - Ectopic Expression of the Agouti Gene. *Faseb Journal, 8*(8), 479-488.

Yeo, G. S., Farooqi, I. S., Aminian, S., Halsall, D. J., Stanhope, R. G., & O'Rahilly, S. (1998). A frameshift mutation in MC4R associated with dominantly inherited human obesity. *Nat Genet, 20*(2), 111-112. doi:10.1038/2404

Yusuf, S., Pitt, B., Davis, C. E., Hood, W. B., Jr., & Cohn, J. N. (1992). Effect of enalapril on mortality and the development of heart failure in asymptomatic patients with reduced left ventricular ejection fractions. *N Engl J Med, 327*(10), 685-691. doi:10.1056/nejm199209033271003

Zakel, U. A., Wudy, S. A., Heinzel-Gutenbrunner, M., Gorg, T., Schafer, H., Gortner, L., . . . Hinney, A. (2005). [Prevalence of melanocortin 4 receptor (MC4R) mutations and polymorphismsin consecutively ascertained obese children and adolescents from a pediatric health care utilization population]. *Klin Padiatr, 217*(4), 244-249. doi:10.1055/s-2005-836589

Zhan, C., Zhou, J., Feng, Q., Zhang, J. E., Lin, S., Bao, J., . . . Luo, M. (2013). Acute and long-term suppression of feeding behavior by POMC neurons in the brainstem and hypothalamus, respectively. *J Neurosci, 33*(8), 3624-3632. doi:10.1523/JNEUROSCI.2742-12.2013

Zhang, F., Gradinaru, V., Adamantidis, A. R., Durand, R., Airan, R. D., de Lecea, L., & Deisseroth, K. (2010). Optogenetic interrogation of neural circuits: technology for probing mammalian brain structures. *Nat Protoc, 5*(3), 439-456. doi:10.1038/nprot.2009.226

Zhang, L., Keung, W., Samokhvalov, V., Wang, W., & Lopaschuk, G. D. (2010). Role of fatty acid uptake and fatty acid beta-oxidation in mediating insulin resistance in heart and skeletal muscle. *Biochim Biophys Acta, 1801*(1), 1-22. doi:10.1016/j.bbalip.2009.09.014

Zhang, Z., Li, M., Lu, R., Alioua, A., Stefani, E., & Toro, L. (2014). The angiotensin II type 1 receptor (AT1R) closely interacts with large conductance voltage- and Ca2+-activated K+ (BK) channels and inhibits their activity independent of G-protein activation. *J Biol Chem, 289*(37), 25678-25689. doi:10.1074/jbc.M114.595603

Ziff, O. J., & Kotecha, D. (2016). Digoxin: The good and the bad. *Trends Cardiovasc Med, 26*(7), 585-595. doi:10.1016/j.tcm.2016.03.011